JOURNAL OF PETROLOGY | VOLUME 45 | NUMBER 5 | PAGES 907–948 | 2004 | DOI: 10.1093/petrology/egg116

Petrogenesis of Proterozoic Lamproites and Kimberlites from the Cuddapah Basin and Dharwar Craton, Southern India

N. V. CHALAPATHI RAO[1]*, S. A. GIBSON[1]†, D. M. PYLE[1] AND A. P. DICKIN[2]

[1]DEPARTMENT OF EARTH SCIENCES, UNIVERSITY OF CAMBRIDGE, DOWNING STREET, CAMBRIDGE CB2 3EQ, UK

[2]DEPARTMENT OF GEOLOGY, McMASTER UNIVERSITY, HAMILTON L8S 4M1, ONT., CANADA

RECEIVED JANUARY 2, 2003; ACCEPTED OCTOBER 16, 2003

Proterozoic mafic potassic and ultrapotassic igneous rocks emplaced in the Cuddapah Basin and Dharwar Craton of the southern Indian shield are among the earliest recorded on Earth. Lamproites intrude the basin and its NE margin, whereas kimberlites intrude the craton to the west of the basin. Kimberlites occur in two spatially separate groups: the non-diamondiferous Mahbubnagar cluster that was emplaced at 1400 Ma and is of a similar age to the Cuddapah lamproites, and the predominantly diamondiferous Anantapur cluster, emplaced at ~1100 Ma. Despite their Proterozoic ages, some of the kimberlites are petrographically fresh. Distinct variations are evident in the major and trace element concentrations of the diamondiferous and non-diamondiferous kimberlites. The latter have higher concentrations of Fe, Ti, Zr, Hf and Sc, and lower Ni contents and La/Sm ratios. All of the kimberlites have high La/Yb ratios (65–180) and positive εNd_i values (0·5–4·5), which suggests that their source regions were metasomatized by small-fraction melts derived from the depleted upper mantle, shortly prior to kimberlite genesis. Cuddapah Basin lamproites have similar La/Yb ratios but much lower εNd_i values (−6 to −7) and appear to have been derived from ancient metasomatized sub-continental lithospheric mantle. The Proterozoic ambient mantle is believed to have had a higher potential temperature than at the present day such that small amounts of lithospheric extension may account for the genesis of the kimberlites and lamproites of southern India without the need for a mantle plume.

KEY WORDS: *Proterozoic; diamonds; India; kimberlites; lamproites*

INTRODUCTION

Global kimberlite and lamproite occurrences are known from the Early Proterozoic to the Quaternary (Janse & Sheahan, 1995). However, certain periods seem to have been the focus for kimberlite and lamproite emplacement. During the Cretaceous many kimberlites and lamproites were emplaced in Africa, South America and North America. This includes the majority of the Group I kimberlites (85–100 Ma) and almost all of the Group II kimberlites (200–100 Ma) of South Africa (Gurney *et al.*, 1991). Skinner *et al.* (1985) recognized the period between 1100 and 1200 Ma as an important global 'mantle event' for kimberlite and lamproite emplacement. Evidence for this event is widespread across the Gondwana supercontinent and also in Greenland. Proterozoic kimberlites and lamproites are relatively rare (Table 1) compared with their Phanerozoic counterparts (Nelson *et al.*, 1989), and petrogenetic studies of the former are few in number.

There is overwhelming evidence that many of the present-day continents of the southern hemisphere formed the Gondwana 'supercontinent' at the end of the Palaeozoic (e.g. Smith & Hallam, 1970). The existence of a preceding Mesoproterozoic supercontinent (Rodinia) at ~1300–1000 Ma is less certain, but has been proposed on the basis of palaeomagnetic data and tectonic reconstructions (e.g. Dalziel, 1997). The reorganization of Rodinia is thought to have been responsible for the formation of Gondwana (e.g. Rogers *et al.*, 1995), and the widespread Pan African radiometric ages (as young as 500 Ma) within the Gondwana fragments are thought to represent a thermal event post-dating the final suturing of this Proterozoic supercontinent. It is in this context that the locations of Proterozoic kimberlites and lamproites in the pre-Cretaceous Gondwana fit assume significance.

*Corresponding author. E-mail: sally@esc.cam.ac.uk

†Present address: Mineralogy Laboratory, Ore Dressing Division, Indian Bureau of Mines, Hingna Road, Nagpur 440016, India.

Table 1: Summary of the radiometric ages of worldwide Proterozoic kimberlites and lamproites

Location	Age (Ma)	Method	Reference
Venezuela (K)	1732 ± 82	Rb–Sr	Nixon *et al*. (1992)
West Greenland (L)	1743 ± 70	K–Ar	Larsen & Rex (1992)
Kuruman Province, South Africa (K)	1700 ± 1600	Rb–Sr	Shee *et al*. (1989)
Premier, South Africa (K)	1202 ± 72	U–Pb	Kramers & Smith (1983)
National, South Africa (K)	1180 ± 30	Rb–Sr	Allsopp *et al*. (1989)
Argyle, Western Australia (L)	1177 ± 47	Rb–Sr	Pidgeon *et al*. (1989)
	1126 ± 9	Rb–Sr	Skinner *et al*. (1985)
Liberia (K)	1072	Rb–Sr	Haggerty (1982)
Bobi, Ivory Coast (L)	1430	Rb–Sr	Nixon *et al*. (1992)
India (L & K)	1090 ± 30 to 1400 ± 10	Rb–Sr	Anil Kumar *et al*. (1993, 2001)
		K–Ar	Chalapathi Rao *et al*. (1996*a*, 1996*b*)
		Ar–Ar	Chalapathi Rao *et al*. (1999)

K, kimberlite; L, lamproite.

A number of kimberlites and lamproites were emplaced during the Proterozoic in the Eastern Dharwar Craton and Cuddapah Basin of the southern Indian shield (Fig. 1). Known kimberlite occurrences in the Dharwar Craton are confined to an area immediately west of the Cuddapah Basin (Fig. 1). They occur as two clusters, in the Anantapur and Mahbubnagar districts of Andhra Pradesh, that are separated from each other by >150 km. In contrast, lamproites are confined to the Cuddapah Basin (Chelima and Zangamarajupalle) and its NE margin (Ramannapeta and Jaggayyapeta; Reddy *et al*., 2000). The kimberlites and lamproites of the Indian sub-continent offer a rare opportunity to investigate Proterozoic tectono-magmatic processes operating when southern India formed a part of the Gondwana supercontinent. Current understanding of the petrogenesis of kimberlites and lamproites has been strongly influenced by studies of examples from South Africa (e.g. Smith, 1983; Tainton & McKenzie, 1994; Mitchell, 1995; Janney *et al*., 2002) Australia (e.g. Jaques *et al*., 1984; Fraser *et al*., 1985), South America (e.g. Gibson *et al*., 1995) and Russia (e.g. Beard *et al*., 1998, 2000; Mahotkin *et al*., 2000). This work complements these recent studies and sheds further insight into the genesis of, and genetic relationship between, kimberlites and lamproites.

GEOLOGICAL SETTING OF THE CUDDAPAH BASIN AND THE EASTERN DHARWAR CRATON

Southern India comprises an extensive supracrustal sequence of Proterozoic rocks, believed to lie above a number of Archaean cratons. The evolution of the Indian shield was initially suggested to have started around Archaean nuclei that developed into three cratons (Dharwar, Singhbhum and Aravalli; Naqvi *et al*., 1974). Subsequent studies revealed additional tectonic sutures, and the Indian shield is now subdivided into seven cratons (e.g. Naqvi & Rogers, 1987). Although the nature of the cratonic boundaries remains unresolved (see Mahadevan, 1995), there is a consensus that the Indian shield has been a single lithospheric unit since mid-Proterozoic times (e.g. Yoshida, 1995; Radhakrishna & Piper, 1999).

The Dharwar Craton mainly comprises schists and gneisses that have undergone greenschist- to granulite-facies metamorphism (Rollinson *et al*., 1981; Allen *et al*., 1985). A NW–SE-trending suite of Early Proterozoic granitic bodies (Closepet granite) divides the Dharwar Craton into western and eastern parts (Naqvi & Rogers, 1987). The Eastern Ghat orogeny affected the Eastern Dharwar Craton, resulting in a narrow, highly deformed granulite-facies belt extending from Madras in the south to near Calcutta in the north. This belt may extend into Eastern Antarctica (e.g. Chetty, 1995). The timing of the Eastern Ghat orogeny is poorly constrained, with age estimates for the granulite-facies metamorphism ranging from 2900 Ma (Sm–Nd whole rock; Paul & Ray Barman, 1988) to ~500 Ma (Grasty & Leelanandam, 1965).

The Cuddapah Basin lies in the Eastern Dharwar Craton (Fig. 1) and includes igneous and sedimentary rocks of Middle to Late Proterozoic age. The basin is crescent shaped, covers an area of 44 000 km^2 and shows increasing metamorphic grade from west to east, attributed to the Eastern Ghat orogeny. The Cuddapah Basin

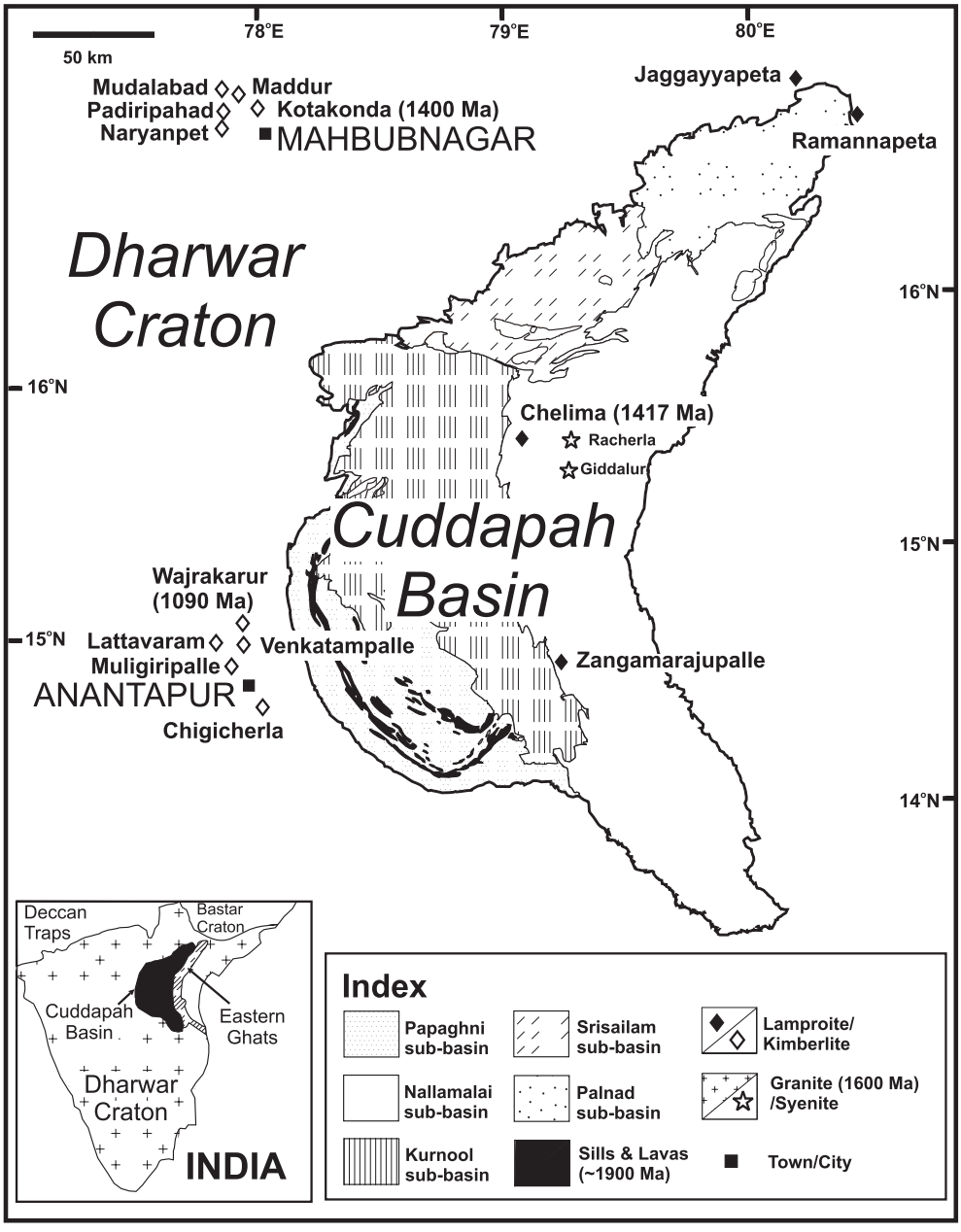

Fig. 1. Geological map of the Cuddapah Basin and surrounding areas (after Nagaraja Rao *et al.*, 1987; Murthy *et al.*, 1987).

includes two sub-basins, the Kurnool and Palnad (see Fig. 1), in which the Upper Proterozoic Kurnool Group sediments were deposited. A marked angular unconformity separates sediments of the older Cuddapah Supergroup from the Kurnool Group. Intrusive and extrusive rocks are present throughout much of the Cuddapah Supergroup, and extensive lava flows, ash beds and sills occur along the SW fringes of the Cuddapah Basin (Reddy, 1988; Anand *et al.*, 2003). Additional intrusives include lamproites (at Chelima and Zangamarajupalle), rare alkali syenites and granitoid domes.

The crust beneath the Cuddapah Basin is 40–50 km thick (Kaila *et al.*, 1979), whereas the lithospheric thickness beneath the Dharwar Craton exceeds 200 km (Bhattacharji & Singh, 1984; Gupta *et al.*, 1991). The thermal structure of the Dharwar lithosphere is considered identical to cratons in Africa, Australia and South America (Gupta, 1993). Evidence for the existence of a thickened Proterozoic Indian lithosphere comes from studies of mantle-derived xenoliths from a kimberlite from the Dharwar Craton [Pipe 3 from Lattavaram in the Anantapur cluster (Fig. 2; Ganguly & Bhattacharya, 1987; Nehru & Reddy, 1989)]. Thermobarometry of

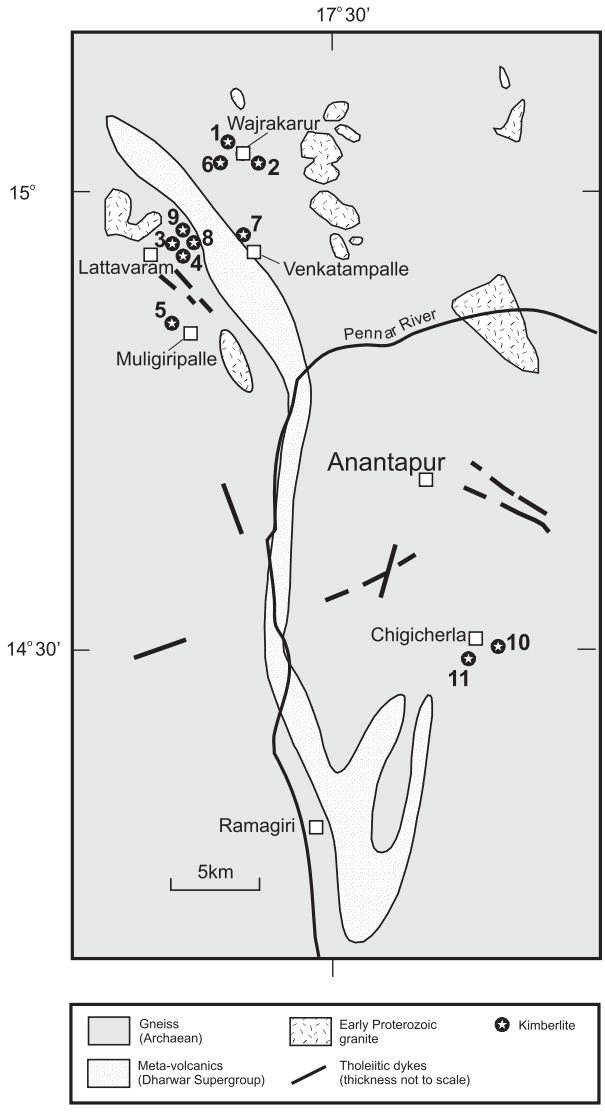

Fig. 2. Location of the Anantapur kimberlites (Pipes 1–11) in the Eastern Dharwar Craton (after Nagaraja Rao *et al.*, 1987; Murthy *et al.*, 1987).

garnet peridotites from this pipe suggests that the mid-Proterozoic lithosphere was at least 170 km thick (see below).

The Archaean basement surrounding the basin is intruded by an extensive swarm of dolerite dykes, which trend ENE–WSW but do not intrude the basin sediments. Radiometric age determinations are of variable precision but suggest that at least three major episodes of dyke emplacement occurred at 1900–1700 Ma, 1400–1300 Ma and 1200–1000 Ma together with a minor younger event at 650 Ma (Murthy *et al.*, 1987; Padmakumari & Dayal, 1987; Mallikharjuna Rao *et al.*, 1995; Chatterjee & Bhattacharji, 2001). The oldest dykes trend east–west and NW–SE and are tholeiitic, whereas the main dyke activity (1300–1400 Ma) comprises tholeiitic to mildly alkaline basalts (Chatterjee & Bhattacharji, 1998). Some north–south-trending mafic dykes, at the northern end of the Cuddapah Basin, are of basaltic komatiite affinity and were emplaced between 1400 and 1300 Ma (Mallikharjuna Rao *et al.*, 1995). Two broad compositional groups of dykes have been recognized: (1) a depleted type similar to mid-ocean ridge basalts (MORB); (2) an enriched type similar to continental flood basalts (Rao & Puffer, 1996).

GEOLOGY AND PETROLOGY OF THE DHARWAR KIMBERLITES

We have used petrography, mineral chemistry and geochemistry to classify the kimberlites and lamproites of southern India following the IUGS scheme proposed by Woolley *et al.* (1996). The freshest possible surface samples, augmented by drill-core samples, were used in this study. Details of sample locations, sample descriptions and photomicrographs are available in Electronic Appendices, which can be downloaded from the *Journal of Petrology* website (http://www.petrology.oupjournals.org), and only the salient aspects are discussed below. The major petrographic features of the studied rocks are summarized in Table 2.

Anantapur kimberlites

Twenty-one kimberlite pipes intrude Archaean granites and gneisses in the Anantapur district (Babu, 1998; Nayak *et al.*, 2001). The pipes were numbered in order of discovery by the Geological Survey of India (GSI) and this terminology is retained here. Pipes 1, 2 and 6 are located near Wajrakarur; Pipes 3, 4, 8 and 9 occur near Lattavaram; Pipes 5 and 7 are located near Muligiripalle and Venkatampalle, respectively, and Pipes 10 and 11 are located close to Chigicherla (Fig. 2).

Crustal xenoliths (chiefly granitic or gneissic rocks) are present in all of the kimberlite pipes, and amphibolite xenoliths also occur in Pipe 7. Mantle xenoliths are reported only from Pipe 3 (lherzolite, harzburgite, dunite and eclogite; Akella *et al.*, 1979; Ganguly & Bhattacharya, 1987; Nehru & Reddy, 1989) and Pipe 10 (spinel harzburgite; Murthy *et al.*, 1994). Typical kimberlite indicator minerals (Cr-diopside, picro-ilmenite and pyrope-garnet) are abundant in all pipes, except 2 and 5, where they are rare. Diamonds have been recovered from all pipes, apart from 2, 5 and 10 (Rao *et al.*, 1991; Satyanarayana *et al.*, 1992). Pipe 1, which has abundant crustal xenoliths and a 'brecciated' appearance, is classified as a diatreme-facies tuffisitic kimberlite (Table 2). All of the others represent hypabyssal-facies kimberlite.

The hypabyssal kimberlites show a characteristic inequigranular porphyritic texture with: (1) subrounded to rounded megacrysts; (2) corroded megacrysts (>5 mm); (3) macrocrysts (0·5–5 mm); (4) subhedral to

Table 2: Petrography of kimberlites and lamproites of the Dharwar Craton

Pipe details	Textural facies	Olivine	Monticellite	Spinel	Clinopyroxene	Phlogopite	Amphibole	Apatite	Perovskite	Diamond	Classification
Anantapur kimberlites											
Pipe 1	diatreme	S, M > Ph	—	TC	—	<2	—	—	2–3	Yes	Kimberlite breccia
Pipe 2	hypabyssal	S, M > Ph	P	TM	—	2–4	—	P	4	No	Phlogopite–monticellite kimberlite
Pipe 3	hypabyssal	F, M > Ph	—	AS	P	2	—	P	3	Yes	Phlogopite-bearing macrocrystic kimberlite
Pipe 4	hypabyssal	F, M > Ph	—	TC	P	2	—	P	3	Yes	Phlogopite kimberlite
Pipe 5	hypabyssal	F, Ph > M	P	TM	P	5–10	—	P	6–8	No	Phlogopite–monticellite kimberlite
Pipe 6	hypabyssal	S, Ph > M	P	TC, TM	—	4	—	P	4	Yes	Phlogopite–monticellite kimberlite
Pipe 7	hypabyssal	F, M > Ph	—	TM	—	3	—	P	3	Yes	Phlogopite kimberlite
Pipe 8	hypabyssal	S, M ≥ Ph	—	C	P	2	—	—	3	Yes	Phlogopite kimberlite
Pipe 9	hypabyssal	S, CL	—	C, TM	—	2	—	—	3	micro	Calcite kimberlite
Pipe 10	hypabyssal	F, M > Ph	—	C	P	3	—	—	4	Poor	Phlogopite kimberlite
Pipe 11	hypabyssal	F, M > Ph	—	TM	P	3	—	P	4	Yes	Phlogopite kimberlite
Mahbubnagar kimberlites											
Maddur	hypabyssal	F, Ph > M	—	TM	—	8	—	P	8	No	Calcite–phlogopite kimberlite
Padiripahad	hypabyssal	S, Ph = M	P	C	P	3	—	P	8	No	Calcite kimberlite
Kotakonda	hypabyssal	S, Ph > M	—	C	—	5–8	—	P	8	No	Phlogopite–monticellite kimberlite
Narayanpet	hypabyssal	F, Ph > M	—	C, TM	P	5–8	—	P	8	No	Perovskite–phlogopite kimberlite
Cuddapah Basin lamproites											
Chelima	hypabyssal	CL	—	—	—	10–15	—	A	—	No	Phlogopite lamproite
Ramannapeta	hypabyssal	S, CL	—	—	P	8–10	P	A	—	No	Phlogopite–richterite lamproite
Zangamarajupalle	hypabyssal	CL	—	—	—	10–15	—	A	—	No	Phlogopite lamproite

F, fresh; CL, calcitized; S, serpentinized; M, macrocryst; Ph, phenocryst; —, absent or not reported; P, present; A, abundant; C, chromite; TM, titano-magnetite; TC, titano-chromite; AS, aluminous spinel. Numbers refer to modal percent.

euhedral phenocrysts (<0·5 mm) of olivine. Modal olivine content and degree of serpentinization varies from pipe to pipe. Olivine is thoroughly serpentinized in Pipes 1, 6, 8 and 9, but fresh in the remaining pipes (Table 2). Some olivines exhibit ragged and embayed margins suggesting resorption prior to serpentinization. Rutile inclusions are noted in some of these olivines. In Pipe 8, olivine pseudomorphs commonly contain opaque cores mantled by carbonate minerals.

Monticellite is an important groundmass phase in Pipes 2, 5 and 6. Its presence is consistent with these rocks being classified as kimberlite, and not lamproite (e.g. Woolley *et al.*, 1996). Phlogopite constitutes an important groundmass phase in all pipes, and is particularly abundant in Pipes 2 and 5, where it occurs either as coarse poikilitic plates or as interstitial grains. Phlogopite macrocrysts (~2 mm) are occasionally present. Some phlogopite shows alteration to serpentine, calcite and/or chlorite. Subhedral to euhedral crystals of perovskite (usually <0·04 mm) occur throughout the groundmass of these pipes, and are particularly abundant in Pipes 2 and 5 (see Table 2). Perovskite may also occur as 'necklaces' around olivine grains, and as inclusions within phlogopite. Various spinels (chromite, titano-magnetite, titano-chromite and aluminous spinel) also constitute important groundmass phases (Table 2). Randomly oriented lath-shaped clinopyroxene crystals occur in some pipes, suggesting late-stage crystallization. Light green laths and plates of clinopyroxene, probably of secondary origin, are reported from Pipe 3 for the first time. Other groundmass phases in the Anantapur kimberlites include calcite, chlorite, apatite, serpentine and clay minerals. Rare minerals such as hazelwoodite (Ni_3S_2), pectolite and melilite have been reported from some of the pipes (Akella *et al.*, 1979; Murthy *et al.*, 1994). Reddy (1987) reported richterite and sanidine in Pipes 2 and 5. However, we observed no amphibole or sanidine in any of the studied samples and suggest that the phases noted by Reddy (1987) may have been derived from granitoid country rocks.

Mahbubnagar kimberlites

Hypabyssal-facies kimberlites, emplaced into migmatites and igneous intrusives, occur near Maddur, Kotakonda, Narayanpet and Padiripahad, and constitute the Mahbubnagar cluster (Fig. 1). Numerous new kimberlite dykes or diatremes have been discovered in this cluster in recent years (Chalapathi Rao *et al.*, 1998). In contrast to the Anantapur kimberlites, preliminary studies suggest that the Mahbubnagar pipes are non-diamondiferous (Satyanarayana, 2002) despite the presence of alluvial diamonds in the vicinity. Chalapathi Rao *et al.* (1998) gave a preliminary account of the indicator minerals and mantle xenoliths in some of these rocks.

Pipes in the Maddur–Narayanpet areas were previously suggested to be olivine lamproites, similar to those in Western Australia (e.g. Nayak *et al.* 1988). However, petrographic, geochemical and isotopic studies demonstrate that they are true kimberlites. Olivine forms euhedral to subhedral phenocrysts and rare, larger (3–5 mm) sub-rounded crystals are also present. Fresh olivine is present in both the Maddur and Narayanpet hypabyssal-facies kimberlites (Table 2). Strongly pleochroic phlogopite forms 0·2–8 mm long euhedral grains in the groundmass, and monticellite inclusions are seen in some phlogopites in the Kotakonda kimberlite. Colourless clinopyroxene is present in the Padiripahad and Narayanpet kimberlites. Perovskite forms an abundant groundmass phase (5–8 modal %) occurring as discrete euhedral grains and as 'garlands' around olivine. The rest of the groundmass predominantly consists of calcite, serpentine, apatite and spinel. The Kotakonda kimberlite also has groundmass rutile, monticellite and kirschsteinite.

GEOLOGY AND PETROLOGY OF THE LAMPROITES FROM THE CUDDAPAH BASIN AND ITS NE MARGIN

The Chelima and Zangamarajupalle lamproite dykes intrude slates and phyllites of the Nallamalai Group, within the Cuddapah Basin (Bhaskar Rao, 1976; Sreeramachandra Rao, 1988). Neither dyke has yet been tested for diamond by modern exploration techniques. The Ramannapeta lamproite intrudes granitoid country rocks at the NE margin of the Cuddapah Basin and lies close to the alluvial workings on the banks of the Krishna River where many famous Indian diamonds, including the Koh-I-Noor, have been recovered. The primary source of these diamonds is uncertain. Earlier workers proposed the Anantapur kimberlites and Chelima lamproite as the source rock for these diamonds (e.g. Rajaraman & Deshpande, 1978). Based on the close proximity (<10 km) of the Ramannapeta lamproite to these workings and the >200 km distance of the nearest known kimberlites, we suggest that the Ramannapeta body may be the primary source for the diamonds of the Krishna valley.

In the Chelima and Zangamarajupalle hypabyssal-facies lamproites, olivine is completely altered and replaced by ferroan dolomite and rarer serpentine. Two olivine generations can be distinguished from pseudomorph textures. Olivine pseudomorphs are rare in the Ramannapeta lamproite. Highly pleochroic, strongly zoned titaniferous phlogopite phenocrysts (0·5–0·7 mm) are abundant in all these rocks (see Table 2). Talc and

chlorite occur as marginal alteration products in the phlogopites of the Chelima lamproite.

Poikilitic laths of a pale pink pleochroic titanian potassic richterite are scattered through the groundmass of the Ramannapeta lamproite. The groundmass also contains abundant pale green or colourless clinopyroxene that lacks the quench textures reported from other lamproites (Mitchell, 1985), and rutile, apatite, serpentine, secondary carbonate and opaque oxides. The abundance of ferroan dolomite and lack of other well-preserved phases (apart from phlogopite) in the Chelima and Zangamarajupalle lamproites may be due to secondary alteration. Therefore, much of the petrological information in these rocks has to be extracted from phlogopite.

The Chelima dyke has been variously classified as minette, lamprophyre, carbonatite–kimberlite and lamproite (e.g. Bergman, 1987; Scott-Smith, 1989). The absence of clinopyroxene precludes this rock from being a minette and the mineral chemistry of the phlogopite is consistent with its classification as a lamproite (see below). The striking petrographic similarity of the Zangamarajupalle lamproite to that at Chelima was noticed by earlier workers, who suggested that both were kimberlites (Bhaskara Rao, 1976; Sreeramachandra Rao, 1988). The composition and zoning trends of the micas and whole-rock geochemistry presented here, however, suggest that both are lamproites.

AGE OF MAGMATISM

The precise emplacement ages of the kimberlites and lamproites are important in constraining models of their origin, whether by lithospheric extension, or the drift of the Indian continent over a mantle plume (e.g. Crough, 1981). Anil Kumar *et al.* (1993) reported phlogopite Rb–Sr ages of ~1090 Ma in some Anantapur kimberlites (Pipes 1, 2, 5 and 7), and the Majhgawan lamproite of central India, and suggested that all southern Indian kimberlites and central Indian lamproites were emplaced around 1090 ± 30 Ma. This contrasts with the much wider age range (850–1350 Ma) reported in earlier work (Paul *et al.*, 1975; Paul, 1979). Preliminary K–Ar dating of phlogopite separates from four Dharwar Craton kimberlites (Kotakonda and Pipe 5 at Muligiripalle) and two Cuddapah Basin lamproites (Chelima and Ramannapeta) yielded Mesoproterozoic ages of 1100–1380 Ma (Chalapathi Rao *et al.*, 1996*a*). These ages, however, have variable precision (±10–50 Ma).

$^{40}Ar/^{39}Ar$ plateau ages of groundmass phlogopite separates from the Kotakonda kimberlite and Chelima lamproites are 1401 ± 5 Ma and 1418 ± 8 Ma, respectively (Chalapathi Rao *et al.*, 1999). These ages are consistent (within error) with conventional K–Ar dates on phlogopite separates from the same samples (Chalapathi Rao *et al.*, 1996*a*). The emplacement of the Kotakonda kimberlite and Chelima lamproite could have been contemporaneous; both are older than the Anantapur kimberlites (~1090 Ma; Anil Kumar *et al.*, 1993). Anil Kumar *et al.* (2001) reported younger phlogopite Rb–Sr ages of 1085 ± 14 and 1099 ± 12 Ma for the Kotakonda and Mudalabad kimberlites of the Mahbubnagar cluster. Those workers also reported a range of Rb–Sr ages for the southern Indian lamproites: Ramannapeta, 1224 ± 14 Ma; Chelima, 1354 ± 17 Ma; Zangamarajupalle, 1070 ± 22 Ma. It is evident that, although further work remains to be done to improve the constraints on their emplacement ages, the Proterozoic kimberlites and lamproites of southern India were non-contemporaneous and emplaced over a protracted period of time.

ANALYTICAL TECHNIQUES

Electron microprobe analyses were conducted using a CAMECA CAMEBAX SX50 in the Department of Earth Sciences, University of Cambridge, using both energy- and wavelength-dispersive spectrometry (EDS and WDS). Routine EDS analyses were obtained on carbon-coated polished thin sections with an accelerating voltage of 20 kV, 10 nA beam current, 3 μm beam diameter and live counting time of 50 s. Both natural and synthetic standards were used for calibration. On-line peak stripping and corrections were performed using LINK Analytical ZAF4 software. WDS was conducted by simultaneous counting on three spectrometers equipped with TAP, LIF and PET crystals with an accelerating voltage of 20 kV, 15 nA beam current and a counting time of 15–20 s for each element. The accuracy is not better than ±1%. Rare earth element (REE) contents of perovskite were determined by WDS with an accelerating voltage of 20 kV and a beam current of 50 nA, using the LiF crystal for REE L lines and Fe Kα; the PET crystal for Ca Kα, Ti Kα and Nb Lα, and the TAP crystal for Sr Lα. The Lβ lines of Pr and Eu were used to minimize interference effects. Standards used were LaB_6, $CeAl_2$, $PrAl_2$, $NdAl_2$, SmF_3, $EuVO_4$, pure Gd, wollastonite (for Ca), TiO_2, pure Nb, pure Fe and Sr-celestine (for Sr).

Whole-rock X-ray fluorescence (XRF) analyses for major and some trace elements (Ba, Cr, Cu, Nb, Ni, Rb, Sc, Sr, V, Y, Zn and Zr) were carried out at the Grant Institute of Geology and Geophysics, University of Edinburgh, on a Phillips PW 1480 automated XRF spectrometer using standard procedures (Norrish & Hutton, 1969). Major elements were analysed on fused discs and trace elements on pressed powder pellets. Data quality was assessed by repeat analysis and analysis of internal standards. Typical uncertainties are <5% for major oxides and <10% for trace elements.

REE and trace elements (Cs, Hf, Ta, Pb, Th and U) were analysed using a VG Plasma Quad PQ2 STE

instrument at the NERC ICP-MS facility, Silwood Park, Surrey. Samples were prepared by open digestion following Jarvis (1990). The instrument was calibrated using three multi-element standard solutions in dilute HNO_3 containing 10 ppb, 20 ppb and 30 ppb of each element. These were analysed in triplicate. Standards BCR-1 and BHVO-1 were run with the samples. The difference in individual light REE (LREE) and middle REE (MREE) concentrations in replicate samples is <10% (Chalapathi Rao, 1997).

Sample dissolutions for Sr- and Nd-isotope ratios were carried out at McMaster University, Hamilton, Canada. All of the samples were leached with warm 6 M HCl and rinsed before dissolution. Sr and Nd isotopic ratios were measured on a VG354 mass spectrometer at McMaster by dynamic multicollection. $^{87}Sr/^{86}Sr$ ratios were normalized for within-run fractionation to $^{86}Sr/^{88}Sr = 0{\cdot}1194$, and are quoted relative to a value of 0·71024 for the NBS 987 standard. $^{143}Nd/^{144}Nd$ ratios were normalized for within-run fractionation to $^{146}Nd/^{144}Nd = 0{\cdot}7219$, and are quoted relative to a value of 0·51185 for the La Jolla standard. Within-run precision of Sr and Nd isotope ratios averages 0·00003 and 0·000015 (2σ), respectively, and the accuracy of calculated initial ratios is estimated to be about 10% of the magnitude of the age corrections. Details of procedures adopted, including run conditions and leaching experiments to back-correct Rb and Sr values, have been given by Gibson *et al.* (1995) and Chalapathi Rao *et al.* (1999).

MINERAL CHEMISTRY

The compositions of mineral phases in 70 mafic potassic rocks from the Cuddapah Basin and Eastern Dharwar Craton were determined by electron microprobe analysis; representative analyses are presented in Table 3.

Olivine

Fresh olivine is present in Pipes 3, 4, 5, 7, 10 and 11 from Anantapur, and the Maddur and Narayanpet kimberlites of the Mahbubnagar cluster. Olivine phenocrysts in the kimberlites range from Fo_{87} to Fo_{92}. Most olivine macrocrysts have similar compositions ($Fo_{84–92}$) although serpentinized olivine from Pipes 2 and 6 (Wajrakarur) range up to Fo_{95}, possibly reflecting Mg enrichment as a result of magnetite precipitation during serpentinization. Some macrocrysts are relatively iron rich ($Fo_{84–86}$), similar to those in some southern African kimberlites (e.g. Boyd, 1974). Because of the considerable compositional overlap, no distinction can be made between olivine phenocrysts and xenocrysts on the basis of their Fo contents. However, olivines from disaggregated mantle xenoliths and phenocrysts from mantle-derived melts may be distinguished on the basis of their CaO contents (Brey *et al.*, 1990; Thompson & Gibson, 2000). A significant proportion of the olivine macrocrysts in the Dharwar kimberlites have CaO <0·18 wt % and are probably xenocrysts (Fig. 3).

Compositional zoning of olivine to iron-rich rims is present in most of the pipes. Ni contents also decrease subtly from core to rim in the phenocrysts. However, reverse zoning is also apparent, especially in Pipe 3 from the Anantapur cluster. Such reverse zoning has been noted in many Group I kimberlites of southern Africa (Moore, 1988). Minor compositional differences between the phenocrysts may result from olivine phenocrysts crystallizing from differing batches of magma. In the Cuddapah lamproites, olivine is either very rare or completely pseudomorphed by calcite, and its composition could not be determined.

Monticellite

Monticellite is an important groundmass phase in Pipes 2, 5 and 6 from Anantapur, and in the Kotakonda kimberlite. Molar Mg/(Mg + Fe) ranges from 0·80 to 0·87 (Table 3) and is slightly lower than in coexisting olivine phenocrysts. Although most monticellites are relatively Mg rich, a few from the Kotakonda kimberlite show appreciable solid solution towards kirschsteinite ($CaFeSiO_4$; Chalapathi Rao *et al.*, 1996*b*). Monticellite crystallizes at low pressures and temperatures after spinel and perovskite, but before late-stage calcite and serpentine (Eggler, 1989). It is characteristically absent from lamproites and Group II kimberlites (Woolley *et al.*, 1996).

Spinel

Spinel is not observed in any of the Cuddapah Basin lamproites. This is a feature characteristic of most lamproites (Mitchell & Bergman, 1991). Mitchell (1986) delineated two trends amongst kimberlite groundmass spinels: a magnesian ulvöspinel trend (Trend 1) containing Ti-rich spinels with substantial amounts of magnesian ulvöspinel molecule and a Ti-magnetite trend (Trend 2) containing a range in composition from aluminous–magnesian chromites to titanian–magnesian chromites, titanian chromites and members of the ulvöspinel magnetite series. Most of the spinels from the Dharwar Craton kimberlites follow Trend 2 (Fig. 4a). The Maddur kimberlite is characterized by abundant titanian magnetite whereas Pipe 8 (Lattavaram), the Kotakonda kimberlite and the Padiripahad kimberlite contain abundant chromite. The rest of the pipes contain different proportions of titanian–magnesian chromite, chromite and Ti-magnetite. Extreme variations in spinel compositions may reflect variation in the bulk composition of their parental magmas. Spinels from the Dharwar Craton kimberlites are relatively poor in aluminium and

Table 3: Representative mineral analyses

	Olivine													
	Olivine macrocrysts							Olivine phenocrysts						
	P3/7 (core)	P-5/7 (core)	G/P7 (core)	CH-10 (core)	P-11/2C (core)	MD-5 (core)	MD/11A (core)	NP (core)	3/PR2B (core)	3/PR2B (rim)	P11/1 (rim)	P11/5 (rim)	MD/5 (rim)	NP (rim)
Oxides (wt %)														
SiO_2	38·91	40·94	40·96	43·60	39·53	39·83	40·19	40·59	40·22	40·27	40·02	40·29	39·74	40·33
TiO_2	n.d.	0·04	n.d.	0·01	n.d.	0·03	0·04	0·09	0·06	0·06	0·03	0·05	0·02	n.d.
Al_2O_3	0·03	n.d.	n.d.	0·03	n.d.	n.d.	n.d.	0·04	0·44	0·51	n.d.	n.d.	n.d.	0·01
Cr_2O_3	n.d.	0·03	0·05	0·01	0·06	0·05	0·03	0·09	0·11	0·13	0·07	0·16	0·10	0·03
FeO_T	16·06	9·68	6·65	7·61	11·30	12·12	13·36	8·29	10·32	10·53	11·17	11·62	11·83	13·57
MnO	0·20	0·15	0·12	0·06	0·09	0·16	0·09	n.d.	0·22	0·14	0·19	0·15	0·12	0·17
MgO	43·66	49·60	51·32	49·80	48·02	47·18	45·80	50·30	48·34	48·09	47·91	48·79	46·93	46·06
CaO	0·04	0·06	0·07	0·02	0·07	0·14	0·13	0·15	0·22	0·21	0·21	0·18	0·18	0·26
Na_2O	0·15	0·25	0·20	0·14	0·27	0·29	0·20	0·23	0·26	0·15	0·27	0·37	0·34	0·23
K_2O	n.d.	n.d.	0·02	n.d.	n.d.	n.d.	n.d.	0·07	0·01	0·01	n.d.	n.d.	n.d.	0·04
NiO	n.d.	0·30	0·34	0·30	0·44	n.d.	0·29	0·31	0·21	0·18	0·35	0·42	n.d.	0·26
P_2O_5	n.d.	0·05	n.d.	0·09	n.d.	0·32	n.d.	n.d.	n.d.	n.d.	n.d.	n.d.	0·33	n.d.
Total	99·05	100·84	99·73	101·69	99·47	99·63	99·84	99·94	100·30	100·15	100·01	101·73	99·93	100·77
$(Mg/Mg + Fe_T)$	0·83	0·90	0·93	0·92	0·88	0·88	0·86	0·92	0·89	0·90	0·88	0·88	0·86	0·91

	Clinopyroxene									
	P3/7 (core)	P4 (core)	P-5/A (core)	P8/10 (core)	P9/1 (core)	CH-5 (core)	P11/1 (core)	NP (core)	MD-5 (core)	RU/1 (core)
Oxides (wt %)										
SiO_2	53·84	52·08	52·60	54·38	51·87	51·19	50·06	49·19	49·42	53·26
TiO_2	0·11	2·15	1·50	0·85	0·23	0·39	4·58	0·17	2·86	1·37
Al_2O_3	n.d.	1·25	0·41	0·22	3·69	2·45	0·59	0·82	1·89	0·24
Cr_2O_3	0·08	0·06	0·13	0·40	0·11	0·06	n.d.	0·01	0·05	0·45
FeO_T	3·27	4·56	6·26	3·47	16·48	12·70	3·86	11·09	5·84	3·97
MnO	0·23	0·09	0·08	0·12	0·20	0·33	0·11	0·33	0·10	0·07
MgO	16·06	14·57	14·22	16·06	13·72	15·14	15·70	13·12	14·13	16·49

Table 3: continued

	Clinopyroxene									
	P3/7 (core)	P4 (core)	P-5/A (core)	P8/10 (core)	P9/1 (core)	CH-5 (core)	P11/1 (core)	NP (core)	MD-5 (core)	RU/1 (core)
CaO	25·58	23·31	22·73	23·84	8·82	17·22	23·87	25·56	23·88	23·68
Na_2O	n.d.	1·14	1·50	0·91	2·12	0·76	0·86	0·11	0·92	0·44
K_2O	0·06	0·76	0·06	0·08	0·77	0·11	0·26	0·02	n.d.	0·02
NiO	0·01	n.d.	n.d.	0·02	n.d.	n.d.	n.d.	n.d.	0·43	n.d.
P_2O_5	n.d.	0·01	n.d.	n.d.	0·08	n.d.	0·02	0·02	0·06	n.d.
Total	99·23	99·98	99·90	100·49	98·15	100·33	99·91	100·46	99·56	99·99

	Phlogopite															
	7/PR2 (core)	P3B (core)	P4/7 (core)	P-5/7 (core)	P6/5 (core)	G/P7/1 (rim)	G/P8 (core)	P9 (core)	CH-5 (core)	P11/2C (core)	MD/11 (core)	NP (core)	PDF/1B (core)	KK7A (core)	C1-C (core)	ZP (core)	RU/1 (core)
Oxides (wt %)																	
SiO_2	43·33	38·81	39·36	41·66	42·90	41·05	40·38	36·60	42·03	39·73	40·76	40·78	40·42	41·88	38·59	39·61	36·17
TiO_2	2·19	1·38	2·27	2·90	2·15	1·22	2·09	2·96	2·69	2·99	2·52	2·99	2·74	1·77	4·84	6·30	8·46
Al_2O_3	5·53	9·44	8·19	5·39	2·56	11·75	11·65	15·27	4·38	8·86	5·13	6·39	4·25	11·06	11·26	10·40	8·45
Cr_2O_3	n.d.	0·01	n.d.	n.d.	n.d.	0·68	0·21	n.d.	0·01	n.d.	n.d.	0·01	n.d.	0·02	0·39	0·30	n.d.
FeO_T	7·04	6·97	6·24	14·88	10·82	4·05	4·62	4·22	11·58	5·25	12·17	10·02	10·93	5·13	9·82	6·03	16·62
MnO	0·07	0·04	n.d.	0·23	0·22	n.d.	0·03	0·09	0·13	0·08	0·05	0·10	0·09	0·02	0·07	0·08	0·18
MgO	23·06	23·96	23·86	19·63	21·12	24·97	24·12	24·98	23·45	25·42	20·86	22·11	23·55	27·55	20·59	20·94	13·99
CaO	0·06	3·40	2·72	0·03	0·18	0·03	0·06	0·23	0·02	n.d.	0·14	0·06	0·11	0·03	0·05	0·14	0·05
Na_2O	1·20	0·06	0·65	0·71	0·72	0·41	0·16	0·34	0·14	0·58	0·43	0·72	0·26	0·22	0·14	0·37	0·30
K_2O	10·57	9·42	10·01	10·64	9·18	11·31	11·59	5·83	9·06	8·57	10·22	10·16	8·76	10·17	10·24	10·28	9·64
Cl	n.d.	n.d.	n.d.	n.d.	0·11	n.d.	n.d.	n.d.	n.d.	n.d.	0·01	n.d.	n.d.	0·03	n.d.	n.d.	n.d.
F	n.d.	1·20	n.d.	0·63	n.d.	n.d.	n.d.	n.d.	n.d.	n.d.	0·44	n.d.	n.d.	1·39	1·46	n.d.	n.d.
P_2O_5	n.d.	n.d.	n.d.	n.d.	n.d.	n.d.	n.d.	n.d.	n.d.	n.d.	n.d.	n.d.	n.d.	n.d.	n.d.	n.d.	n.d.
Total	93·05	94·40	93·30	96·17	91·95	95·56	94·99	90·50	93·47	91·58	92·48	93·35	91·13	97·74	97·44	94·47	93·86

	Amphibole (richterite)							
	RU/1 (core)	RU/1 (core)	RU/1 (core)	NR/1 (core)	NR/1 (core)	NR/1 (core)	NR/1 (core)	NR/7 (core)
Oxides (wt %)								
SiO_2	51·80	53·12	54·14	54·73	54·53	50·18	51·27	49·56
TiO_2	3·63	3·15	1·15	1·31	1·35	6·18	4·81	5·92
Al_2O_3	0·28	0·18	0·02	0·15	0·07	0·40	0·38	0·97
Cr_2O_3	0·05	0·01	0·01	n.d.	0·06	n.d.	n.d.	0·12
FeO_T	12·46	11·71	8·95	16·39	7·07	11·96	14·28	11·02
MnO	0·35	0·20	0·16	0·19	0·25	0·46	0·34	0·29
MgO	14·39	14·88	17·81	12·59	18·98	12·99	11·82	14·54
CaO	5·51	5·16	4·33	3·31	5·39	5·04	5·73	6·45
Na_2O	3·80	4·16	4·64	5·03	3·69	3·95	3·19	3·10
K_2O	3·83	4·68	4·82	4·18	4·88	4·35	3·99	4·28
Total	96·10	97·25	96·20	97·89	96·26	95·50	95·82	96·14

	Perovskite									
	P3	P4	P4	CH10	P11/2C	KK10	MD/11	NP	PD/2	PD/2
Oxides (wt %)										
La_2O_3	1·13	0·86	0·83	0·54	0·62	0·31	0·26	0·45	0·21	0·36
Ce_2O_3	2·67	2·05	2·27	1·07	1·45	0·78	0·41	0·89	0·47	0·66
Pr_2O_3	0·33	0·29	0·18	0·29	0·31	0·08	0·04	0·05	0·02	0·07
Nd_2O_3	1·12	0·78	0·83	0·54	0·56	0·35	0·17	0·36	0·29	0·25
Sm_2O_3	0·12	0·09	0·08	0·05	0·05	0·02	0·02	0·03	0·01	0·02
Eu_2O_3	n.d.	n.d.	n.d.	n.d.	n.d.	n.d.	n.d.	n.d.	n.d.	n.d.
Gd_2O_3	0·01	0·02	0·08	0·09	0·01	0·03	n.d.	0·06	0·04	0·03
CaO	36·61	37·11	37·58	38·84	37·81	39·92	39·37	39·81	40·29	39·97
TiO_2	54·75	54·54	55·13	55·88	56·12	58·61	58·65	57·55	58·08	57·91
Nb_2O_5	1·83	1·39	1·45	0·37	0·34	0·22	0·27	0·27	0·32	0·30
FeO_T	1·10	0·92	0·94	2·09	2·00	0·92	0·93	0·86	0·95	0·93
Total	99·67	98·05	99·37	99·75	99·27	101·24	100·12	100·32	100·79	100·50
REE	5·37	4·09	4·26	2·57	2·99	1·57	0·91	1·83	1·15	1·39

Table 3: continued

	Perovskite									
	P3	P4	P4	CH10	P11/2C	KK10	MD/11	NP	PD/2	PD/2
Trace elements (ppm)										
La	9590	7360	7040	4590	5210	2600	2220	3800	2620	3060
Ce	22800	17490	19380	9170	12380	6680	3520	7570	4050	5670
Pr	2820	2440	1520	2440	2650	650	370	440	210	620
Nd	9590	6690	7110	4620	4770	2980	1470	3090	2520	2130
Sm	1040	850	700	460	420	190	150	220	100	170
Eu	n.d.	n.d.	n.d.	n.d.	n.d.	n.d.	n.d.	n.d.	n.d.	n.d.
Gd	60	140	650	740	60	260	n.d.	530	370	260
Nb	9840	7470	7810	1980	1840	1180	1470	1470	1720	1600
	Monticellite									
	7/PR2 (core)	7/PR2 (rim)	4/PR2 (core)	4/PR2 (rim)	P-5/A (core)	G/P5 (core)	P5 (core)	KK4 (core)	KK11 (core)	
Oxides (wt %)										
SiO_2	37·07	36·86	36·76	36·22	36·91	35·96	36·96	40·78	40·58	
TiO_2	0·08	0·18	0·11	0·15	0·11	0·47	0·09	0·12	0·20	
Al_2O_3	0·01	n.d.	n.d.	n.d.	0·48	0·63	0·51	0·92	2·09	
Cr_2O_3	0·06	0·04	0·05	0·04	0·06	0·08	0·10	0·06	n.d.	
FeO_T	7·26	6·17	7·97	9·85	8·17	13·32	8·32	20·11	11·30	
MnO	0·38	0·25	0·25	0·35	0·34	0·24	0·32	n.d.	0·10	
MgO	21·80	22·37	21·21	19·36	21·26	16·96	21·17	15·27	30·36	
CaO	33·41	33·41	33·32	33·50	33·14	31·99	33·17	22·87	14·81	
Na_2O	0·19	0·16	0·24	0·18	0·31	0·33	0·15	0·40	0·44	
K_2O	0·05	0·05	0·05	0·08	n.d.	0·17	0·02	0·06	n.d.	
NiO	0·05	0·07	0·13	0·10	0·10	0·13	0·01	0·14	0·11	
Total	100·39	99·55	100·05	99·84	100·87	100·15	100·86	100·58	101·02	

	Spinel														
	NW1-9 (core)	8/PR2A (core)	P3/5 (core)	P4 (core)	P5/10 (core)	P6/5 (core)	G/P7/1 (rim)	P8 (core)	P9 (core)	CH-8 (core)	P11/2A (core)	KK10 (core)	MD/11A (core)	PDF/10 (core)	NP/10 (core)
Oxides (wt %)															
SiO_2	0·19	0·19	0·10	0·17	0·16	0·22	0·24	0·22	0·19	0·29	0·19	0·38	0·16	0·39	0·52
TiO_2	6·11	3·63	0·09	8·30	9·82	4·55	4·82	3·17	4·31	5·41	5·38	3·54	14·66	4·40	4·54
Al_2O_3	6·95	3·41	14·27	0·31	2·11	1·34	9·17	4·66	9·68	5·80	4·16	13·37	0·56	9·26	9·31
Cr_2O_3	46·39	33·30	56·31	0·63	10·88	27·43	51·83	55·97	50·84	45·56	26·14	30·85	2·05	34·99	51·17
Fe_2O_3	7·68	27·93	0·06	54·67	38·13	33·70	3·55	4·97	3·03	10·72	29·71	21·17	38·18	17·54	4·71
FeO	19·45	24·03	0·34	30·39	33·30	22·82	17·20	22·93	16·81	21·67	26·19	19·11	40·78	19·26	15·81
MnO	0·42	0·58	0·23	0·75	1·75	0·84	0·18	0·79	0·11	0·92	1·33	0·46	2·31	0·87	0·55
MgO	12·01	6·41	13·29	4·21	3·13	7·01	12·96	7·48	12·60	9·08	5·68	10·51	0·11	10·58	12·96
CaO	0·30	0·09	n.d.	0·47	0·19	0·09	0·10	0·10	0·24	0·18	0·12	0·26	0·34	0·51	0·05
Na_2O	0·05	0·21	0·28	0·16	0·15	0·24	0·16	0·17	0·13	0·30	0·21	0·37	0·26	0·01	0·43
K_2O	n.d.	0·08	n.d.	0·08	0·01	0·02	0·06	n.d.	n.d.	0·03	0·01	n.d.	n.d.	0·04	0·07
P_2O_5	n.d.	n.d.	n.d.	0·01	n.d.	n.d.	0·05	n.d.	n.d.	0·08	n.d.	n.d.	n.d.	0·01	0·06
NiO	0·21	n.d.	0·09	n.d.	n.d.	0·27	0·28	0·06	0·26	0·24	n.d.	0·02	0·02	0·08	0·20
Total	99·65	99·89	99·59	100·12	99·31	98·27	100·27	100·03	97·94	99·95	99·64	100·02	99·41	97·83	99·90

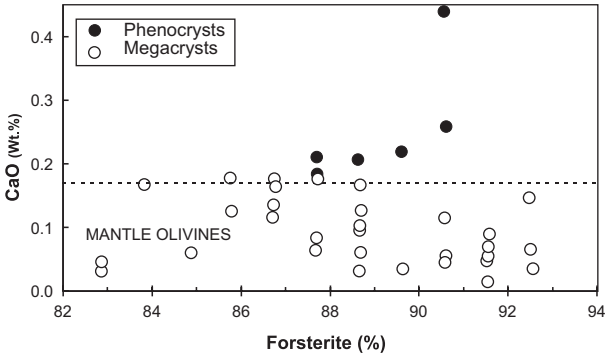

Fig. 3. Variation of Fo [Mg/(Mg + Fe)] and CaO contents in olivines from the Dharwar kimberlites. Olivines with >0·18 wt % CaO are believed to have crystallized from the kimberlite melt whereas those with <0·18 wt % CaO are thought to be xenocrysts (Brey *et al.*, 1990; Thompson & Gibson, 2000).

magnesium compared with those from southern Africa (Fig. 4b); those from Pipes 1 and 3 (Anantapur) have the highest Al_2O_3 and MgO contents.

Clinopyroxene

Clinopyroxene occurs as a groundmass phase in the Anantapur kimberlites (Pipes 3, 4, 5, 8, 10, 11) and in the Maddur, Narayanpet and Padiripahad pipes from the Mahbubnagar cluster. Most clinopyroxenes are diopsides and those in Pipe 10 are the most Fe rich. The TiO_2 contents of diopside in the Maddur kimberlite and Pipes 4, 5 and 11 are high (up to 4 wt %) compared with the other pipes. With the exception of Pipe 10 (Chigicherla), the Al_2O_3 contents of kimberlite diopside are <1·0 wt %. In Pipe 10, Al_2O_3 ranges from 1 to 2·5 wt %, suggesting that the clinopyroxene may be xenocrystal (see Mitchell, 1986). Crust-derived xenocrystic augite occurs in Pipe 9. Clinopyroxene is a rare groundmass phase in Group I kimberlites (see Mitchell, 1995), but has been reported from some archetypal kimberlites from the Dharwar Craton (Scott-Smith, 1989) and Greenland (Scott, 1981). Its occurrence may be due to contamination of the magma by crustal xenoliths.

In the lamproites, clinopyroxene occurs only in the samples from Ramannapeta, where it is a pure diopside and shows little compositional variation. This is considered characteristic of lamproite diopsides and is attributed to either rapid quenching of the magma after the onset of pyroxene crystallization (Mitchell, 1985) or its early replacement as a liquidus phase by amphibole (Mitchell & Bergman, 1991). The TiO_2 content of clinopyroxene in the Ramannapeta lamproite ranges from 1·37 to 2·2 wt % and Cr_2O_3 and Al_2O_3 contents are 0·06–0·48 wt % and 0·2–0·53 wt %, respectively. Such diopsides are considered to be typical of lamproites (Bergman, 1987).

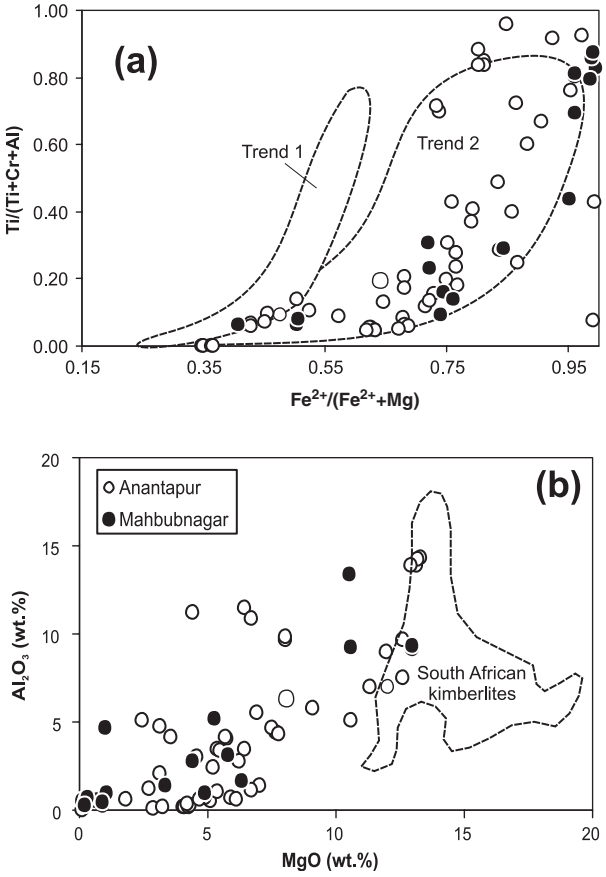

Fig. 4. (a) $Fe^{2+}/(Fe^{2+} + Mg^{2+})$ vs Ti/(Ti + Cr + Al) (mol fraction) for groundmass kimberlite spinels projected onto the front face of the 'reduced' spinel prism. The trends exhibited by spinels in kimberlites and lamproites are modified from Mitchell (1986). (b) MgO (wt %) vs Al_2O_3 (wt %) of spinels from the Anantapur and Mahbubnagar kimberlites. The shaded zone is the field for some southern African kimberlite spinels (after Scott-Smith & Skinner, 1984).

Phlogopite

Phlogopite, along with olivine, is the most characteristic ferromagnesian mineral in kimberlites and lamproites, where it occurs as megacrysts, macrocrysts and microphenocrysts. Megacrysts (>1 cm) are xenocrystal and may be derived from mantle peridotites (Dawson & Smith, 1975), but it is not always possible to distinguish them from phenocrysts (Mitchell, 1995). All of the kimberlite phlogopites have TiO_2 <4·5 wt % (Fig. 5) and zoning trends that indicate enrichment in Al_2O_3 and depletion in TiO_2. Minor variations in zoning patterns shown by some micas may reflect changes in the magma composition on a small scale or mixing processes. Some Pipe 4 and Pipe 6 micas have relatively low Al_2O_3 (<4 wt %) but substantial tetrahedrally coordinated Fe^{3+} and are therefore tetraferriphlogopites. They strongly resemble phlogopites from the Orroroo kimberlites, Australia (Scott-Smith *et al.*, 1984), and others from West Greenland (Emeleus & Andrews, 1975).

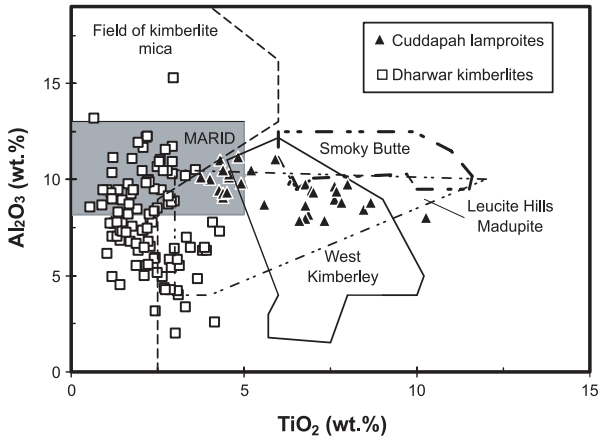

Fig. 5. TiO_2 vs Al_2O_3 for micas from the Anantapur and Mahbubnagar kimberlites with those from other areas. Fields for selected kimberlites, lamproites and the MARID (mica–amphibole–rutile–ilmenite–diopside) suite of xenoliths are from Dawson & Smith (1977), Smith *et al.* (1978), Scott-Smith *et al.* (1989) and Mitchell & Bergman (1991).

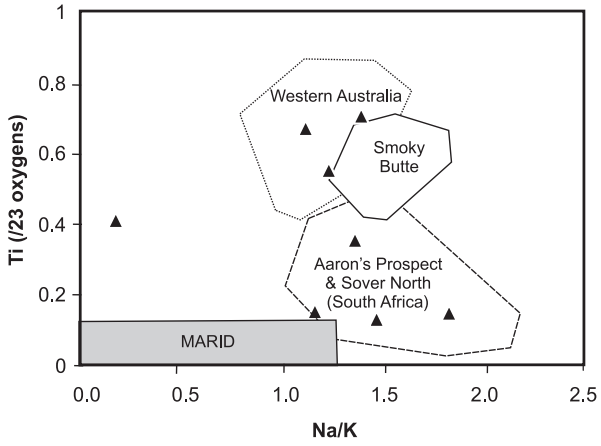

Fig. 6. Variation of Ti (/23 oxygens) vs Na/K in amphibole from the Ramannapeta lamproite. Fields for Aaron's Prospect and Sover North are from Tainton (1992), MARID from Dawson & Smith (1977), Western Australian and Smoky Butte from Mitchell & Bergman (1991).

Lamproite micas are more strongly zoned than those in the kimberlites (Fig. 5). They are all titaniferous (>4 wt %), with Zangamarajupalle micas containing up to 10·5 wt % TiO_2. Ramannapeta and Zangamarajupalle micas show core–rim zoning trends of increasing TiO_2 and FeO_T and falling MgO and Al_2O_3. Although most of the Chelima micas also show marked Ti enrichment, a few show slight Ti depletion that may reflect mixing processes. In the lamproite phlogopites, the cation sum (Al + Si) is typically less than 8 atoms per 23 oxygens, so some Fe^{3+} probably occupies the tetrahedral site (e.g. Farmer & Boettcher, 1981). The high TiO_2 content of the Chelima, Ramannapeta and Zangamarajupalle micas is consistent with the classification of the host rocks as lamproites.

Cr_2O_3 contents of the kimberlite micas are mostly below the levels of detection, but Pipe 7 contains chromian micas with 0·5–0·7 wt % Cr_2O_3. Lamproite micas collectively show relatively high Cr_2O_3 values (0·2–0·35 wt %). Fluorine contents of kimberlite and lamproite micas worldwide are very poorly documented. The Cuddapah lamproite phlogopites contain 0·49–1·57 wt % F, with the highest values in the Chelima micas. In contrast, the Dharwar kimberlite micas have F contents ranging up to 3·1 wt %, whereas the Kotakonda micas consistently contain around 2 wt % F. The fluorine concentrations obtained here are consistent with the compositions of primary phlogopites (Smith *et al.*, 1981), and are higher than in phlogopites from South African kimberlite peridotite nodules (Matson *et al.*, 1986).

Amphibole

Pleochroic amphibole (richterite) is found only in the Ramannapeta lamproite (Table 3). It is rich in TiO_2 (1·2–6·1 wt %) and K_2O (3·8–4·5 wt %), but poor in Al_2O_3 (0·4 wt %) and CaO (<6·4 wt %). Bergman (1987) noted that richterites of such composition are 'unique' to lamproites. The Ramannapeta richterite TiO_2 contents are more varied than in most other lamproites, where TiO_2 is characteristically >3 wt % (Mitchell & Bergman, 1991), although richterites with 0·38–1·37 wt % TiO_2 are found in the groundmass of some Kansas lamproites (Cullers *et al.*, 1996). The Ramannapeta richterite has appreciably higher TiO_2 than richterites in MARID suite nodules (e.g. Dawson & Smith, 1977, fig. 6) and richterite-bearing peridotites (Wagner *et al.*, 1996). FeO_T and Na_2O contents show little variation. The Ramannapeta richterite appears to have a tetrahedral site deficiency (Si + Al <8), so either Fe^{3+} or Ti^{4+} may enter the tetrahedral sites (e.g. Mitchell *et al.*, 1987; Hwang *et al.*, 1994). Richterites in the Ramannapeta lamproites are broadly similar in composition to those from Barkley West (South Africa) and Western Australia (Fig. 6).

Perovskite

Perovskite is an important groundmass phase in the Dharwar kimberlites but is present only in minor amounts in the Cuddapah lamproites. Perovskites have CaO (~38 wt %) and TiO_2 (~58 wt %) contents near that of the stoichiometric end-member, indicating little substitution by other elements. FeO* (as total iron) contents of perovskites range from 0·79 to 1·02 wt % in the non-diamondiferous Mahbubnagar kimberlites and from 0·92 to 2·22 wt % in the diamondiferous Anantapur kimberlites. These are similar to the Fe contents of kimberlite perovskites from elsewhere (Mitchell, 1986), indicating little Fe substitution in the Ti site. Nb_2O_5

Table 4: Whole-rock analyses of Proterozoic kimberlites and lamproites from southern India

	Anantapur kimberlites (1090 Ma)																		
Location:	Pipe 1 (Wajrakarur)		Pipe 2 (Wajrakarur)				Pipe 3 (Lattavaram)					Pipe 4 (Lattavaram)			Pipe 5 (Muligiripalle)				
Grid ref.:	15°1′58″, 70°23′6″		15°1′26″, 70°24′30″				14°55′25″, 77°18′09″					14°55′25″, 77°19′30″			14°59′50″, 77°19′30″				
Sample no.:	NW1-9	6/PR1B	3/PR2B	4/PR2	7/PR2	8/PR2A	P3B	P3A	P3/5	P3/7	P3	P4/7	P4/A	P4	G/P5	P-5/7	P5	P-5/A	P5/10
SiO_2	59·10	43·90	33·70	33·22	35·38	33·10	36·86	37·15	37·13	33·37	36·45	38·32	38·14	38·15	34·65	35·18	32·28	35·47	33·86
TiO_2	0·86	1·34	2·58	2·68	2·29	2·59	1·69	1·59	1·64	1·56	1·61	1·47	1·52	1·35	4·11	4·36	5·36	4·43	4·47
Al_2O_3	9·69	4·40	5·79	5·60	6·07	5·38	3·45	3·35	3·36	3·18	3·37	3·51	3·62	3·45	4·22	3·99	3·68	4·53	3·97
$Fe_2O_3^*$	5·68	7·26	12·58	13·27	11·96	12·90	10·21	10·06	10·23	8·85	10·04	10·00	10·01	9·73	13·49	13·08	14·34	12·08	14·62
MnO	0·07	0·16	0·22	0·24	0·21	0·22	0·16	0·15	0·16	0·16	0·16	0·15	0·16	0·15	0·19	0·18	0·19	0·15	0·21
MgO	10·50	11·57	18·60	20·31	17·30	19·69	28·40	28·93	28·73	29·02	28·00	30·23	29·43	29·77	20·02	21·01	22·08	19·60	19·88
CaO	5·49	25·97	15·60	12·88	16·50	15·79	8·16	7·80	7·90	8·15	8·00	6·93	7·67	8·33	11·82	11·28	11·01	12·99	11·46
Na_2O	1·71	0·17	0·39	0·17	0·45	0·62	0·26	0·26	0·19	0·05	0·24	0·17	0·21	0·25	0·34	0·37	0·27	0·29	0·41
K_2O	1·76	0·03	2·26	2·47	0·92	2·16	0·84	0·74	0·79	0·97	0·77	1·31	1·28	0·99	1·37	1·59	1·49	1·30	1·19
P_2O_5	0·38	0·70	0·93	0·78	0·90	0·69	0·52	0·50	0·50	0·56	0·50	0·48	0·54	0·53	1·16	0·85	0·53	0·80	0·92
LOI	4·46	3·39	6·55	7·78	7·22	5·72	8·87	8·81	8·85	12·67	10·83	6·88	6·24	6·10	7·84	7·14	8·19	7·06	8·09
Total	99·70	98·89	99·20	99·40	99·20	98·86	99·42	99·34	99·48	98·54	99·97	99·45	98·82	98·80	99·21	99·03	99·42	98·70	99·08
C.I.	5·70	1·80	1·90	1·70	2·40	1·70	1·30	1·30	1·30	1·20	1·30	1·30	1·30	1·30	1·80	1·70	1·50	1·90	1·80
Mg no.	0·76	0·73	0·72	0·72	0·71	0·72	0·83	0·83	0·85	0·84	0·85	0·84	0·83	0·84	0·72	0·73	0·73	0·74	0·70
Ba	735	3170	3368	1197	2449	1836	877	897	927	2932	1129	1697	2381	1796	1209	1398	1021	1812	1149
Cr	422	523	809	980	903	1259	1244	1150	1145	1111	1166	1296	1267	1188	822	864	920	813	861
Cs	0·71	0·35	3·24	1·43	1·82	1·91	2·72	2·16	1·96	1·67	2·25	3·43	3·00	3·69	6·25	4·48	3·79	3·67	6·58
Cu	19·0	62·8	125	111	89·1	77·3	82·9	80·1	74·9	56	80·5	71·6	77·7	68·4	202	132	110	119	145
Hf	2·97	3·51	5·01	3·34	4·02	4·47	2·96	2·39	2·43	3·36	3·15	2·82	3·33	2·69	12·37	10·25	7·99	10·37	9·72
Nb	84	195	199	145	192	209	123	124	111	151	122	122	123	121	149	156	152	154	139
Ni	373	357	503	575	557	1316	1303	1373	1371	1284	1343	1376	1324	1403	772	884	858	740	796
Pb	12·6	13·57	8·05	9·24	10·6	11·83	7·47	7·68	7·18	10·9	7·97	7·56	9·57	7·98	14·2	13·1	18·43	14·8	15
Rb	43	0·9	238	245	196	131	108	100	100	139	100	126	130	106	153	134	143	103	146
Sc	9·8	15·0	24·5	25·3	22·9	15·6	13·9	13·2	12·4	13·0	13·6	13·4	12·2	9·3	19·5	17·4	18·4	13·9	19·7
Sr	339	290	1167	741	1189	605	692	657	662	616	661	560	604	654	835	1025	1145	944	1033

	Anantapur kimberlites (1090 Ma)																		
Location:	Pipe 1 (Wajrakarur)		Pipe 2 (Wajrakarur)				Pipe 3 (Lattavaram)					Pipe 4 (Lattavaram)			Pipe 5 (Muligiripalle)				
Grid ref.:	15°1′58″, 70°23′6″		15°1′26″, 70°24′30″				14°55′25″, 77°18′09″					14°55′25″, 77°19′30″			14°59′50″, 77°19′30″				
Sample no.:	NW1-9	6/PR1B	3/PR2B	4/PR2	7/PR2	8/PR2A	P3B	P3A	P3/5	P3/7	P3	P4/7	P4/A	P4	G/P5	P-5/7	P5	P-5/A	P5/10
Ta	4·34	8·87	11·00	8·43	11·10	12·63	7·12	7·36	6·52	9·17	7·21	7·04	7·43	7·55	8·87	9·72	10·3	9·7	8·5
Th	12·7	21·1	19·4	13·5	18·1	22·1	11·4	6·72	5·61	14·6	11·7	12·1	13·2	12·7	15·6	15·2	13·33	15·9	16·5
U	2·54	6·01	3·56	2·6	3·3	3·79	2·14	2·01	1·93	2·62	2·15	2·26	2·4	2·13	3·39	3·29	2·56	3·02	3·11
V	78·3	95	172	152	95·7	107	111	108	110	186	113	94·0	107	90·7	295	243	201	245	354
Y	11·4	15·4	19·7	12·9	17·1	19·0	10·5	9·12	7·95	11·7	10·9	10·4	11·3	10·9	21·0	19·6	16·9	19·7	17·9
Zn	55·0	54·0	89·8	66·5	87·7	73·8	68·1	69·0	67·0	63·0	68·3	71·2	71·4	72·0	91·7	87·0	81·1	80·8	99·8
Zr	117	138	215	129	159	174	124	96·6	96·2	128	128	113	133	129	478	394	274	379	403
La	76·3	172	132	94·3	130	143	81·5	75·9	70·8	99·9	79·2	81·9	83·9	82·7	107	116	107	117	97·9
Ce	143	271	233	168	232	259	146	131	121	171	141	149	152	153	213	231	216	238	191
Pr	14·83	28·27	24·70	17·70	24·77	27·57	15·30	14·57	13·73	17·33	15·10	15·67	15·67	15·16	24·13	24·90	23·73	25·87	21·73
Nd	50·0	97·6	87·7	64·9	87·3	95·6	53·2	52·1	47·1	58·8	52·7	53·5	55·2	53·2	85·0	92·2	86·2	94·2	78·3
Sm	7·17	13·93	13·27	9·76	12·90	14·40	7·95	7·45	6·64	8·39	7·84	7·95	8·11	7·96	13·37	14·40	14·20	15·73	12·39
Eu	1·91	3·71	3·48	2·61	3·83	4·02	2·09	1·91	1·86	1·91	1·97	2·20	2·26	2·20	3·48	4·06	3·94	4·23	3·65
Gd	8·67	14·57	18·20	9·30	16·70	17·60	9·29	7·07	8·60	9·05	7·75	10·23	8·66	10·33	14·60	13·33	12·67	13·73	13·33
Tb	0·71	1·23	1·20	0·79	1·16	1·27	0·75	0·60	0·67	0·71	0·64	0·71	0·67	0·75	1·35	1·20	1·20	1·31	1·10
Dy	3·56	4·77	5·09	3·39	4·74	5·11	2·81	2·56	2·42	3·01	2·99	3·05	3·30	3·05	5·42	5·39	5·17	5·50	4·79
Ho	0·52	0·64	0·83	0·52	0·74	0·86	0·47	0·43	0·40	0·48	0·46	0·51	0·51	0·49	0·88	0·90	0·80	0·88	0·76
Er	1·32	1·41	2·04	1·20	1·74	1·82	0·99	0·93	0·87	1·13	1·06	1·24	1·20	1·21	2·05	1·94	1·89	2·02	2·03
Tm	0·17	0·17	0·24	0·14	0·21	0·25	0·14	0·10	0·11	0·14	0·11	0·14	0·12	0·14	0·26	0·24	0·19	0·22	0·23
Yb	1·00	1·01	1·41	0·92	1·22	1·40	0·73	0·68	0·66	0·76	0·78	0·78	0·77	0·77	1·53	1·35	0·97	1·35	1·32
Lu	0·13	0·11	0·19	0·11	0·17	0·18	0·11	0·07	0·08	0·09	0·09	0·11	0·10	0·10	0·22	0·18	0·10	0·15	0·17

Table 4: continued

	Anantapur kimberlites (1090 Ma)																		
Location:	Pipe 6 (Wajrakarur)		Pipe 7 (Venkatampalle)		Pipe 8 (Lattavaram)					Pipe 9		Pipe 10 (Chigicherla)			Pipe 11 (Chigicherla)				
Grid ref.:	15°1′28″, 77°22′10″		14°56′1″, 77°23′		14°55′25″, 77°18′11″					14°55′25″, 77°17′41″		14°31′30″, 77°17′42″			14°32′15″, 77°41′10″				
Sample no.:	P6/5	P6/1	G/P7	G/P7/1	P8/5	P8/10	P8	G/P8/1	G/P8	P9	P9/1	CH-10	CH-8	CH-5	P11/5	P11/2C	P11/2A	P11/1	P11/2
SiO_2	36·60	35·13	34·10	33·79	39·70	41·23	42·04	42·20	40·30	23·50	34·53	39·24	38·34	40·65	38·22	39·29	39·35	38·90	39·37
TiO_2	4·13	2·45	0·78	0·81	1·83	1·60	1·71	1·55	1·50	0·62	0·79	2·22	2·29	2·09	2·26	2·29	2·29	2·33	2·19
Al_2O_3	4·63	6·20	3·42	4·01	4·66	4·83	5·39	5·43	5·41	2·06	3·91	4·09	3·98	4·53	3·99	4·19	4·39	4·32	4·14
$Fe_2O_3^*$	13·98	12·52	7·78	7·92	9·79	9·31	9·28	9·02	9·07	7·37	6·38	10·82	10·82	10·28	11·39	11·66	11·67	11·61	11·52
MnO	0·19	0·21	0·13	0·14	0·14	0·14	0·22	0·14	0·14	0·11	0·10	0·16	0·16	0·14	0·16	0·17	0·16	0·16	0·16
MgO	20·74	19·54	30·17	28·50	25·16	24·39	23·07	24·16	24·52	7·99	16·16	25·38	23·95	21·13	26·58	26·70	26·01	25·84	27·13
CaO	13·32	13·55	8·33	8·87	8·48	8·92	8·75	8·66	8·54	29·31	18·55	8·75	8·67	10·35	10·13	9·49	9·80	9·89	9·18
Na_2O	0·17	1·17	0·16	0·31	0·29	0·35	0·31	0·34	0·34	0·04	0·07	0·35	0·37	0·39	0·27	0·33	0·28	0·28	0·36
K_2O	0·62	2·07	0·70	0·79	0·52	0·53	0·52	0·63	0·58	0·12	0·33	0·94	0·99	0·87	0·64	0·71	0·69	0·78	0·66
P_2O_5	0·55	0·80	0·78	0·80	0·47	0·52	0·51	0·38	0·34	0·69	0·86	0·46	0·42	0·32	0·59	0·47	0·46	0·46	0·47
LOI	4·48	5·57	12·18	12·31	7·94	7·41	7·32	7·45	7·96	27·20	17·08	6·73	9·19	8·78	4·19	4·23	4·34	4·38	4·32
Total	99·41	99·21	98·53	98·25	98·98	99·23	99·12	99·96	98·70	99·01	98·76	99·14	99·18	99·53	98·42	99·53	99·44	98·95	99·50
C.I.	1·90	1·90	1·20	1·30	1·70	1·80	2·00	1·90	1·80	0·87	2·30	1·60	1·70	2·00	1·50	1·50	1·60	1·60	1·60
Mg no.	0·72	0·73	0·87	0·86	0·81	0·82	0·81	0·82	0·82	0·65	0·81	0·80	0·79	0·78	0·80	0·80	0·79	0·79	0·80
Ba	2154	1911	4278	4919	1251	1006	920	1333	1034	2022	3652	2669	1128	1374	1788	1265	929	1184	1489
Cr	713	817	1213	1156	947	982	937	908	915	1492	1491	861	971	995	1024	1012	914	1018	999
Cs	4·06	2·53	2·19	2·54	15·2	15·87	6·26	16·87	15·73	1·96	2·83	8·35	6·87	5·18	2·53	3·04	2·8	2·96	2·8
Cu	101	88·2	41·5	46·5	62·7	53·6	82·3	53·3	63·6	46·9	89·4	145	85·1	96·8	80·1	84·8	116·9	86·9	83·1
Hf	6·23	3·30	2·77	2·85	3·46	2·95	3·40	3·62	3·18	2·25	2·38	4·83	4·31	4·51	5·21	5·15	4·39	4·56	4·99
Nb	168	202	238	264	113	109	121	108	106	249	275	110	106	100	111	109	103	109	105
Ni	474	507	1336	1199	1135	1107	1112	1070	1052	1699	1216	1295	1223	1123	1291	1274	784	1220	1324
Pb	7·63	8·02	15·27	16·47	7·02	6·91	10·3	10·73	10·7	19·1	13·53	10·9	9·95	9·68	6·9	7·21	6·09	13·43	6·75
Rb	142	200	82	88	77	79	55	83	69	13	44	146	133	75	82	93	66	97	86
Sc	27·3	23·7	13·5	17·5	10·5	11·0	9·8	9·3	6·6	18·2	12·1	19·7	14·3	11·7	15·8	15·1	23	14·1	13·9
Sr	609	933	1526	1564	614	654	709	636	592	730	1265	1033	986	641	1378	1548	1569	1379	1555
Ta	9·89	11·8	8·81	10·16	6·96	6·71	7·25	6·41	6·22	8·64	10·73	6·28	6·1	5·6	6·06	6·3	5·89	5·93	5·96
Th	13·7	19·7	31·23	33·4	10·8	10·27	12·6	10·93	10·2	35·43	27·5	13·2	10·09	13·17	12·13	12·17	8·64	10·47	11·1
U	3·33	4·00	5·00	5·47	2·67	2·39	3·37	3·33	4·85	3·41	4·38	2·97	2·84	6·10	2·42	2·24	2·1	2·11	2·28

	Anantapur kimberlites (1090 Ma)																			
Location:	Pipe 6 (Wajrakarur)		Pipe 7 (Venkatampalle)		Pipe 8 (Lattavaram)					Pipe 9		Pipe 10 (Chigicherla)			Pipe 11 (Chigicherla)				
Grid ref.:	15°1′28″, 77°22′10″		14°56′1″, 77°23′		14°55′25″, 77°18′11″					14°55′25″, 77°17′41″		14°31′30″, 77°17′42″			14°32′15″, 77°41′10″				
Sample no.:	P6/5	P6/1	G/P7	G/P7/1	P8/5	P8/10	P8	G/P8/1	G/P8	P9	P9/1	CH-10	CH-8	CH-5	P11/5	P11/2C	P11/2A	P11/1	P11/2
V	141	138	75·3	90·1	99·8	98·1	104	118	135	63·4	77·1	120	103	142	107	108	197	118	102
Y	17·5	18·7	17·7	19·9	17·1	10·4	11·3	10·6	10·2	26·0	18·0	13·3	12·3	11·5	14·3	14·4	12·4	15·0	14·0
Zn	91·1	89·2	53·9	55·7	65·2	66·1	55·4	61·6	61	46·2	52·6	99·8	74·7	63·5	80·9	79·2	69·9	82·3	78·5
Zr	246	135	123	130	133	120	134	137	124	106	111	193	176	177	211	198	168	201	196
La	112	137	212	234	72·8	71·8	74·3	67·5	69·8	253	210	86·5	84·7	77·2	88·2	87·2	86·1	85·1	84·9
Ce	206	244	355	396	133	131	141	123	126	379	337	168	163	164	170	173	161	165	164
Pr	21·37	25·83	35·67	38·17	13·97	13·67	15·03	12·87	13·40	37·50	35·40	18·60	18·37	18·23	19·00	18·93	18·30	18·67	17·77
Nd	76·0	93·0	112	127	50·2	48·0	51·8	45·6	45·6	122	117	69·3	65·3	63·9	69·7	69·8	65·3	67·9	65·4
Sm	12·30	14·33	14·50	16·57	7·62	7·39	8·17	6·76	6·83	15·83	16·83	9·76	9·47	9·82	10·23	10·93	9·77	10·87	9·78
Eu	3·31	3·89	3·77	4·18	2·15	2·09	2·37	2·03	1·97	4·23	4·12	2·73	2·61	2·55	3·02	2·67	2·49	2·61	2·73
Gd	12·40	14·20	22·20	18·70	7·85	7·44	7·68	7·31	8·98	16·50	17·27	11·27	11·60	11·27	12·80	10·37	9·76	9·97	10·06
Tb	1·10	1·27	1·12	1·23	0·67	0·67	0·75	0·64	0·71	1·30	1·27	0·82	0·82	0·81	0·97	0·97	0·79	0·80	0·79
Dy	4·65	5·16	4·69	5·73	2·95	2·89	3·15	2·76	2·59	5·70	5·14	3·64	3·42	3·34	3·80	3·90	3·51	4·02	3·78
Ho	0·77	0·83	0·73	0·83	0·44	0·43	0·49	0·44	0·44	0·93	0·83	0·57	0·52	0·51	0·60	0·64	0·54	0·63	0·59
Er	1·82	1·94	1·93	1·91	1·01	0·98	1·05	1·04	1·07	1·98	1·94	1·31	1·13	1·16	1·36	1·34	1·21	1·36	1·16
Tm	0·23	0·22	0·22	0·22	0·11	0·12	0·14	0·12	0·14	0·25	0·21	0·17	0·14	0·14	0·17	0·18	0·14	0·17	0·16
Yb	1·51	1·27	1·27	1·33	0·76	0·78	0·74	0·74	0·75	1·43	1·31	0·89	0·88	0·91	1·06	1·07	0·88	1·09	0·99
Lu	0·18	0·15	0·17	0·16	0·08	0·09	0·10	0·09	0·11	0·19	0·16	0·10	0·11	0·12	0·14	0·13	0·12	0·13	0·11

Table 4: continued

	Mahbubnagar kimberlites (1400 Ma)															
Location:	Narayanpet				Maddur				Kotakonda				Padiripahad			
Grid ref.:	16°45′4″, 77°30′2″				16°51′ 54″, 77°30′2″				16°45′50″, 77°39′2″				16°49′58″, 77°35′10″			
Sample no.:	NP	NP/5	NP/10	NP/7	MD/11	MD-7	MD/11A	MD-5	KK7A	KK11	KK4	KK10	PDF/1B	PDF/10	PDF/1A	PDF/1
SiO_2	32·69	31·74	31·94	32·50	36·62	34·90	36·72	35·99	32·46	31·89	32·23	32·26	31·91	30·76	32·19	32·02
TiO_2	5·40	5·01	5·13	5·02	4·27	4·36	4·31	4·05	3·76	3·77	3·80	3·72	4·40	4·28	4·55	4·45
Al_2O_3	3·75	4·11	4·11	4·20	4·53	4·41	4·52	4·47	3·71	3·89	3·72	3·31	3·50	3·15	3·60	3·55
$Fe_2O_3^*$	14·17	13·46	13·65	13·30	14·30	13·70	14·40	13·67	12·97	13·89	13·94	13·94	14·41	14·13	14·36	14·14
MnO	0·21	0·19	0·19	0·19	0·20	0·19	0·20	0·19	0·19	0·21	0·22	0·22	0·20	0·21	0·21	0·21
MgO	22·62	22·72	23·29	23·10	21·20	21·17	21·35	20·93	24·02	23·15	23·81	25·78	22·89	23·63	22·90	23·04
CaO	10·08	10·60	10·58	10·90	12·96	12·96	12·98	13·49	11·54	11·85	11·30	9·05	11·18	12·60	11·15	10·94
Na_2O	0·09	0·03	0·09	0·11	0·14	0·14	0·15	0·20	0·05	0·04	0·09	0·04	0·06	0·02	0·04	0·13
K_2O	1·01	0·48	0·51	0·55	0·37	0·55	0·31	0·59	0·74	0·94	0·86	1·07	1·05	0·10	1·04	1·03
P_2O_5	0·56	0·42	0·45	0·41	0·57	0·50	0·59	0·53	0·86	0·68	0·79	0·46	0·88	0·71	0·79	0·76
LOI	8·52	10·16	9·25	9·12	4·10	6·46	3·71	5·04	8·86	8·88	8·75	9·05	8·54	9·58	8·56	8·68
Total	99·10	98·92	99·19	99·40	99·26	99·34	99·24	99·15	99·16	99·19	99·51	98·90	99·02	99·17	99·39	98·95
C.I.	1·50	1·50	1·50	1·50	1·90	1·80	1·90	1·80	1·40	1·40	1·40	1·30	1·40	1·40	1·40	1·40
Mg no.	0·73	0·74	0·75	0·75	0·72	0·73	0·72	0·72	0·76	0·74	0·75	0·76	0·73	0·74	0·73	0·74
Ba	1553	1852	2932	2254	2370	1526	2370	1283	1283	1134	1108	1040	1216	292	1066	1134
Cr	969	917	959	942	898	896	897	860	1003	960	990	1045	963	825	979	944
Cs	5·23	10·97	12·03	11·3	5·82	4·81	6·26	4·65	1·48	1·44	1·29	1·21	5·1	0·57	4·97	4·99
Cu	130·2	115·4	115·8	111	134·1	124·4	140·3	132	147·8	136·5	131·9	72·3	149·8	159·2	146·7	153·7
Hf	8·05	5·82	6·9	6·09	7·78	5·04	7·73	6·11	7·12	6·3	6·33	5·19	7·51	6·48	7·44	7·53
Nb	174	153	152	141	117	106	116	104	157	153	144	145	155	147	151	150
Ni	815	789	785	773	771	768	772	780	934	910	922	963	835	919	819	840
Pb	11·67	7·12	9·5	7·44	6·66	6·02	6·74	5·4	17·13	22·23	9·15	7	10·93	4·83	10·43	10·47
Rb	110	66	74	78	116	91	112	106	90	101	93	89	89	10·9	84	83
Sc	21·2	22·8	25·9	22·3	20·8	18·8	21·4	18·4	23·0	21·9	20·6	23·9	22·9	20·6	24·5	20·7
Sr	427	565	552	607	1131	821	1312	1034	708	653	748	421	956	750	926	944
Ta	11·73	9·88	10·57	9·62	8·29	7·36	8·65	7·64	9·38	8·55	8·72	9·55	10·13	9·25	10·37	7·50
Th	14·47	12·03	13·03	12·4	10·57	6·67	11·5	9·05	16·83	14·23	12·36	12·6	13·23	10·24	13·6	10·93
U	5·32	3·17	3·18	3·09	2·7	2·44	2·73	2·56	3·56	3·37	3·96	3·05	6·26	4·23	6·10	13·43
V	217	199	200	199	269	228	266	246	268	227	256	164	167	99	157	151
Y	18·1	14·8	15·2	13·6	14·7	11·2	14·9	12·9	21·3	20·8	19·5	20·0	16·3	14·5	16·5	16·2

	Mahbubnagar kimberlites (1400 Ma)															
Location:	Narayanpet				Maddur				Kotakonda				Padiripahad			
Grid ref.:	16°45′4″, 77°30′2″				16°51′ 54″, 77°30′2″				16°45′50″, 77°39′2″				16°49′58″, 77°35′10″			
Sample no.:	NP	NP/5	NP/10	NP/7	MD/11	MD-7	MD/11A	MD-5	KK7A	KK11	KK4	KK10	PDF/1B	PDF/10	PDF/1A	PDF/1
Zn	78·6	71·7	69·4	70·4	86·4	76·8	86·2	78·2	77·5	94·7	105	62·9	77·6	59	74·8	73·5
Zr	296	241	233·7	208	302	190	298	235	293	256	260	191	321	260	292	281
La	117	100	103	93·4	70·8	66·5	70·8	61·6	121	110	116	115	107	99·8	108	108
Ce	223	192	202	184	139	129	137	122	239	215	220	222	207	190	209	206
Pr	24·97	21·23	21·57	19·70	15·53	14·43	15·30	13·67	27·53	24·50	24·10	25·57	23·03	21·23	22·97	23·07
Nd	90·8	78·3	79·7	72·4	56·1	51·8	57·1	51·8	98·8	89·5	92·3	95·2	85·3	76·1	84·6	85·2
Sm	13·60	12·47	12·47	11·90	9·16	8·49	9·57	8·84	15·77	14·37	14·12	15·90	13·46	11·90	13·16	13·31
Eu	3·82	3·19	3·71	3·19	2·67	2·44	2·84	2·38	4·47	4·01	3·89	4·11	3·65	3·35	3·77	3·78
Gd	15·93	12·03	12·13	11·60	11·97	9·90	9·72	8·37	17·33	15·63	15·09	14·63	13·07	12·50	12·03	12·22
Tb	1·16	1·01	1·12	1·01	0·97	0·90	0·86	0·82	1·50	1·31	1·27	1·23	0·99	0·99	1·12	0·92
Dy	5·12	4·17	4·57	4·05	3·94	3·35	4·19	3·77	6·12	5·71	5·72	6·14	4·29	4·13	4·83	4·45
Ho	0·80	0·63	0·68	0·61	0·65	0·53	0·64	0·61	0·94	0·92	0·90	0·85	0·71	0·66	0·70	0·70
Er	1·82	1·49	1·66	1·46	1·54	1·16	1·51	1·47	2·15	2·01	2·19	1·98	1·84	1·82	1·90	1·93
Tm	0·23	0·13	0·18	0·15	0·19	0·14	0·17	0·15	0·25	0·24	0·21	0·21	0·18	0·17	0·17	0·17
Yb	1·28	0·83	0·88	0·74	1·09	0·77	1·07	0·91	1·42	1·34	1·20	1·09	1·08	1·02	0·99	1·06
Lu	0·16	0·10	0·11	0·10	0·15	0·12	0·13	0·11	0·18	0·17	0·17	0·13	0·12	0·13	0·13	0·12

Table 4: continued

	Cuddapah lamproites (1418 Ma)							
Location:	Ramannapeta		Chelima				Zangamarajupalle	
Grid ref.:	17°03′25″, 80°7′10″		15°27′, 78°42′				14°76′ 7″, 78°88′3″	
Sample no.:	RU1	NR/1	NR/7	C5	C1-A	C1-C	ZP	ZP1
SiO_2	44·95	47·14	46·81	35·44	48·56	47·60	43·23	42·79
TiO_2	3·33	3·00	2·96	5·57	3·18	3·50	4·81	4·71
Al_2O_3	6·93	7·02	7·09	4·24	2·81	3·21	5·59	5·49
$Fe_2O_3^*$	11·82	11·58	11·69	7·21	7·08	7·96	10·42	10·38
MnO	0·17	0·15	0·16	0·09	0·07	0·05	0·12	0·11
MgO	14·40	14·09	13·99	9·07	13·13	14·12	14·25	14·79
CaO	10·29	8·51	8·72	17·21	9·36	8·21	6·14	6·01
Na_2O	0·35	0·47	0·47	0·09	0·01	0·01	0·06	0·05
K_2O	2·55	2·68	2·67	2·11	1·91	1·05	4·57	4·87
P_2O_5	0·90	0·72	0·95	1·47	1·36	0·64	1·43	1·40
LOI	3·86	3·46	3·58	15·92	12·51	12·65	8·11	7·97
Total	99·55	98·82	99·09	98·42	99·98	99·00	98·73	98·57
C.I.	3·00	3·20	3·30	3·50	3·40	3·30	2·50	2·40
Mg no.	0·68	0·68	0·67	0·68	0·76	0·75	0·70	0·71
Ba	1454	1689	1478	1327	585	588	943	928
Cr	588	716	769	629	980	1118	664	670
Cs	1·06	1·11	1·05	7·63	3·81	4·25	40·8	38·7
Cu	47	38·8	50·3	77·9	67·47	73·1	64·7	69·5
Hf	12·47	12·77	12·11	29·6	12·93	16·37	11·77	11·22
Nb	102	86	100	242	154	174	163	190
Ni	407	517	536	427	799	927	498	511
Pb	15·77	12·67	15·3	27·4	58·77	138	27·5	30·13
Rb	61	54	52	144	78	69	312	320
Sc	19·3	20·7	19·5	19·6	19·4	18·9	22·6	21·7
Sr	673	588	618	1031	699	732	964	971
Ta	5·98	5·32	5·67	12·43	8·43	10·4	7·95	7·65
Th	11·8	11·0	11·0	20·8	17·3	24·1	18·8	20·5
U	1·67	4·5	4·1	5·19	2·86	3·63	4·82	4·72
V	161·9	151	145	112	84·2	72·8	121	116
Y	20·9	21·43	21·65	40·27	20·2	24·53	27·93	36·1

	Cuddapah lamproites (1418 Ma)							
Location:	Ramannapeta		Chelima				Zangamarajupalle	
Grid ref.:	17°03′25″, 80°7′10″		15°27′, 78°42′				14°76′ 7″, 78°88′3″	
Sample no.:	RU1	NR/1	NR/7	C5	C1-A	C1-C	ZP	ZP1
Zn	129·7	121	128	87	222	301	48·6	51·2
Zr	401	450	410	1149	518	627	478	490
La	106	124	120	366	240	207	254	250
Ce	234	237	231	709	473	417	493	491
Pr	26·77	25·7	26·5	76·9	56·7	45·8	55·3	54·1
Nd	96·3	92·2	95·7	263	197	163	196	194
Sm	15·03	13·6	15·1	32·4	25·4	21·9	27·0	26·3
Eu	4·22	3·48	4·17	8·17	6·10	5·59	7·02	7·01
Gd	13·93	13·57	13·62	30·27	26·10	19·40	23·20	22·70
Tb	1·38	1·27	1·31	2·54	1·53	1·68	1·98	2·01
Dy	5·98	5·74	5·73	10·13	6·03	7·07	7·98	7·91
Ho	0·96	0·95	0·91	1·65	0·90	1·08	1·22	1·21
Er	2·21	2·23	2·08	4·05	2·06	2·46	3·11	3·09
Tm	0·26	0·26	0·26	0·55	0·26	0·30	0·34	0·32
Yb	1·59	1·77	1·60	3·15	1·48	1·66	2·04	2·01
Lu	0·19	0·22	0·20	0·40	0·19	0·18	0·26	0·26

*Total Fe is given as Fe_2O_3.
Concentrations of major oxides are in wt % and trace elements in ppm. LOI, loss on ignition; C.I., contamination index (Clement, 1982) = $(SiO_2 + Al_2O_3 + Na_2O)/(MgO + K_2O)$; Mg number = 100Mg/(Mg + Fe). Sample locations are given in the Electronic Appendix (http://www.petrology.oupjournals.org).

contents are markedly different in the Anantapur (0·34–2·33 wt %) and Mahbubnagar (0·22–0·32 wt %) kimberlites, and low compared with Nb contents in perovskites from kimberlites elsewhere. This is consistent with the bulk-rock Nb contents (see below).

LREE oxide contents range from 0·88 to 1·97 wt % in the Mahbubnagar perovskites and from 2·57 to 5·37 wt % in Anantapur perovskites. La/Sm ratios in the perovskites range from 6·5 to 8·5 and from 8 to 12·5 in the Mahbubnagar and Anantapur kimberlites, respectively. These are identical to the La/Sm ratios of the host kimberlites (see below) and confirm the significant role of perovskite in controlling the LREE contents of kimberlites.

Apatite

Apatite is a ubiquitous phase in southern Indian kimberlites and lamproites, and shows no significant variation in composition.

Carbonate

Calcite is an abundant primary and secondary phase in kimberlites, whereas lamproites are virtually devoid of primary calcite, and any carbonate is of secondary origin (Mitchell & Bergman, 1991). Calcite occurs in Pipes 7 and 9 (Anantapur). Ferroan dolomite is present in the Chelima and Zangamarajupalle lamproites, where its texture suggests that it is a secondary phase.

Rutile

Rutile is a common accessory phase in the Dharwar kimberlites, where it chiefly occurs as needle-shaped crystals in olivine. Although it is considered an uncommon mineral in lamproites (Mitchell & Bergman, 1991), rutile is a fairly abundant groundmass phase in the Chelima and Zangamarajupalle lamproites. It is relatively poor in Cr_2O_3 (<0·3 wt %) compared with rutile from the Maddur kimberlite (1·43 wt %).

WHOLE-ROCK GEOCHEMISTRY

Whole-rock chemical analyses of 69 representative samples of southern Indian Proterozoic kimberlites and lamproites are presented in Table 4. Kimberlites and lamproites incorporate varying proportions of crustal and mantle xenoliths on ascent from the mantle to the Earth's surface, and they are highly susceptible to hydrothermal alteration. It is therefore necessary to evaluate the extent of contamination and alteration in these samples before interpreting their bulk-rock compositions.

Alteration and contamination indices

Loss on ignition (LOI) values of the southern Indian kimberlites and lamproites typically range from 3·9 to 12·3 wt %; Pipe 1 (22·1 wt %), Pipe 9 (27·2 wt %) and the Chelima lamproite (14·2 wt %) have relatively high LOI as a result of the presence of secondary carbonate minerals and talc. As mentioned above, some samples are petrographically fresh (Anantapur Pipes 3, 4, 5, 7, 10 and 11, and the Maddur and Narayanpet pipes from the Mahbubnagar cluster) and these tend to have lower LOI (3·7–10 wt %). Analyses of these latter rocks provide important constraints on the effects of hydrothermal alteration, especially on highly mobile elements such as Rb and K.

We have used Clement's (1982) contamination index (C.I.) to assess the extent of crustal contamination of the samples:

$$\text{C.I.} = (SiO_2 + Al_2O_3 + Na_2O)/(MgO + K_2O).$$

This index is a measure of the proportions of clay minerals and tectosilicates relative to ferro-magnesian minerals (olivine, phlogopite), and has been widely used in assessing kimberlite and lamproite whole-rock major oxide chemistry (e.g. Mitchell, 1986; Taylor *et al.*, 1994; Beard *et al.*, 2000). Kimberlites with C.I. $<1{\cdot}4$ are generally regarded as uncontaminated. The contamination index is influenced by alteration, but also by olivine accumulation. The relatively low Ni contents of the Dharwar kimberlites, however, suggest that their contamination indices have not been significantly influenced by olivine accumulation. Anantapur Pipe 1 has relatively high SiO_2 (59·1 wt %), Al_2O_3 (7·1 wt %) and Na_2O (0·9 wt %) contents and hence a high contamination index ($\sim$5·7), which is consistent with the presence of abundant crustal xenoliths in this diatreme-facies kimberlite. The remaining Anantapur hypabyssal-facies kimberlites have C.I. values of 0·87–2·4 (Table 4). The more micaceous and non-diamondiferous Anantapur kimberlites have moderately elevated values, i.e. Pipe 2 (1·7–2·9) and Pipe 5 (1·5–1·9), whereas the rest have C.I. $\sim$1·5. Contamination indices for the non-diamondiferous Mahbubnagar kimberlites vary from 1·3 to 1·9. The Maddur kimberlite and the Cuddapah lamproites have high contamination indices (2·5–3·5) reflecting their high modal phlogopite contents (Fig. 7).

Major elements

MgO contents range from 21 to 25 wt % in the Mahbubnagar kimberlites and from 18 to 29 wt % in the Anantapur kimberlites (excluding altered rocks from Pipes 1 and 9). All of the Dharwar kimberlites show a well-defined increase in CaO and Al_2O_3 with decreasing MgO, and all have low SiO_2 contents (28–40 wt %). The $Fe_2O_3^*$ (Total Fe) range of the diamondiferous

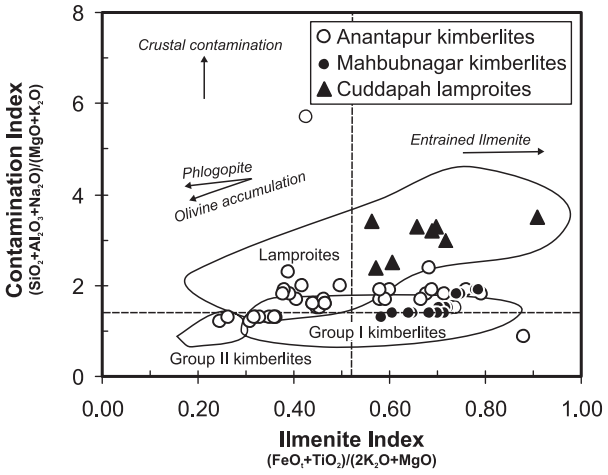

Fig. 7. Contamination index (Clement, 1982) vs Ilmenite Index (Taylor *et al.*, 1994). The fields of worldwide lamproites, Group I and II kimberlites are shown for comparison. Data sources: Gurney & Ebrahim (1973); Scott (1979); Smith *et al.* (1985); Fraser (1987); Spriggs (1988); Tainton (1992); Taylor *et al.* (1994); Greenwood *et al.* (1999).

Anantapur kimberlites (6·9–13·4 wt %) is lower than that of non-diamondiferous kimberlites from Mahbubnagar (13·5–14·8 wt %). The latter also have higher TiO_2 contents (3·8–7·2 wt %) than those from Anantapur (0·7–4·7 wt %; Fig. 8). We have used the 'Ilmenite Index' of Taylor *et al.* (1994) to identify kimberlites and lamproites that may have accumulated and/or assimilated ilmenite megacrysts and xenocrysts (Fig. 7). This index (Ilm.I.) is defined thus:

$$\text{Ilm.I.} = (FeO_t + TiO_2)/(2K_2O + MgO).$$

Anantapur kimberlites have the lowest Ilm.I.; all samples except those from Pipes 1, 2, 5, 6 and 9 have Ilm.I. <0·52 and are not believed to have accumulated or dissolved ilmenite megacrysts. All of the non-diamondiferous Mahbubnagar kimberlites have Ilm.I. ranging from 0·61 to 0·79. The K_2O contents and the K_2O/Na_2O ratios of the diamondiferous Anantapur kimberlites are in the range of 0·6–1·7 wt % and 1·8–5·5, respectively. The K_2O contents are uniformly low in the non-diamondiferous Mahbubnagar kimberlites (0·9 wt %; Fig. 8). P_2O_5 contents of the Dharwar kimberlites range from 0·5 to 1·5 wt %.

Cuddapah Basin lamproites have relatively low MgO contents (<15 wt %) and show limited major elemental compositional variation at a given MgO value. They do not lie on the extension of linear arrays defined by the kimberlites, i.e. they have a distinct chemistry (Fig. 8). A single lamproite sample (Chelima: C5 sample) plots amongst the Anantapur kimberlites in Fig. 8. This has an unusually high LOI (15·92 wt %, Table 4) and appears to have undergone extreme secondary carbonation that has resulted in a low SiO_2 (35·4 wt %) and high CaO (17·21 wt %) content. The remaining Cuddapah Basin lamproites have higher SiO_2 (42–46 wt %) than the kimberlites and are similar to other lamproite occurrences worldwide (Fig. 9). The relatively high SiO_2 (46·3 wt %), CaO (9·2 wt %) and Na_2O (0·43 wt %) contents of the Ramannapeta lamproite are consistent with its high modal proportion of groundmass phlogopite (Table 2). The lamproites have $Fe_2O_3^*$ contents that range from 7·5 to 11·4 wt % and the TiO_2 enrichment (3·1–4·8 wt %) corresponds to the Ti-rich nature of their phlogopite and, in the case of Chelima and Zangamarajupalle, to rutile abundance. They have relatively high K_2O (~2–4·8 wt %) and hence high K_2O/Na_2O ratios (>6). The low K_2O content (1–2 wt %) of the Chelima lamproite (C1-C) is probably due to its highly altered nature. All of these rocks may therefore be classified as potassic–ultrapotassic (Foley *et al.*, 1987). P_2O_5 contents of the Cuddapah Basin lamproites range from 0·64 to 1·5 wt %, with Chelima and Zangamarajupalle having the highest abundances (up to 1·1 wt % and 1·4 wt %), consistent with their relatively high modal apatite contents.

Trace elements

The variability of compatible element abundances in kimberlites is due to widely varying macrocryst/phenocryst–matrix ratios and does not necessarily reflect the composition of the liquids from which their parental melts were generated (Mitchell, 1986). Both Ni and Cr show a good positive correlation with MgO (Fig. 8) in the kimberlites. The Mahbubnagar kimberlites show lesser variation and lower abundances of Ni (772–932 ppm) and Cr (888–1000 ppm) than the Anantapur kimberlites (491–1367 ppm Ni, 765–1491 ppm Cr). Sc contents of kimberlites from Pipes 2, 5 and 6 are slightly higher (13–27 ppm) than those of the other Anantapur kimberlites (<15 ppm), consistent with their higher modal phlogopite contents (Table 2). Non-diamondiferous Mahbubnagar kimberlites show uniformly high Sc contents (~20 ppm). Vanadium in kimberlites is hosted primarily by phlogopite and spinel. The Mahbubnagar kimberlites collectively show higher V abundances (144–253 ppm) than most of the Anantapur kimberlites.

The diamondiferous Anantapur kimberlites have Zr <200 ppm and Hf between 2 and 5 ppm (Table 4). Non-diamondiferous Pipe 5 (Muligiripalle) has relatively high Zr (400–478 ppm) and Hf (>10 ppm). The non-diamondiferous Mahbubnagar kimberlites have moderate Zr (>200 ppm) and Hf (5·5–7·5 ppm) contents. The Rb contents of the Anantapur kimberlites range from 73 to 203 ppm whereas those of Mahbubnagar range from 67 to 89 ppm (Table 4). The high Nb contents of the non-diamondiferous Mahbubnagar kimberlites and non-diamondiferous Pipes 2 and 5 from the Anantapur cluster are consistent with their high modal percent of

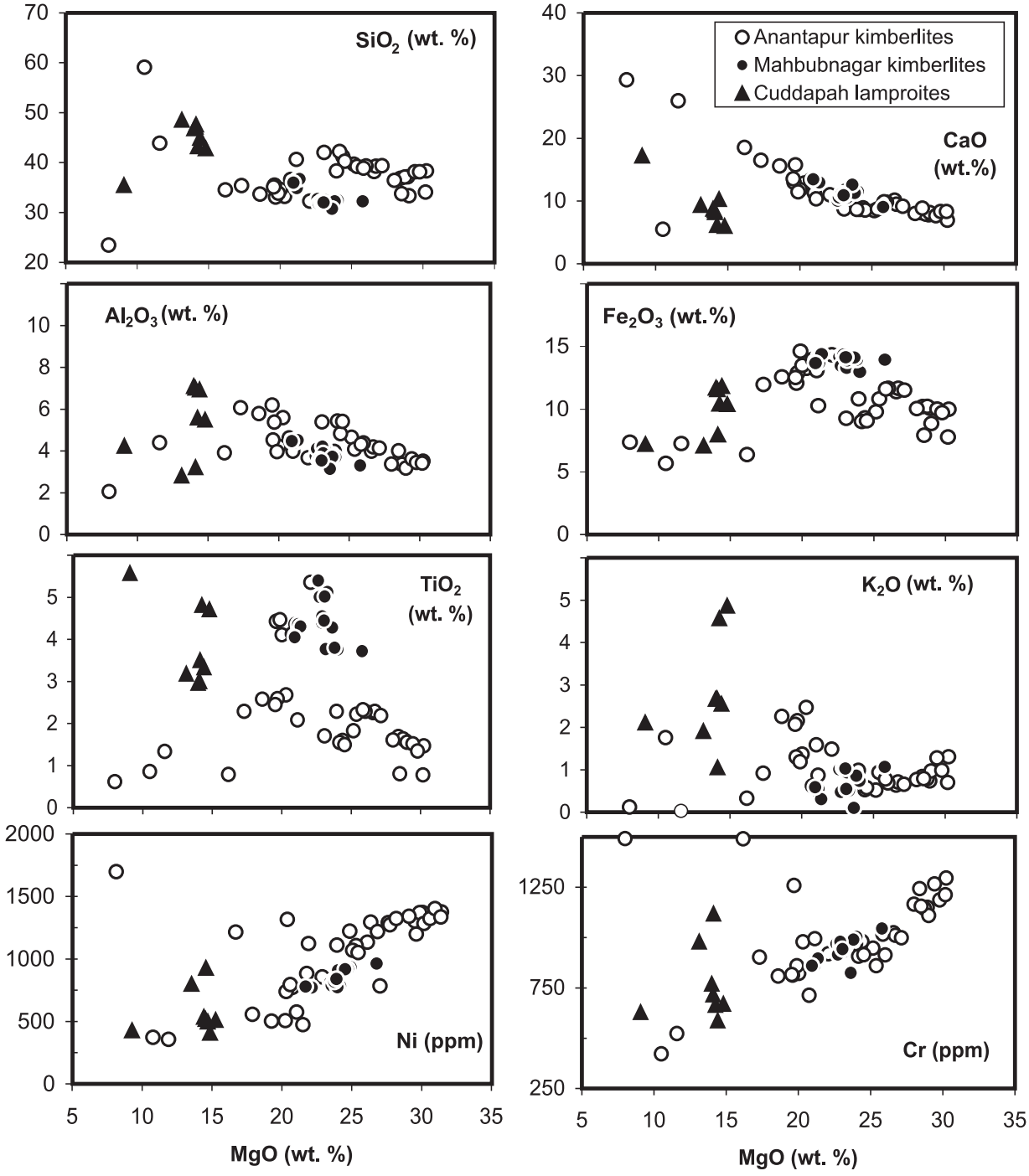

Fig. 8. Major and trace element variation diagrams for the Dharwar Craton kimberlites and Cuddapah Basin lamproites, southern India. Data are from Table 4.

perovskite. Highly diamondiferous Pipe 7 has the highest concentrations of Nb (250 ppm) for a given TiO_2 content.

In the Cuddapah lamproites, Ni (487–718 ppm) and Cr (667–909 ppm) concentrations are low relative to the Dharwar kimberlites but Sc contents are high (20 ppm). Relatively high values of Zn in the Chelima (300 ppm) and Ramannapeta (120 ppm) lamproites may reflect secondary alteration. The lamproites have higher Zr (400–1149 ppm), Hf (10–30 ppm) and Rb contents (55–316 ppm) and higher K/Rb (12–50) than the

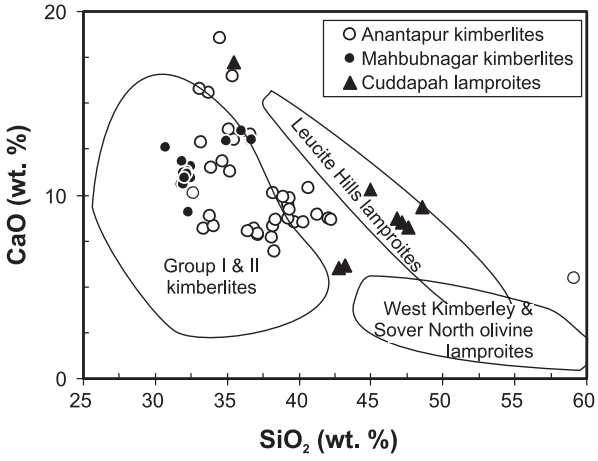

Fig. 9. Compositional range of SiO_2 and CaO for the Dharwar Craton kimberlites and Cuddapah Basin lamproites, southern India. Data sources: West Kimberley olivine lamproites and Leucite Hills lamproites, Fraser (1987); kimberlites, Gurney & Ebrahim (1973); Scott (1979); Smith *et al.* (1985); Spriggs (1988); Tainton (1992); Taylor *et al.* (1994); Greenwood *et al.* (1999).

kimberlites (2·6–10·4). The extremely high K/Rb (50) of the Ramannapeta lamproite is primarily due to its low Rb abundance (60 ppm). This lamproite has low Nb (~100 ppm) and low modal perovskite compared with the other kimberlites and lamproites.

On normalized multi-element plots the majority of the southern Indian kimberlites and lamproites exhibit troughs at K and rarely at Rb (Fig. 10). Such negative anomalies may reflect either hydrothermal alteration or the presence of residual phases in contributing melt source regions. The altered nature of Pipes 1 and 9 might be responsible for their relatively low concentrations of both K and Rb (Fig. 10), which is supported by their high LOI and high contamination indices (Table 4). Negative Rb and K anomalies were recorded in the Group I and II kimberlites of southern Africa (e.g. Smith *et al*, 1985; Mitchell, 1995) and a trough at K is seen in many mafic–potassic rocks (e.g. Gibson *et al.*, 1995). The negative Rb anomaly of the Ramannapeta lamproite could be due to either hydrothermal alteration or residual amphibole (K-richterite) in its mantle source, whereas a relative depletion in K and the lack of a corresponding negative Rb anomaly in most of the southern Indian kimberlites and lamproites suggests that the residual mantle phase may be phlogopite. Our interpretations are consistent with experimental data suggesting that phlogopite, but not richterite, is likely to be a residual phase during melting of metasomatized peridotite (Van der Laan & Foley, 1994). Separation of phlogopite macrocrysts may also produce negative troughs at K on normalized multi-element plots but we have no conclusive evidence of this process occurring in the kimberlites and lamproites of southern India (e.g. see vector for phlogopite in Fig. 7).

The positive Ti spikes of the Mahbubnagar and some non-diamondiferous Anantapur kimberlites correlate with relatively high modal amounts of perovskite. The relatively high concentrations of Ti, Nb, Fe and Hf in the non-diamondiferous kimberlites may reflect melting and/or entrainment of ilmenite from their mantle source regions. Ilmenite has a high intrinsic oxygen fugacity, which is well above the stability field of solid carbon. Negative Ti anomalies are not considered characteristic of kimberlites (Mitchell, 1995) but they are present in the Tres Ranchos (Brazil), Premier and Bellsbank (South Africa) kimberlites (see Fig. 10) and in the diamondiferous Anantapur Pipes 1, 7 and 9. Although alteration may account for Ti depletion in Pipes 1 and 9, the presence of a residual Ti-bearing phase in the source for the Pipe 7 kimberlite seems a more plausible explanation for its Ti depletion. The C.I. of this pipe (1·20–1·30, Table 4) is the lowest of the Anantapur pipes. It also has a low Ilm.I. (<0·52) suggesting little or no entrainment of ilmenite megacrysts. Negative spikes at P in some of the rocks may reflect residual apatite in their source. Pipe 7 is the most highly diamondiferous of the southern Indian kimberlites and shows considerable differences from the other pipes in its overall geochemistry.

Rare earth elements

Concentrations of REE are relatively unaffected by secondary processes, such as leaching or weathering, and their relatively high abundances mean that they are not significantly affected by contamination with crustal material. Perovskite and apatite are the main REE-bearing phases in kimberlites and lamproites (Mitchell & Bergman, 1991). The kimberlites and lamproites of southern India are strongly enriched in LREE with La abundances of 300–1100 times chondrite (Fig. 10). Pipes 7 and 9 from Anantapur, however, are more enriched in their LREE (~700 times chondrite) than the other kimberlites and have similar concentrations to the lamproites (700–1100 times chondrite). Within-pipe REE variations are in general minor and occur only in Anantapur Pipes 1 and 2. Heavy REE (HREE) abundances are low, and range from 5 to 10 times chondrite. Consequently, La/Yb ratios are high and show a wide range (from 70 to 176). All samples are enriched in LREE relative to MREE, with La/Sm ratios of 7–12 (Fig. 11).

It is well established that melts with high La/Yb ratios (60–180) can be produced by very small (<1%) degrees of partial melting of a phlogopite–garnet lherzolite (e.g. Mitchell & Brunfelt, 1975; Mitchell & Bergman, 1991; Tainton & McKenzie, 1994). Furthermore, to generate such melts with high REE abundances the mantle source must have been previously enriched (e.g. Menzies &

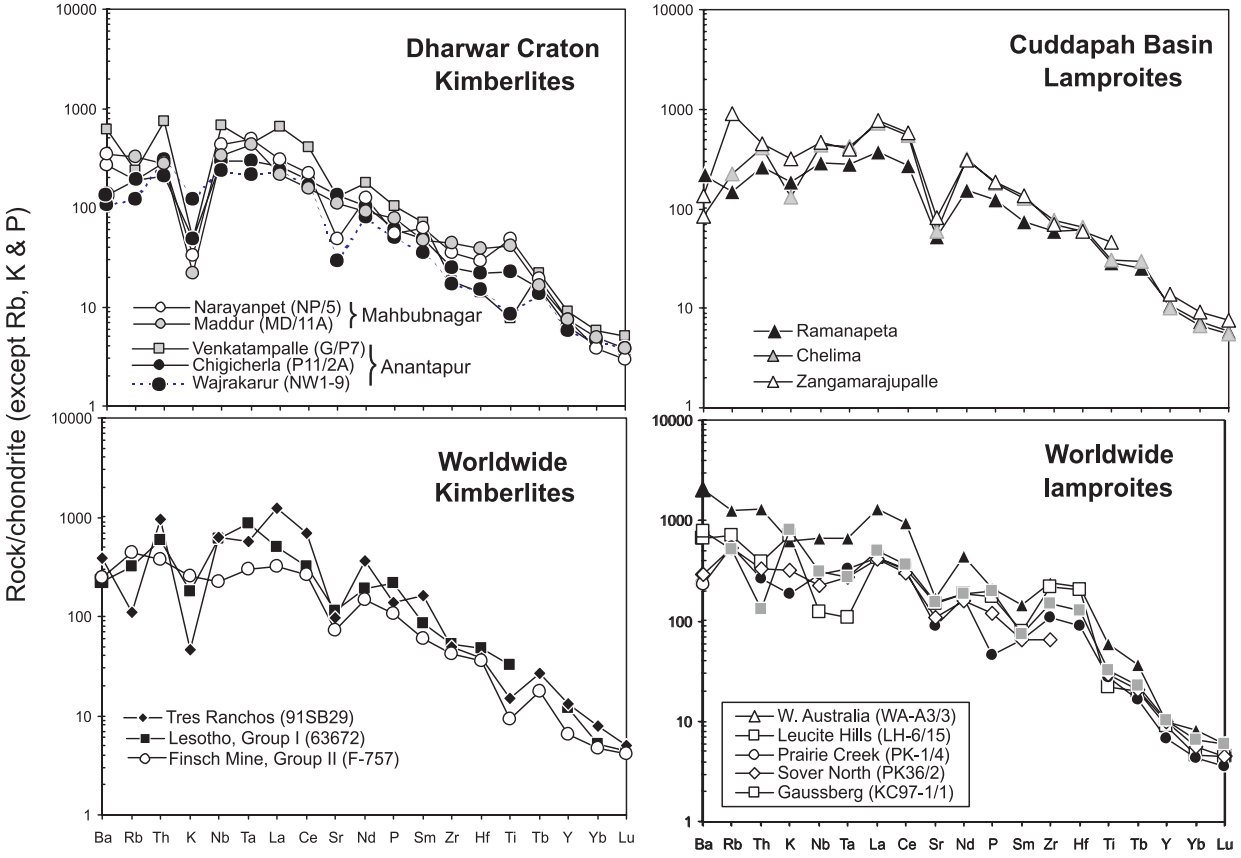

Fig. 10. Comparison of normalized multi-element patterns of the Dharwar Craton kimberlites and Cuddapah Basin lamproites with other worldwide occurrences. Normalization factors are from Thompson *et al.* (1984). Data sources: Table 4; Thompson *et al.* (1984); Fraser (1987); Tainton (1992); Gibson *et al.* (1995); Murphy *et al.* (2002).

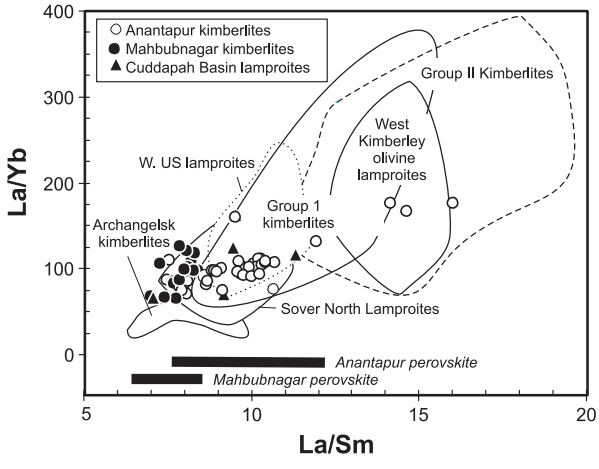

Fig. 11. Variation of La/Sm and La/Yb ratios in the Dharwar Craton kimberlites and Cuddapah Basin lamproites, southern India. The La/Sm ratios of perovskites in the Anantapur and Mahbubnagar kimberlites are shown for comparison, as are the fields of worldwide kimberlites and lamproites. Data sources: Table 4; Gurney & Ebrahim (1973); Scott (1979); Smith *et al.* (1985); Fraser (1987); Spriggs (1988); Tainton (1992); Taylor *et al.* (1994); Greenwood *et al.* (1999).

Wass, 1983; Vollmer & Norry, 1983). Evidence for metasomatism in the sub-Dharwar lithosphere comes from the REE data for the garnet lherzolite xenolith from Pipe 3 (Lattavaram), which are similar (particularly in terms of its LREE enrichment) to those for the metasomatized garnet lherzolites from southern Africa (see Nehru & Reddy, 1989).

Radiogenic isotopes

Bulk-rock Sr- and Nd-isotope determinations were undertaken on eight kimberlites and four lamproites (Table 5). These samples were selected on the basis of petrographic evidence (of minimal crustal contamination) and, where possible, low LOI (indicating restricted alteration) and high Rb contents. The measured isotopic ratios of the Anantapur kimberlites have been corrected to an emplacement age of 1090 Ma, whereas those for Mahbubnagar have been corrected to 1400 Ma. All lamproites were corrected to an emplacement age of 1418 Ma.

The diamondiferous Anantapur kimberlites have initial $^{87}Sr/^{86}Sr$ ratios ($^{87}Sr/^{86}Sr_i$) that range from 0·7021 (Pipe 2,

Table 5: Sr and Nd isotopic ratios of representative samples of Dharwar Craton kimberlites and Cuddapah Basin lamproites

	Cuddapah Basin lamproites			
	Chelima		Zangamarajupalle	Ramanapeta
	C5	C1-C	ZP	NR/1
Age (Ma):	1418	1418	1418	1418
Rb (ppm)	33·86	69·0	312·0	13·1
Sr (ppm)	368	732	964	556
$^{87}Sr/^{86}Sr_m$	0·72229	0·74462	0·74115	0·70656
$^{87}Sr/^{86}Sr_i$	0·71689	0·73904	0·72209	0·70518
εSr	19·98	51·50	27·38	3·32
Sm (ppm)	32·37	—	27·00	13·60
Nd (ppm)	263·4	—	196·3	92·2
$^{143}Nd/^{144}Nd_m$	0·51116	—	0·51122	0·51134
$^{143}Nd/^{144}Nd_i$	0·51046	—	0·51044	0·51051
εNd	−6·76	—	−7·17	−6·23

	Dharwar Craton kimberlites							
	Mahbubnagar			Anantapur				
	NP/10	MD/11A	KK7A	7/PR2	P3/5	G/P7	P8/10	P11/2C
Age (Ma):	1400	1400	1400	1090	1090	1090	1090	1090
Rb (ppm)	5·62	24·72	18·24	20·9	20·71	31·75	4·03	4·12
Sr (ppm)	360	1161	511	858	368	543	489	1335
$^{87}Sr/^{86}Sr_m$	0·70367	0·70828	0·70482	0·70319	0·70562	0·71007	0·70492	0·70378
$^{87}Sr/^{86}Sr_i$	0·70277	0·70705	0·70275	0·70209	0·70309	0·70744	0·70455	0·70364
εSr	−0·14	5·95	−0·15	−1·61	−0·20	5·99	1·88	0·59
Sm (ppm)	12·47	9·57	15·78	12·90	6·64	14·50	7·39	10·93
Nd (ppm)	78·3	57·1	98·8	87·3	47·1	112·3	48·0	69·8
$^{143}Nd/^{144}Nd_m$	0·51197	0·51200	0·51197	0·51197	0·51191	0·51182	0·51196	0·51197
$^{143}Nd/^{144}Nd_i$	0·51110	0·51106	0·51107	0·51133	0·51130	0·51125	0·51129	0·51129
εNd	4·31	3·95	4·24	1·96	0·73	0·44	1·06	1·15

Sr and Nd isotope determinations were undertaken at McMaster University. All of the samples were leached with 6 M HCl prior to dissolution. Rb and Sr concentrations are those determined for samples after leaching by atomic absorption spectrometry. Details of procedures are given in the Analytical Techniques section. Ages of emplacement were used to calculate initial ratios. Sample locations and petrographic descriptions are given in the Electronic Appendices (http://www.petrology.oupjournals.org).

Wajrakarur) to 0·7073 (Pipe 7, Venkatampalle) and correspond to εSr_i values of −1·6 to 6 (Fig. 12). These $^{87}Sr/^{86}Sr_i$ ratios agree with the few ratios previously published for the Anantapur kimberlites (Paul, 1979; Anil Kumar *et al.*, 1993). The Mahbubnagar kimberlites show a similar range from 0·7027 (Kotakonda) to 0·7070 (Maddur). The kimberlite suites have $^{143}Nd/^{144}Nd_i$ ratios ranging from 0·51105 (Kotakonda) to 0·51133 (Maddur). These correspond to εNd_i values that range from +4·3 to +4·6 for the non-diamondiferous Mahbubnagar pipes and from +0·5 to +2 for the diamondiferous Anantapur kimberlites (Fig. 12). These values, in conjunction with the $^{143}Nd/^{144}Nd_i$ ratios from Basu & Tatsumato (1979), show that all of the Eastern Dharwar Craton kimberlites have initial Nd isotopic signatures higher than Bulk Earth.

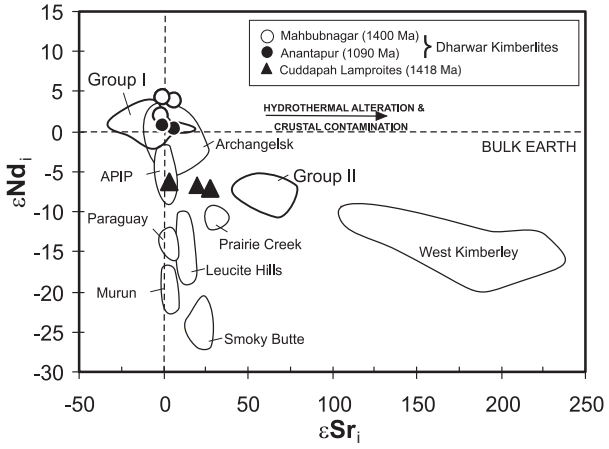

Fig. 12. εSr_i vs εNd_i for the Dharwar Craton kimberlites and Cuddapah Basin lamproites, southern India. APIP is the field for mafic potassic igneous rocks from the Alto Paranaíba Igneous Province, Brazil. Data sources are Table 5 and those given by Gibson *et al.* (1995) and Mahotkin *et al.* (2000).

The Cuddapah lamproites have relatively high $^{87}Sr/^{86}Sr_i$ (from 0·7059, Ramannapeta, to 0·7218, Zangamarajupalle) that correspond to εSr_i of 3–52. Two samples of the Chelima lamproites have very high $^{87}Sr/^{86}Sr_i$ ratios (0·7168 and 0·7390); these may reflect the presence of abundant secondary carbonate. Crawford & Compston (1973) also recorded high $^{87}Sr/^{86}Sr_m$ (0·7286) for the Chelima lamproite. The high $^{87}Sr/^{86}Sr_i$ (0·7218) for the Zangamarajupalle lamproite may similarly be due to secondary alteration. We are therefore cautious about interpreting the petrogenetic significance of these ratios. The lamproites have $^{143}Nd/^{144}Nd_i$ ratios significantly lower than those of the kimberlites, with εNd_i ranging from −7·3 to −8·3 (Table 5). The lamproites appear to be predominantly derived from melt source regions with lower time-integrated Sm/Nd ratios than Bulk Earth. The $^{87}Sr/^{86}Sr_i$ ratios do not show a systematic variation with $^{143}Nd/^{144}Nd_i$, suggesting that these two isotope systems are decoupled. This is almost certainly caused by the mobilization of Sr during hydrothermal alteration.

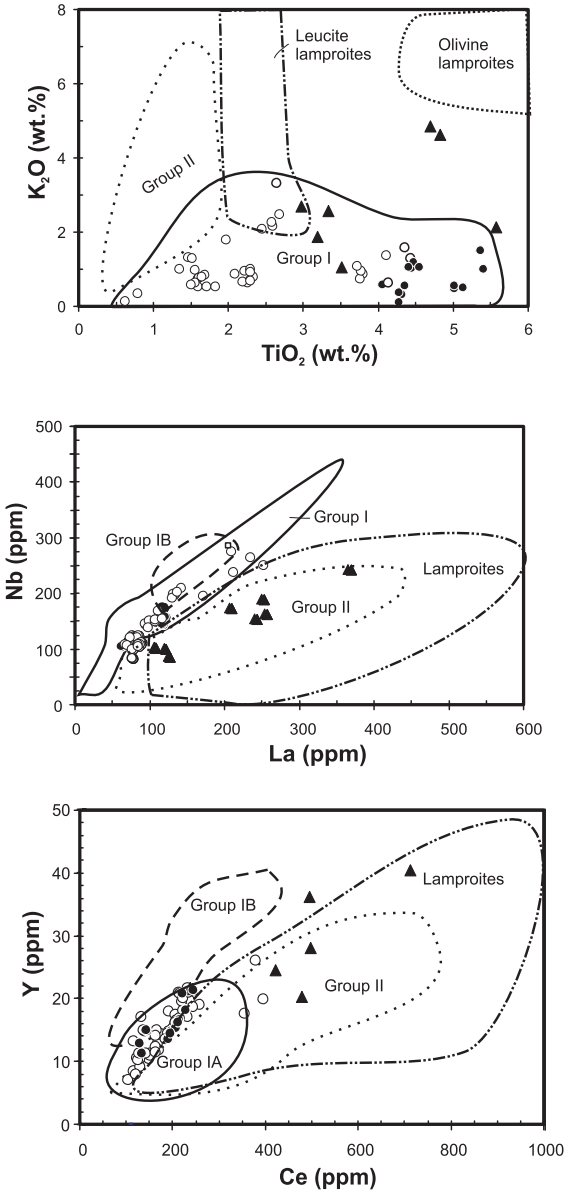

Fig. 13. Plots of TiO_2 vs K_2O, La vs Nb and Ce vs Y for Dharwar Craton kimberlites and Cuddapah Basin lamproites, southern India. Data sources: Table 4; Gurney & Ebrahim (1973); Scott (1979); Smith *et al.* (1985); Fraser (1987); Spriggs (1988); Tainton (1992); Taylor *et al.* (1994); Greenwood *et al.* (1999). Symbols are the same as in Fig. 11.

COMPARISON WITH WORLDWIDE OCCURRENCES

The Dharwar kimberlites are mica-rich and petrographically resemble the phlogopite-bearing kimberlites from the USA. The high TiO_2 and low K_2O contents, low La/Nb (0·6–0·9) and Ce/Y ratios (7–20) of both the diamondiferous Anantapur and non-diamondiferous Mahbubnagar kimberlites are similar to those of Group IA 'on-craton' kimberlites from southern Africa (Fig. 13). They are less rich in LREE than Group II South African kimberlites but have higher incompatible element abundances than the Proterozoic Premier kimberlite (Group I) of South Africa (McDonald *et al.*, 1995). The εNd_i values of the Anantapur and Mahbubnagar kimberlites are similar to those of Group I kimberlites from southern Africa (Smith, 1983), North America (Alibert & Albarède, 1988) and Greenland (Nelson, 1989).

The Maddur kimberlite from the Mahbubnagar cluster and Pipe 11 from the Anantapur cluster show a small Sr dip on normalized multi-element plots (Fig. 10), a feature that is common in kimberlites and lamproites worldwide. This can be attributed either to the presence of residual

clinopyroxene (Smith *et al.*, 1985) or residual phosphate (Mitchell, 1995) in the mantle source, or to depletion of the mantle source in Sr during a previous phase of melt extraction (Tainton & McKenzie 1994). The REE plots do not show any apparent depletion in MREE (Eu to Ho) and lack the downward concave shape that is characteristic of some other Gondwanaland kimberlites, e.g. the Aries kimberlite of Western Australia (Edwards *et al.*, 1992) and the Koidu kimberlite of West Africa (Taylor *et al.*, 1994).

The Cuddapah Basin lamproites appear to be less rich in K_2O than other olivine lamproites (West Kimberley and Smoky Butte) but have contents comparable with those of lamproites from the Leucite Hills and Prairie Creek (Fig. 13). They have relatively high La/Nb (1–1·5) and variable Ce/Y ratios (10–27) that are similar to lamproites worldwide (e.g. Western Australia; western USA; Sover North, South Africa). On normalized multi-element plots (Fig. 10), the Cuddapah lamproites lack the peaks at Zr and Hf that characterize some other worldwide lamproites (e.g. those from Western Australia and the western USA). The Cuddapah lamproites have slightly higher Nd isotopic ratios than lamproites from Western Australia (McCulloch *et al.*, 1983; Jaques *et al.*, 1989) and Prairie Creek (Arkansas, USA; Fraser *et al.*, 1985) but similar ratios to mafic potassic–ultrapotassic rocks from the Alto Paranaíba Province, Brazil (Gibson *et al.*, 1995) and Italy (Hawkesworth & Vollmer, 1979).

PETROGENESIS

The compositions of mafic potassic–ultrapotassic magmas can be used to investigate the relative contributions of asthenosphere- and lithosphere-derived melts and to probe compositional variations in the sub-continental lithospheric mantle (Gibson *et al.*, 1995, 1996). Studies over the last decade have suggested that Group I and II southern African kimberlites and lamproites are genetically distinct and that their parental melts were derived from different source regions (e.g. Mitchell & Bergman, 1991; Mitchell, 1995). The close spatial and temporal association of kimberlites and lamproites in southern India provides an opportunity to test the extent to which these models and observations hold in other portions of the Gondwana supercontinent.

Role of crustal contamination

Southern Indian kimberlites and lamproites have much higher abundances of incompatible trace elements such as Sr (550–1526 ppm), Nb (80–250 ppm) and Zr (180–600 ppm) than the continental crust. All of the studied rocks have Mg/(Mg + Fe) $>0{\cdot}69$ and high Ni contents (>500 ppm), which are indicative of the 'primitive' nature of the magmas. Furthermore, the major oxide compositions of these rocks show low abundances of Al_2O_3 (<10 wt %) and Na_2O ($<0{\cdot}5$ wt %) that cannot be accounted for by crustal contamination. The granitic rocks through which the kimberlites of the Eastern Dharwar Craton have been emplaced have relatively low LREE/HREE ratios (La/Yb = 30; Divakara Rao *et al.*, 1994). The absence of positive Eu anomalies and the low HREE and Y contents of the samples provide further additional evidence against significant crustal contamination. Thus, it can be concluded that variation in the Nd-isotopic signature of the kimberlites and lamproites is not simply due to crustal contamination, but reflects that of their contributing mantle source regions.

Source enrichment and mantle heterogeneity

Mantle metasomatism is typically attributed to either (1) fluids or melts generated by subduction processes (e.g. Peacock, 1990; Maury *et al.*, 1992; Murphy *et al.*, 2002), or (2) volatile- and K-rich, low-viscosity melts that leak continuously to semi-continuously from the asthenosphere and accumulate in the overlying lithosphere (e.g. McKenzie, 1989; Gibson *et al.*, 1995; Wilson *et al.*, 1995). The nature of the metasomatizing agent may vary widely from silicate to carbonate melts rich in CO_2 and H_2O (e.g. Wyllie, 1987; Wallace & Green, 1988), to Na metasomatism derived by peridotite slab–melt interaction (e.g. Takahashi, 1988; Kepezhinskas *et al.*, 1995). The composition of these metasomatic melts is believed to change continuously as they percolate through the mantle from their source regions (Navon & Stolper, 1987). Kimberlite melt may also form an important metasomatizing agent (Kinny & Dawson, 1992), and Tainton & McKenzie (1994) have suggested that phlogopite and K-richterite-bearing peridotites may have been generated by infiltration of a metasomatic melt with a composition similar to that of kimberlites.

Normalized multi-element plots (Fig. 10) for kimberlites and lamproites of southern India do not show any subduction-related characteristics, such as large negative anomalies at Ta, Nb and Ti, and we therefore attribute the source enrichment to metasomatizing melts derived from the convecting mantle. McKenzie (1989) proposed that small-melt fractions—enriched in K_2O, incompatible elements and volatiles—have the ability to migrate continuously or semi-continuously from the asthenosphere and invade the sub-continental lithospheric mantle. He suggested that these melts would freeze in the lithosphere where the ambient temperature was below their solidus and they would therefore be concentrated in thin zones over a wide range of depths. McKenzie (1989) pointed out that this process could continue over a long period of time, resulting in substantial volumes of frozen melt accumulating in the mechanical boundary layer as

veins, dykes or sills. Their compositions would depend on the contents of CO_2 and H_2O but strongly resemble those of kimberlites, lamproites and carbonatites. Remelting of these modified layers by heating (mantle plume) or by extension (decompression melting) can lead to the generation of potassic–ultrapotassic rock types, such as kimberlites and lamproites, and long-term storage of these areas result in enriched mantle.

Experimental studies on the liquidus compositions of lamproites and other ultrapotassic rocks suggest that their enriched source regions melted under H_2O-rich, reducing conditions (e.g. Foley, 1988, 1992, 1993; Mitchell & Bergman, 1991) in contrast to the CO_2-rich nature of the kimberlite source regions (e.g. Canil & Scarfe, 1990; Edgar & Charbonneau, 1993; Girnis *et al.*, 1995). Hence, their observed petrological and compositional differences are attributed to variations in the content and nature of volatiles in their source regions. The presence of accessory phases in vein assemblages, rich in incompatible elements, was suggested to be essential for the generation of lamproites and other ultrapotassic rocks (Becker *et al.*, 1999). A lamproite-like trace element pattern can result from melting of a veined assemblage if both apatite and a titanate mineral are present in addition to diopside, phlogopite and K-richterite; however, the concentrations of these phases must be small (Edgar & Mitchell, 1997).

There is considerable debate as to the role of the convecting mantle in kimberlite genesis. The presence of syngenetic inclusions of majoritic garnets within diamonds (Moore *et al.*, 1991) and ultra-deep (>400 km) xenoliths in some southern African kimberlites with ocean-island basalt (OIB)-like isotopic signatures, i.e. Group I kimberlites, led some workers to suggest that they are convecting mantle melts derived from a 'transition zone' source (Ringwood *et al.*, 1992), or even from the core–mantle boundary (Haggerty, 1994). Invoking similar criteria, some of the kimberlites with Group I type isotopic signatures from the Eastern Dharwar Craton have been suggested to be products derived from partial melting of sources in the 'transition zone' (Murthy *et al.*, 1997). In contrast, Tainton & McKenzie (1994) suggested that Group I and II kimberlites and lamproites are all predominantly derived from lithospheric mantle sources and that the difference in isotopic compositions requires that the source enrichment occurred at different times but not necessarily by different processes.

The isotopic systematics of southern Indian kimberlites and lamproites demonstrate the existence of variably enriched source regions beneath the intracratonic Cuddapah Basin and Eastern Dharwar Craton. The $^{143}Nd/^{144}Nd$ ratios of the Cuddapah lamproites require that their predominant contributing mantle source region(s) was isolated from the convecting mantle for a significant period of time, prior to their emplacement. Even though the Ramannapeta lamproite differs from the Chelima and Zangamarajupalle lamproites in terms of mineralogy and geochemistry, it has a similar Nd isotopic composition (εNd_i of $-6{\cdot}4$ to $-8{\cdot}29$). Although we cannot rule out a small melt contribution from the convecting mantle, the predominant melt source of the lamproites appears to have resided within the mechanical boundary layer of the lithospheric mantle (see below). The positive εNd_i values ($\sim$4) of the non-diamondiferous Mahbubnagar pipes would have been only slightly less than the depleted upper mantle at 1400 Ma ($\varepsilon Nd = 6$; e.g. McCulloch & Bennett, 1994). This, combined with the high La/Sm ratios (6·9–8·6) of the kimberlites, suggests that their mantle source regions were enriched by small-fraction melts, derived from the depleted upper mantle, shortly prior to final melt generation. The slightly lower εNd_i values (1·15–0·4) of the diamondiferous Anantapur kimberlites (and also the non-diamondiferous Padiripahad kimberlite from the Mahbubnagar cluster) correspond to the high macrocryst/phenocryst ratio (Table 2) and high Ni contents (Fig. 8) in these samples. We suggest that these kimberlites contain a greater proportion of entrained sub-continental lithospheric mantle peridotite than the Mahbubnagar kimberlites.

REE inversion modelling

We have used the REE inversion program (INVMEL) developed by McKenzie & O'Nions (1991) to model the melt distribution with depth that may have been responsible for the observed REE patterns in the Dharwar kimberlites and Cuddapah lamproites. The inversion technique uses the REE abundances and the slope (La/Yb) of the normalized pattern to constrain the melt distribution with depth, given an assumed source composition.

Xenolith data from the Dharwar Craton kimberlites are sparse, but some are similar to the 'depleted' garnet peridotite xenoliths entrained by southern African kimberlites (Ganguly & Bhattacharya, 1987; Nehru & Reddy, 1989). Therefore, we adopted as a source composition a garnet peridotite with 70% olivine, 22% orthopyroxene, 3% clinopyroxene and 5% garnet, phlogopite and apatite, corresponding to the composition of depleted garnet phlogopite peridotite xenoliths from the Kaapvaal craton (Erlank *et al.*, 1987). In addition, chrome-spinel was added to the lherzolite source, and a correction was made to Ni to remove the effects of olivine xenocrysts (see Tainton & McKenzie, 1994).

Modelled REE concentrations are sensitive to the amount of melting and the depth at which it takes place. The amount of melting is important as it determines the extent to which phases (e.g. garnet, clinopyroxene) remain in the residue, and the depth of melting also influences the source mineralogy. Tainton

& McKenzie (1994) investigated inversion models for Group I and II kimberlites from the Kaapvaal craton and the Argyle lamproite of Western Australia, and suggested that the observed REE patterns required three stages of melting: (1) depletion of the peridotite source by extraction of ~20% melt in the garnet stability field; (2) metasomatic enrichment with a MORB type melt; (3) small-fraction melting of this enriched harzburgite source. The extensive initial melting event is required to produce the observed low concentrations of HREE in kimberlites and lamproites. Subsequent metasomatic enrichment is required to produce the observed LREE abundances.

We inverted the REE concentrations of the Dharwar kimberlites and Cuddapah lamproites using similar parameters to test whether the Tainton & McKenzie model holds good for these samples. We used the entire dataset for hypabyssal-facies kimberlites and lamproites from southern India (Table 4) in our inversion models.

Because most kimberlites are hybrid rocks, containing a significant proportion of entrained lithospheric material, interpretation of the primary magma compositions from bulk-rock analyses must be treated with caution. This is especially the case for the Anantapur kimberlites that have a high olivine macrocryst/phenocryst ratio. However, as the bulk-rock LREE/MREE ratios of the kimberlites are comparable with those in perovskites, which occur as an abundant euhedral early-crystallizing groundmass phase (Fig. 11), we suggest that these ratios are representative of those in the primary magma. This suggestion is consistent with previous studies of the REE contents of perovskite that have demonstrated that the whole-rock REE abundances in kimberlites and lamproites correspond primarily to the modal amounts of this mineral rather than any other phase (e.g. Jones & Wyllie, 1984; Mitchell & Reed, 1988; Mitchell & Steele, 1992).

The fractionated HREE ratios (e.g. $[Ho/Lu]_n = 2{\cdot}5–5$) of the Dharwar Craton kimberlites and Cuddapah Basin lamproites imply that partial melting occurred in the presence of garnet. As melting takes place entirely in the garnet stability region, the depth to the top of the melting column cannot be predicted. However, as some of the kimberlites contain diamond we have placed the top of the melting column at 150 km. This is the depth of intersection of the diamond–graphite transition with the cratonic geotherm (see below). Anand *et al.* (2003) estimated that the thickness of the lithosphere beneath the intracratonic Cuddapah Basin was ~145 km prior to extension and we have used this as a maximum depth in our lamproite models.

The calculated REE abundances fit the observed values (Fig. 14) and the predicted amounts of mantle source depletion and enrichment are almost indistinguishable. These values, together with the calculated major element composition of the source, are summarized in Table 6. The difference between observed and calculated REE concentrations is less than twice the SD in all cases and hence is not significant. The amount of source depletion for the kimberlites and lamproites ranges from 18 to 28% over a depth range of 68–89 km. The proportion of metasomatic melt enrichment varies from 2 to 4% for the majority of Anantapur and Mahbubnagar kimberlites, and from 6 to 7% for highly diamondiferous Pipe 7 (Venkatampalle) and Pipe 9 (Lattavaram). Metasomatic melt enrichment of the lamproite mantle source region ranges from 4% (Ramannapeta) to 8% (Chelima and Zangamarajupalle) and is indistinguishable from that of the kimberlites. Increasing the degree of enrichment by metasomatic melt addition results in a poorer fit to the HREE data, whereas decreasing enrichment worsens the fit for LREE. The amounts of initial melt depletion and subsequent enrichment estimated for the mantle source regions of the southern Indian kimberlites and lamproites are similar to those for southern African kimberlites (Table 6).

The model that best fits the REE data does not, however, fully account for the observed concentrations of some trace elements (Fig. 14). This may be partly due to limitations in our assumptions regarding partition coefficient data. Nevertheless, some deductions made from these plots may provide additional information about the nature of the source. With the exception of non-diamondiferous Pipe 5 (Muligiripalle), the observed concentrations of K are low and suggest either the presence of residual phlogopite in the source, or hydrothermal alteration. Observed concentrations of Zr and Hf are lower than the predicted values for highly diamondiferous Pipes 7 and 9; this may be due to the presence of residual zircon in the source region. Concentrations of high field strength elements (Nb, Ta and Ti) in the kimberlites are generally underestimated by the model and this together with the high Ilm.I. (see above) suggests that a titanate phase may have been present in their melt source regions. Sr concentrations are overestimated and the lower Sr in all of the Dharwar kimberlite pipes may be attributed to: (1) the involvement of a carbonate phase; (2) errors in the assumed partition coefficient (Tainton & McKenzie, 1994); or (3) extensive depletion of a calcium-bearing phase in the melt source region. Alteration by secondary carbonation (as in the case of lamproites) may lead to elevated Sr concentrations in the calculated compositions.

We consider that minor discrepancies between predicted and observed models, as discussed above, are not due to the assumptions in our modelling but are source related. For example, the low observed K values compared with the melting models can be attributed to phlogopite; the REE partition coefficients for both phlogopite (and also K-richterite) are considerably smaller than those for diopside in the nodules and therefore the influence of

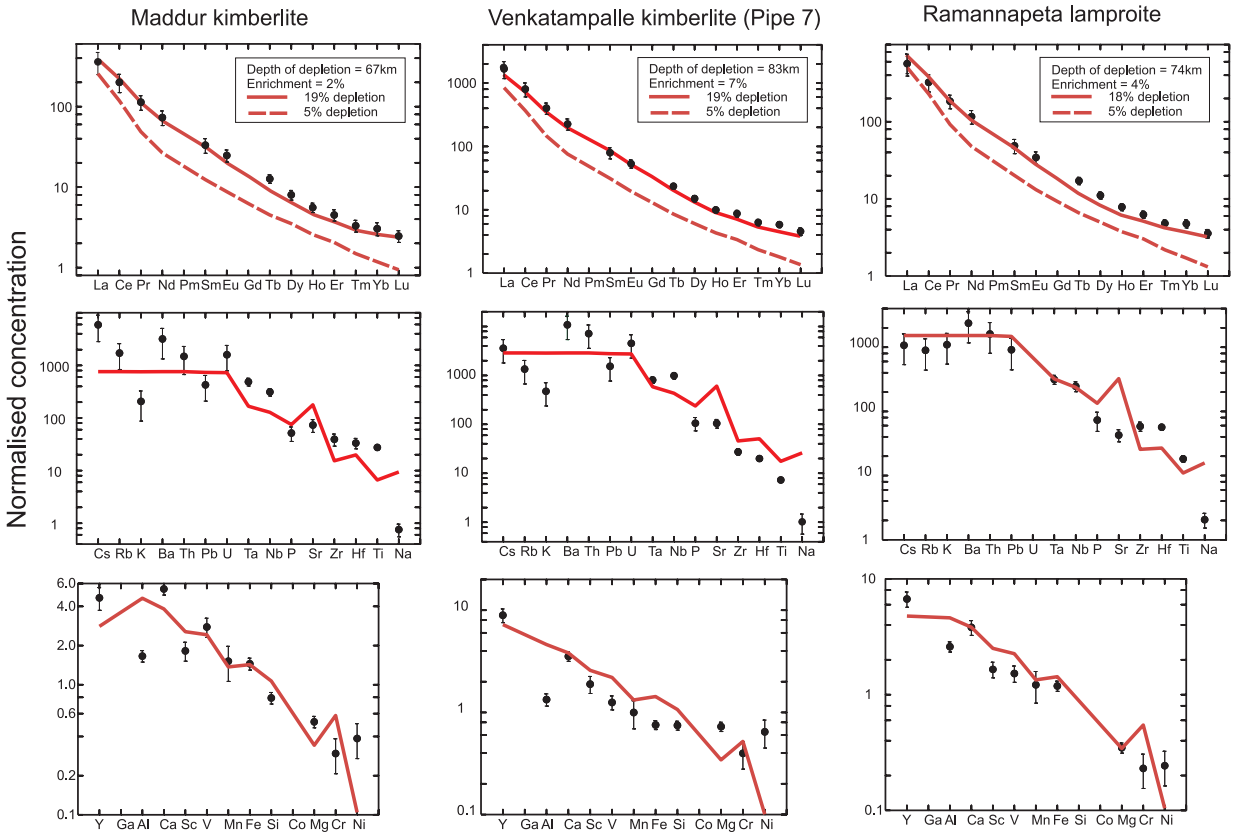

Fig. 14. REE and other trace element concentrations normalized with respect to MORB source (McKenzie & O'Nions, 1991) for Dharwar Craton kimberlites and Cuddapah Basin lamproites, southern India. ●, mean observed concentration ratios; the error bars correspond to 1 SD. The amount of depletion as well as the metasomatic enrichment required to generate the observed REE distributions are also shown at the top in all REE plots.

residual phlogopite on the REE concentrations in the melt can be neglected (Erlank *et al.*, 1987). Likewise, the possibility that the melt that metasomatized the source could have been carbonatitic, rather than silicic, in nature can also be ruled out as (1) kimberlite magmas and metasomatic melts are dominantly silicic, and carbonate would have only a modest effect on bulk-partition coefficients (see Harte, 1983), and (2) extensive depletion of the source, followed by enrichment, is still required to model the HREE concentrations in kimberlites or lamproites even if the partition coefficients for pure carbonatite are used (Tainton & McKenzie, 1994).

Extensive melting (~20%) of the source to form a harzburgite is a prerequisite for the generation of kimberlites and lamproites of the Eastern Dharwar Craton. Evidence for at least one episode of extensive melting beneath the Eastern Dharwar Craton during the Archaean and Early Proterozoic is provided by the presence of komatiites and metavolcanics in the greenstone belts (Rajamani *et al.*, 1985, 1989; Mallikharjuna Rao *et al.*, 1995). Tainton & McKenzie (1994) showed that the melt distribution curve obtained from the REE inversion of a komatiite, but not a tholeiite, can satisfy the extraction of ~20% melt from a region in which garnet is stable. They also calculated that komatiitic melting results in the thickening of the lithosphere by a factor of two, thereby placing the depleted source well within the graphite–diamond transition (i.e. 150 km). Experimental studies have also highlighted the importance of a harzburgite mantle source for lamproite genesis (e.g. Foley *et al.*, 1987; Jaques *et al.*, 1989; Mitchell & Bergman, 1991).

GEODYNAMIC MODEL FOR THE PROTEROZOIC DHARWAR KIMBERLITES AND CUDDAPAH LAMPROITES

Mantle plumes have been widely invoked in the genesis of kimberlites and lamproites, especially for those of Mesozoic age (e.g. Crough *et al.*, 1980; England & Houseman, 1984). Heat conducted from the mantle plumes, or advected by plume-derived small-fraction melts, is believed to have caused melting of the overlying metasomatized lithospheric mantle and generated the kimberlites and lamproites. The role of mantle plumes

Table 6: Source rock major oxide compositions (wt %) of southern Indian kimberlites and lamproites calculated from REE inversion using the program INVMEL (McKenzie & O'Nions, 1991)

	mg-no.	cr-no.	SiO_2	TiO_2	Al_2O_3	CaO	Na_2O	K_2O	Depletion (%)	Depth (km)	Enrichment (%)
Dharwar Craton kimberlites											
Anantapur cluster											
Pipe 2 (Lattavaram)	92·6	42·7	44·50	0·06	0·35	0·26	0·06	0·02	20	79	3
Pipe 3 (Lattavaram)	91·9	43·7	44·64	0·07	0·35	0·41	0·06	0·02	23	71	3
Pipe 4 (Lattavaram)	91·5	29·6	44·80	0·09	0·65	0·83	0·09	0·03	20	71	4
Pipe 5 (Muligiripalle)	91·8	40·8	44·70	0·07	0·41	0·64	0·06	0·02	21	71	3
Pipe 6 (Wajrakarur)	91·6	34·8	44·70	0·07	0·51	0·74	0·07	0·02	20	70	3
Pipe 7 (Venkatampalle)	91·6	21·5	44·90	0·15	0·94	1·01	0·15	0·04	19	83	7
Pipe 8 (Lattavaram)	91·4	26·5	44·70	0·07	0·77	0·95	0·07	0·02	18	69	3
Pipe 9 (Lattavaram)	92·3	26·4	44·80	0·13	0·70	0·52	0·12	0·04	28	85	6
Pipe 10 (Chigicherla)	91·6	34·8	44·70	0·07	0·51	0·74	0·07	0·02	20	70	3
Pipe 11 (Chigicherla)	91·6	34·8	44·70	0·07	0·51	0·74	0·07	0·02	20	70	3
Mahbubnagar cluster											
Maddur	91·6	36·6	44·70	0·05	0·48	0·74	0·05	0·01	19	67	2
Kotakonda	91·8	36·6	44·80	0·09	0·47	0·41	0·64	0·09	22	73	4
Narayanpet	91·5	31·1	44·70	0·07	0·61	0·83	0·07	0·02	19	68	3
Padiripahad	91·6	35·6	44·70	0·07	0·50	0·73	0·07	0·02	20	69	3
Cuddapah Basin lamproites											
Chelima	91·5	18·1	45·10	0·17	1·15	1·15	0·17	0·05	22	89	8
Ramannapata	91·5	24·7	44·80	0·09	0·83	0·97	0·09	0·03	19	74	4
Zangamarajupalle	91·8	21·1	45·10	0·17	0·93	0·85	0·17	0·05	25	89	8
Comparison with other kimberlites and lamproites (Tainton & McKenzie, 1994)											
Bellsbank (Group II kimberlite)	91·8	28	44·90	0·15	0·80	0·8	0·15	0·04	24	85	7
Finsch (Group II kimberlite)	91·0	14	45·00	0·18	1·80	1·7	0·17	0·05	17	100	8
Kimberley & Lesotho											
(Group I kimberlite)	91·3	17	45·00	0·11	1·50	1·5	0·11	0·05	20	85	8
Sover North lamproite	91·1	16	45·00	0·21	1·60	1·5	0·21	0·06	20	90	10

Best-fit REE concentrations were produced by a three-stage model. This involves an initial melt depletion event (18–25%) between 67 and 89 km. This harzburgite source was then enriched by small-degree MORB source melts generated by 0·3–0·8% melting in the garnet stability field (see text for more details).

in the genesis of Proterozoic kimberlites is poorly constrained. There is, however, considerable evidence for the role of mantle plumes in the genesis of Proterozoic basalts (e.g. LeCheminant & Heaman, 1989) and Archaean komatiites (Abbott, 1996; Tomlinson *et al.*, 1998; Gibson, 2002) but each of these examples involves relatively large-degree melting of the convecting mantle. To further understand the petrogenesis of the Dharwar kimberlites and the Cuddapah lamproites we have attempted to reconstruct the Proterozoic geothermal gradient (Fig. 15) using the following information.

(1) The cooling Earth models of Turcotte & Schubert (1982) and Richter (1988) predict that the potential temperature of the convecting mantle at the time of genesis of the Dharwar kimberlites and Cuddapah lamproites would have been ~1400°C. We have assumed an adiabatic gradient of 0·6°C/kbar (McKenzie & Bickle, 1988).

(2) Previous studies of garnet lherzolite and harzburgite xenoliths from the Anantapur kimberlites (Pipe 3) have reported the compositions of equilibrium phases (Ganguly & Bhattacharya, 1987; Nehru & Reddy, 1989). We have recalculated equilibration temperatures for these xenoliths using the geothermometer of Harley (1984) for the garnet harzburgites and those of Bertrand & Mercier (1985) and Brey & Kohler (1990) for the

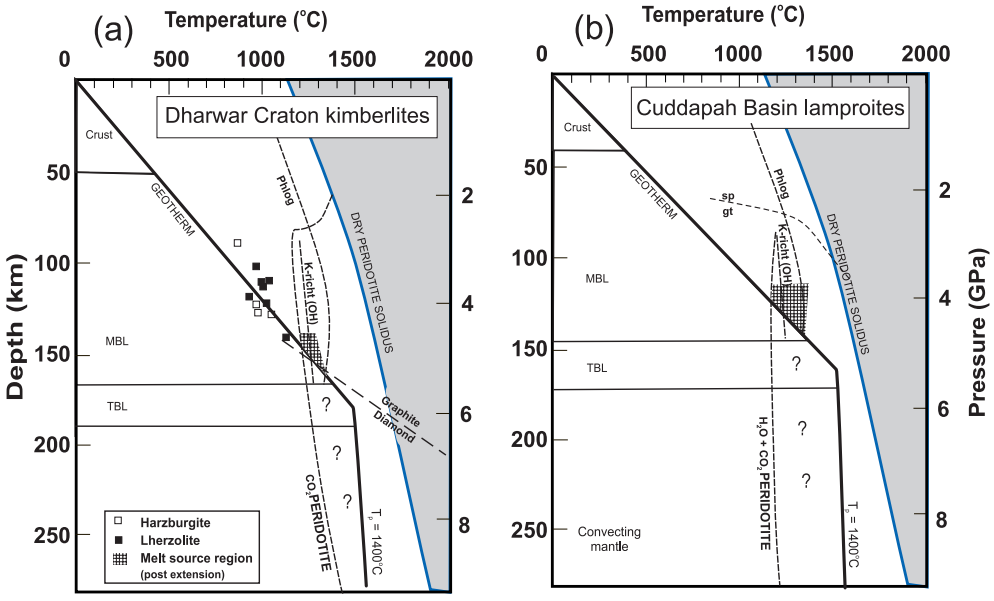

Fig. 15. Thermal structure of the southern Indian lithosphere during the Mid-Proterozoic. The geothermal gradients and appropriate solidi and stability fields at the time of kimberlite and lamproite genesis are shown in (a) and (b), respectively (see text for discussion). Dry peridotite solidus is from Hirschmann (2000), CO_2-rich and $H_2O + CO_2$-rich peridotite solidi are from Eggler (1977) and Canil & Scarfe (1990). The graphite–diamond and garnet–spinel transition zones are from Kennedy & Kennedy (1976) and Klemme & O'Neill (2000), respectively. The stability field for K-richterite is from Van der Laan & Foley (1994) and Konzett *et al.* (1997), and that for phlogopite is from Sato *et al.* (1997). *P–T* estimates for mantle xenoliths were obtained simultaneously using the data of Ganguly & Bhattacharya (1987) and Nehru & Reddy (1989) and the equations of Macgregor (1974), Harley (1984), Bertrand & Mercier (1985), Nickel & Green (1985) and Brey & Kohler (1990). The estimated base of the Proterozoic Mechanical Boundary Layer (MBL) beneath the Cuddapah Basin is from Anand *et al.* (2003). The postulated melt zone in the MBL, following lithospheric extension and perturbation of the illustrated geotherm, is shown by the hatched zone. There is no conclusive evidence of a melt contribution to the kimberlites and lamproites from the Thermal Boundary Layer (TBL) or convecting mantle as indicated by the '?' symbols.

garnet lherzolites. These equations were solved simultaneously with the geobarometers of Macgregor (1974), Nickel & Green (1985) and Brey & Kohler (1990), and the results are shown in Fig. 15.

(3) The Anantapur kimberlites are known to be diamondiferous. The Proterozoic geothermal gradient below the Dharwar Craton must therefore pass through the diamond stability field. We have located this in Fig. 15a using the experimental results of Kennedy & Kennedy (1976).

(4) A recent study of Early Proterozoic tholeiitic basalts from the intracratonic Cuddapah Basin has suggested that the mechanical boundary layer (MBL) was ~145 km thick, prior to lithospheric extension (Anand *et al.*, 2003). This is the only information that we have to constrain the depth of melting involved in the genesis of the Cuddapah lamproites (Fig. 14b).

We have combined the above information with the results of experimental studies on CO_2- and H_2O-rich peridotite (Canil & Scarfe, 1990), anhydrous peridotite (Hirschmann, 2000), phlogopite (Sato *et al.*, 1997) and K-richterite (Van der Laan & Foley, 1994; Konzett *et al.*, 1997), to constrain the source regions of the primary kimberlite and lamproite melts. If our Mesoproterozoic geothermal gradient for the Dharwar Craton is correct, then Fig. 15a suggests that the primary melts of the diamondiferous Anantapur kimberlites could have been generated near the base of the MBL (at depths of ~160 km) from a CO_2-rich peridotite source by minor amounts of lithospheric extension. Phlogopite would also be stable under these conditions and this would explain the K anomalies that we have observed on normalized multi-element plots. Our geochemical data suggest that the non-diamondiferous kimberlites (i.e. Pipes 2, 5 and 10 from Anantapur, and all of those from Mahbubnagar) have passed through lithospheric mantle containing a significant amount of ilmenite. This may represent material from partially melted veined lithospheric mantle; ilmenite would, however, be residual only at very small degrees of partial melting (Foley, 1992). We do not have any evidence for a convecting mantle source contribution to the kimberlites but we believe that a significant melt contribution came from the subcontinental lithospheric mantle.

Our Nd-isotopic study of the lamproites suggests that they were generated from ancient enriched lithospheric mantle sources beneath the intracratonic Cuddapah Basin. Figure 15b suggests that the lamproites may have been generated from a metasomatized harzburgite near the base of the MBL, i.e. at depths of

~145 km. K-richterite (OH) and phlogopite would be only marginally stable under these conditions, which is consistent with the relatively potassic nature of these rocks. The regional metasomatic events, which have influenced the source regions of the kimberlites and lamproites, might also be responsible for the enrichment of the source regions of of the Mid-Proterozoic alkaline plutons in the Eastern Ghat mobile belt. These are poorly dated but seem to be broadly contemporaneous with, or younger than, the lamproites. The contemporaneous generation of different types of small-volume igneous rocks has been noted in other igneous provinces where there are variations in lithospheric thickness (e.g. Gibson *et al.*, 1995).

None of the scenarios that we have outlined above require elevated Proterozoic mantle potential temperatures or invoke significant melting of the convecting mantle. The ~300 Myr interval of mid-Proterozoic kimberlite and lamproite emplacement in the Eastern Dharwar Craton and Cuddapah Basin is more consistent with a model of lithospheric mantle melting by extension rather than linked with a mantle plume. Indeed, the ~1·9 Ga initiation and subsequent evolution of the Cuddapah Basin can be largely explained by lithospheric extension (Anand *et al.*, 2003). The age of the Chelima lamproite (1417 ± 8·2 Ma; Chalapathi Rao *et al.*, 1999), which intrudes the youngest unit of the Cuddapah Supergroup of rocks, is considered to be the minimum age for the termination of extension in the Cuddapah Basin. The thick sedimentary succession and genesis of tholeiitic lavas and sills does not require the involvement of a mantle plume but can be explained by the high ambient potential temperature (1500°C) of the underlying convecting mantle during the Early Proterozoic (Anand *et al.*, 2003). Mafic dyke swarms in the Dharwar Craton may also have been generated by lithospheric extension. These are, however, poorly dated and little is known about their petrogenesis.

CONCLUSIONS

(1) Detailed study of the petrology and mineral chemistry of Proterozoic mafic potassic igneous rocks from southern India suggests that those occurring within the Cuddapah Basin and at its NE margin are lamproites and those within the Dharwar Craton are kimberlites. The kimberlites are non-diamondiferous in the ~1400 Ma Mahbubnagar cluster and predominantly diamondiferous in the ~1090 Ma Anantapur cluster. Many are remarkably fresh, given their Proterozoic age.

(2) The non-diamondiferous kimberlites from Mahbubnagar and Anantapur are characterized by higher contents of Fe, Ti, Zr, Hf and Sc and lower La/Sm ratios and Ni contents than the diamondiferous Anantapur kimberlites.

(3) The absence of Ta and Nb negative anomalies in normalized multi-element patterns suggests that metasomatic enrichment of the sub-continental lithospheric mantle was caused by the migration of low-temperature, small-fraction melts from the convecting mantle (McKenzie, 1989) rather than by subduction-derived melts (Murphy *et al.*, 2002).

(4) The positive εNd_i values and high La/Sm ratios of the Dharwar kimberlites suggest that their melt source regions were enriched by small-melt fractions derived from the depleted upper mantle shortly prior to kimberlite genesis. The low εNd_i values of the diamondiferous Anantapur kimberlites relative to most of the Mahbubnagar kimberlites suggest that the former have entrained a greater amount of material from the sub-continental lithospheric mantle. This is consistent with the higher proportion of olivine macrocrysts in the Anantapur kimberlites.

(5) REE ratios of both the kimberlites and lamproites suggest that they are the products of low-degree partial melting of a garnet peridotite mantle source. Inversion modelling of REE concentrations suggests that the source regions of the Dharwar Craton kimberlites and lamproites have been extensively depleted (~20%) prior to metasomatic enrichment and subsequent partial melting. These observations are consistent with those for Group I and II kimberlites and lamproites from Kaapvaal craton of southern Africa (Tainton & McKenzie, 1994). The diamondiferous Anantapur kimberlites appear to have been derived from more LREE-enriched mantle sources than the non-diamondiferous Mahbubnagar kimberlites. The observed petrological and geochemical differences between the kimberlites and lamproites reflect: (a) differences in the volatile contents of their respective source regions; (b) final depth of melting; (c) subsequent low-pressure crystallization of these magmas.

(6) The occurrence of kimberlites in the Dharwar Craton, lamproites in the Cuddapah Basin and other alkaline rocks within the Eastern Ghat Mobile belt is due to extension of lithosphere of variable thickness during the Mid-Proterozoic.

ACKNOWLEDGEMENTS

We are grateful to S. V. Satyanarayana, K. R. P. Rao, Mohd Burhanuddin, K. Shivaji, B. K. Nagaraja Rao, M. G. Rao and K. S. Bhaskar Rao of the Geological Survey of India (Southern Region, Hyderabad) for their help during N.V.C.R.'s fieldwork; to D. James, K. Jarvis and B. Gibson for assistance with analytical work; and to D. McKenzie for providing the inversion code. A Cambridge University Nehru Trust Scholarship, Cambridge Philosophical Society grant and a bursary from the Wolfson College to N.V.C.R. made this research possible. Thorough reviews of an earlier draft

of this manuscript by K. Bell, J. B. Dawson, P. Janney and D. G. Pearson, and the editorial comments of M. Wilson, are gratefully acknowledged. This is Department of Earth Sciences Contribution ES.7522.

SUPPLEMENTARY DATA

Supplementary data from this paper are available on *Journal of Petrology* online.

REFERENCES

Abbott, D. H. (1996). Plumes and hotspots as sources of greenstone belts. *Lithos* **37**, 113–127.

Akella, J., Rao, P. S., McCallister, R. H., Boyd, F. R. & Meyer, H. O. A. (1979). Mineralogical studies on the diamondiferous kimberlites of Wajrajkarur area, south India. In: Boyd, F. R. & Meyer, H. O. A. (eds.) *Kimberlites, Diatremes and Diamonds: their Geology, Petrology and Geochemistry, Volume 1*. Washington, DC: American Geophysical Union, pp. 172–177.

Alibert, C. & Albarède, F. (1988). Relationships between mineralogical, chemical and isotope properties of some North American kimberlites. *Journal of Geophysical Research* **93**, 7643–7691.

Allen, P., Condie, K. C. & Narayana, B. L. (1985). The geochemistry of prograde and retrograde charnockite–gneiss reactions in southern India. *Geochimica et Cosmochimica Acta* **49**, 323–336.

Allsopp, H. L., Bristow, J. W., Smith, C. B., Brown, R., Gleadow, A. J. W., Kramers, J. D. & Garvie, O. G. (1989). A summary of radiometric dating methods applicable to kimberlites and related rocks. *Geological Society of Australia Special Publication* **14**, 343–357.

Anand, M., Gibson, S. A., Subbarao, K. V., Kelley, S. P. & Dickin, A. P. (2003). Early Proterozoic melt generation processes beneath the intra-cratonic Cuddapah Basin, Southern India. *Journal of Petrology* **44**, 2139–2171.

Anil Kumar, Padmakumari, V. M., Dayal, A. M., Murthy, D. S. N. & Gopalan, K. (1993). Rb–Sr ages of Proterozoic kimberlites of India: evidence for contemporaneous emplacement. *Precambrian Research* **62**, 227–232.

Anil Kumar, Gopalan, K., Rao, K. R. P. & Nayak, S. S. (2001). Rb–Sr ages of kimberlites and lamproites from Eastern Dharwar Craton, South India. *Journal of the Geological Society of India* **58**, 135–142.

Babu, T. M. (1998). *Diamonds in India. Geological Society of India, Bangalore, Economic Geology Series Publication*, 332 pp.

Basu, A. R. & Tatsumoto, M. (1979). Sm–Nd systematics in kimberlites and in the minerals of garnet-lherzolite inclusions. *Science* **205**, 398–401.

Beard, A. D., Downes, H., Hegner, E., Sablukov, S. M., Vetrin, V. R. & Balogh, K. (1998). Mineralogy and geochemistry of Devonian ultramafic minor intrusions of the southern Kola peninsula, Russia: implication for the petrogenesis of kimberlites and melilites. *Contributions to Mineralogy and Petrology* **130**, 288–303.

Beard, A. D., Downes, H., Hegner, E. & Sablukov, S. M. (2000). Geochemistry and mineralogy of kimberlites from the Arkhangelsk region, NW Russia: evidence for transitional kimberlite magma types. *Lithos* **51**, 47–73.

Becker, H., Wenzel, T. & Volker, F. (1999). Geochemistry of glimmerite veins in peridotites from Lower Austria—implications for the origin of K-rich magmas in collision zones. *Journal of Petrology* **40**, 315–338.

Bergman, S. C. (1987). Lamproites and other K-rich igneous rocks: review of their occurrence, mineralogy and geochemistry. In: Fitton, J. G. & Upton, B. G. J. (eds) *Alkaline Igneous Rocks. Geological Society, London, Special Publications* **30**, 103–190.

Bertrand, P. & Mercier, J. C. C. (1985). The mutual solubility of coexisting ortho- and clinopyroxene; toward an absolute geothermometer for the natural system? *Earth and Planetary Science Letters* **76**, 109–122.

Bhaskara Rao, B. (1976). A note on the micaceous kimberlite in the Cumbum Formations near Zangamarajupalle, Cuddapah district, Andhra Pradesh. *Indian Minerals* **30**, 55–58.

Bhattacharji, S. & Singh, R. N. (1984). Thermomechanical structure of the southern part of the Indian shield and its relevance to Precambrian basin evolution. *Tectonophysics* **105**, 103–120.

Boyd, F. R. (1974). Olivine megacrysts from the kimberlites of Monastery and Frank Smith Mines, South Africa. *Carnegie Institution of Washington Yearbook* **73**, 282–285.

Brey, G. P. & Kohler, T. (1990). Geothermobarometry in four-phase lherzolites. Part II: New thermobarometers and practical assessment of existing thermobarometers. *Journal of Petrology* **31**, 1353–1378.

Brey, G. P., Kohler, T. & Nickel, K. G. (1990). Geothermobarometry in four-phase lherzolites. Part I: Experimental results from 10 to 60 kb. *Journal of Petrology* **31**, 1313–1352.

Canil, D. & Scarfe, C. M. (1990). Phase relationships in peridotite + CO_2 system up to 12 GPa: implications for the origin of kimberlites and carbonate stability in the Earth's upper mantle. *Journal of Geophysical Research* **95**, 15805–15816.

Chalapathi Rao, N. V. (1997). Petrogenesis of Proterozoic kimberlites and lamproites from the Cuddapah Basin and Dharwar Craton, southern India. Ph.D. thesis, University of Cambridge.

Chalapathi Rao, N. V., Miller, J. A., Pyle, D. M. & Madhavan, V. (1996*a*). New Proterozoic K–Ar ages for some kimberlites and lamproites from the Cuddapah Basin and Dharwar Craton, south India: evidence for non-contemporaneous emplacement. *Precambrian Research* **79**, 363–369.

Chalapathi Rao, N. V., Reed, S. J. B., Pyle, D. M. & Beattie, P. D. (1996*b*). Larnitic kirschsteinite from the Kotakonda kimberlite, Andhra Pradesh, India. *Mineralogical Magazine* **60**, 513–516.

Chalapathi Rao, N. V., Gibson, S. A., Pyle, D. M. & Dickin, A. P. (1998). Contrasting isotopic mantle sources for Proterozoic lamproites and kimberlites from the Cuddapah Basin and eastern Dharwar Craton: implication for Proterozoic mantle heterogeneity beneath southern India. *Journal of the Geological Society of India* **52**, 683–694.

Chalapathi Rao, N. V., Miller, J. A., Gibson, S. A., Pyle, D. M. & Madhavan, V. (1999). Precise $^{40}Ar/^{39}Ar$ dating of Kotakonda kimberlite and Chelima lamproite, India: implication to the timing of mafic dyke swarm activity in the Eastern Dharwar Craton. *Journal of the Geological Society of India* **53**, 425–433.

Chatterjee, N. & Bhattacharji, S. (1998). Formation of Proterozoic tholeiite intrusives in and around Cuddapah Basin, south India and their Gondwana counterparts in East Antarctica, and compositional variation in their mantle sources. *Neues Jahrbuch für Mineralogie, Abhandlungen* **174**, 79–102.

Chatterjee, N. & Bhattacharji, S. (2001). Petrology, geochemistry and tectonic setting of the mafic dykes and sills associated with the evolution of the Proterozoic Cuddapah Basin of South India. *Proceedings of the Indian Academy of Sciences (Earth & Planetary Sciences)* **110**, 433–453.

Chetty, T. R. K. (1995). A correlation of Proterozoic shear zones between Eastern Ghats, India and Enderby Land, Eastern Antarctica. In: Yoshida, S. & Santosh, M. (eds) *India and Antarctica during the Precambrian. Geological Society of India Memoir* **34**, 205–220.

Clement, C. R. (1982). A comparative geological study of some major kimberlite pipes in northern Cape and Orange Free State. Ph.D. thesis, University of Cape Town.

Crawford, A. R. & Compston, W. (1973). The age of the Cuddapah and Kurnool systems, southern India. *Journal of the Geological Society of Australia* **19**, 453–464.

Crough, S. T. (1981). Mesozoic hot spot epeirogeneity in Eastern North America. *Geology* **9**, 2–6.

Crough, S. T., Morgan, W. J. & Hargraves, R. B. (1980). Kimberlites: their relation to mantle hot spots. *Earth and Planetary Science Letters* **50**, 260–274.

Cullers, R. L., Dorais, M. J., Berendsen, P. & Chaudhuri, S. (1996). Mineralogy and petrology of Cretaceous sub-surface lamproite sills, south-eastern Kansas, USA. *Lithos* **38**, 185–206.

Dalziel, I. W. D. (1997). Overview: Neoproterozoic–Paleozoic geography and tectonics: review, hypothesis, environmental speculations. *Geological Society of America Bulletin* **109**, 16–42.

Dawson, J. B. & Smith, J. V. (1975). Chemistry and origin of phlogopite megacrysts in kimberlite. *Nature* **253**, 336–338.

Dawson, J. B. & Smith, J. V. (1977). The MARID (mica–amphibole–rutile–ilmenite–diopside) suite of xenoliths in kimberlite. *Geochimica et Cosmochimica Acta* **41**, 309–323.

Divakara Rao, V., Subba Rao, M. V., Rama Rao, P. & Pantulu, G. V. C. (1994). Geochemistry, age and origin of Perur granite, Chittoor district, Andhra Pradesh. *Journal of the Geological Society of India* **44**, 637–644.

Edgar, A. D. & Charbonneau, H. E. (1993). Melting experiments on a SiO_2-poor CaO-rich aphanitic kimberlite from 5–10 GPa and their bearing on the source of kimberlite magmas. *American Mineralogist* **78**, 132–142.

Edgar, A. D. & Mitchell, R. H. (1997). Ultra high pressure–temperature melting experiments on an SiO_2-rich lamproite from Smoky Butte, Montana: derivation of siliceous lamproite magmas from enriched sources deep in the continental mantle. *Journal of Petrology* **38**, 457–477.

Edwards, D., Rock, N. M. S., Taylor, W. R., Griffin, W. J. & Ramsay, R. R. (1992). Mineralogy and petrology of the Aries diamondiferous kimberlite pipe, central Kimberley block, Western Australia. *Journal of Petrology* **33**, 1157–1191.

Eggler, D. H. (1977). The principle of the zone of invariant vapor composition; an example in the system CaO–MgO–SiO_2–CO_2–H_2O and implications for the mantle solidus. *Carnegie Institution of Washington Yearbook* **76**, 428–435.

Eggler, D. H. (1989). Kimberlites: how do they form? *Geological Society of Australia Special Publication* **14**, 489–504.

Emeleus, C. H. & Andrews, J. R. (1975). Mineralogy and petrology of kimberlite dyke and sheet intrusions and included peridotite xenoliths from SW Greenland. *Physics and Chemistry of the Earth* **9**, 179–198.

England, P. & Houseman, G. (1984). On the geodynamic setting of kimberlite genesis. *Earth and Planetary Science Letters* **67**, 109–122.

Erlank, A. J., Waters, F. G., Hawkesworth, C. J., Haggerty, S. E., Allsopp, H. L., Rickard, R. S. & Menzies, M. (1987). Evidence for mantle metasomatism in peridotite nodules from the Kimberley pipes, South Africa. In: Menzies, M. A. & Hawkesworth, C. J. (eds) *Mantle Metasomatism*. London: Academic Press, pp. 221–311.

Farmer, G. L. & Boettcher, A. L. (1981). Petrological and crystal chemical significance of some deep-seated phlogopites. *American Mineralogist* **66**, 1154–1163.

Foley, S. F. (1988). The genesis of continental basic alkaline magmas—an interpretation in terms of redox melting. *Journal of Petrology, Special Lithosphere Issue*, 138–161.

Foley, S. F. (1992). Petrological characterisation of the source composition of K-magmas: geochemical and experimental constraints. *Lithos* **28**, 187–204.

Foley, S. F. (1993). An experimental study of olivine lamproite: first results from the diamond stability field. *Geochimica et Cosmochimica Acta* **57**, 483–489.

Foley, S. F., Venturelli, G., Green, D. H. & Toscani, L. (1987). The ultra-potassic rocks: characteristics, classification and constraints for petrogenetic models. *Earth-Science Reviews* **24**, 81–134.

Fraser, K. J. (1987). Petrogenesis of kimberlites from South Africa and lamproites from Western Australia and North America. Ph.D. thesis, The Open University, Milton Keynes, 270 pp.

Fraser, K. J., Hawkesworth, C. J., Erlank, A. J., Mitchell, R. H. & Scott-Smith, B. H. (1985). Sr, Nd and Pb isotope and minor element geochemistry of lamproites and kimberlites. *Earth and Planetary Science Letters* **76**, 57–70.

Ganguly, J. & Bhattacharya, P. K. (1987). Xenoliths in Proterozoic kimberlites from southern India: petrology and geophysical implications. In: Nixon, P. H. (ed.) *Mantle Xenoliths*. New York: John Wiley, pp. 249–266.

Gibson, S. A. (2002) Major element heterogeneity in Archean to Recent mantle plume starting-heads. *Earth and Planetary Science Letters* **195**, 59–74.

Gibson, S. A., Thompson, R. N., Leonardos, O. H., Dickin, A. P. & Mitchell, J. G. (1995). The Late Cretaceous impact of the Trindade mantle plume: evidence from large-volume, mafic, potassic magmatism in SE Brazil. *Journal of Petrology* **36**, 189–229.

Gibson, S. A., Thompson, R. N., Dickin, A. P. & Leonardos, O. H. (1996). High Ti- and low-Ti mafic potassic magmas: key to plume–lithosphere interactions and continental flood basalt genesis. *Earth and Planetary Science Letters* **141**, 325–341.

Girnis, A. P., Brey, G. P. & Ryabchikov, I. D. (1995). Origin of Group IA kimberlites: fluid-saturated melting experiments at 45–55 kbar. *Earth and Planetary Science Letters* **134**, 283–296.

Grasty, R. L. & Leelanandam, C. (1965). Isotopic ages of basic charnockite and khondalite from Kondapalle, Andhra Pradesh, India. *Mineralogical Magazine* **35**, 529–535.

Greenwood, J. C., Gibson, S. A., Thompson, R. N., Weska, R. K. & Dickin, A. P. (1999). Cretaceous kimberlites from the Paranatinga–Batovi region, Central Brazil: geochemical evidence for subcratonic lithosphere mantle heterogeneity. In: Gurney, J. J., Gurney, J. L., Pascoe, M. D. & Richardson, S. H. (eds) *Proceedings of the Seventh International Kimberlite Conference, 1*. Cape Town: Red Roof Design, pp. 291–298.

Gupta, M. L. (1993). Is Indian shield hotter than other Gondwana shields? *Earth and Planetary Science Letters* **115**, 275–285.

Gupta, M. L., Sundar, A. & Sharma, S. R. (1991). Heat flow and heat generation in the Archaean Dharwar Cratons and implications for the southern Indian shield geotherm and lithospheric thickness. *Tectonophysics* **194**, 107–122.

Gurney, J. J. & Ebrahim, S. (1973). Chemical composition of Lesotho kimberlites. In: Nixon, P. H. (ed.) *Lesotho Kimberlites*. Maseru: Lesotho National Development Corporation, pp. 280–284.

Gurney, J. J., Moore, R. O., Otter, M. L., Kirkley, M. B., Hops, J. J. & McCandless, T. E. (1991). Southern African kimberlites and their xenoliths. In: Kampunju, A. B. & Lubala, R. T. (eds) *Magmatism in Extensional Tectonic Settings: the Phanerozoic African Plate*. New York: John Wiley, pp. 495–536.

Haggerty, S. E. (1982). Kimberlites in Western Liberia: an overview of the geological setting in a plate tectonic framework. *Journal of Geophysical Research* **87**, 811–826.

Haggerty, S. E. (1994). Super kimberlites: a geodynamic window to the Earth's core. *Earth and Planetary Science Letters* **122**, 57–69.

Harley, S. L. (1984). Comparison of the garnet–orthopyroxene geobarometer with recent experimental studies, and applications to natural assemblages. *Journal of Petrology* **25**, 697–712.

Harte, B. (1983). Mantle peridotites and processes—the kimberlite sample. In: Hawkesworth, C. J. & Norry, M. J. (eds) *Continental Basalts and Mantle Xenoliths*. Nantwich: Shiva, pp. 46–91.

Hawkesworth, C. J. & Vollmer, R. (1979). Crustal contamination versus mantle enrichment, $^{143}Nd/^{144}Nd$ and $^{87}Sr/^{86}Sr$ evidence from Italian volcanics. *Contributions to Mineralogy and Petrology* **69**, 151–165.

Hirschmann, M. M. (2000). Mantle solidus: experimental constraints and the effects of peridotite composition. *Geochemistry, Geophysics, Geosystems* 2000GC000070.

Hwang, P., Taylor, W. R., Rock, N. M. S. & Ramsay, R. R. (1994). Mineralogy, geochemistry and petrogenesis of the Metters Bore No. l lamproite pipe, Calwynyardah Field, West Kimberley Province, Western Australia. *Mineralogy and Petrology* **51**, 195–226.

Janney, P. E., le Roex, A. P., Carlson, R. W. & Viljoen, K. S. (2002). A chemical and multi-isotope study of the Western Cape Olivine Melilitite Province, South Africa: implications for the sources of kimberlites and the origin of the HIMU signature in Africa. *Journal of Petrology* **43**, 2339–2370.

Janse, A. J. A. & Sheahan, P. A. (1995). Catalogue of worldwide diamond and kimberlite occurrences: a selective and annotative approach. *Journal of Geochemical Exploration* **53**, 73–111.

Jaques, A. L., Lewis, J. D., Smith, C. B., Gregory, G. P., Ferguson, J., Chappell, B. W. & McCulloch, M. T. (1984). The diamond-bearing ultrapotassic (lamproitic) rocks of the west Kimberley region, western Australia. In: Kornprobst, J. (ed.) *Kimberlites I. Kimberlites and Related Rocks*. Amsterdam: Elsevier, pp. 225–254.

Jaques, A. L., Sun, S.-S. & Chappell, B. W. (1989). Geochemistry of Argyle (AK1) lamproite pipe, Western Australia. *Geological Society of Australia Special Publication* **14**, 170–188.

Jarvis, K. E. (1990). A critical evaluation of two sample preparation techniques for low-level determination of some geologically incompatible elements by ICP-MS. *Chemical Geology* **83**, 89–103.

Jones, A. P. & Wyllie, P. J. (1984). Minor elements in perovskites from kimberlite and distribution of rare earth elements: an electron probe study. *Earth and Planetary Science Letters* **69**, 128–140.

Kaila, K. L., Roychowdhury, K., Reddy, P. R., Krishna, V. G., Harinarain, Subbotin, S. I., Sollogub, V. B., Chekunov, A. V., Kharetchko, G. E., Lazarenko, M. A. & Illchenko, T. V. (1979). Crustal structure along the Kavali–Udipi profile in the Indian peninsular shield from deep seismic soundings. *Journal of the Geological Society of India* **20**, 307–333.

Kennedy, C. S. & Kennedy, G. C. (1976). The equilibrium boundary between graphite and diamond. *Journal of Geophysical Research* **81**, 2467–2470.

Kepezhinskas, P. K., Defant, M. J. & Drummond, M. S. (1995). Na metasomatism in the island arc mantle by slab–melt peridotite interaction: evidence from mantle xenoliths in the Northern Kamchatka Arc. *Journal of Petrology* **36**, 1505–1527.

Kinny, P. D. & Dawson, J. B. (1992). A mantle metasomatic injection event linked to Late Cretaceous kimberlite magmatism. *Nature* **360**, 726–728.

Klemme, S. & O'Neill, H. St. C. (2000). The near-solidus transition from garnet lherzolite to spinel lherzolite. *Contributions to Mineralogy and Petrology* **138**, 237–248.

Konzett, J., Sweeney, R. J., Thompson, A. B. & Ulmer, P. (1997). Potassium amphibole stability in the upper mantle: an experimental study in a peralkaline KNCMASH system to 8·5 GPa. *Journal of Petrology* **38**, 537–568.

Kramers, J. D. & Smith, C. B. (1983). A feasibility study of U–Pb and Pb–Pb dating of kimberlites using groundmass mineral fractions and wholerock samples. *Chemical Geology* **1**, 23–38.

Larsen, L. M. & Rex, D. C. (1992). A review of the 2500 Ma span of alkaline–ultramafic–potassic and carbonatitic magmatism in West Greenland. *Lithos* **28**, 367–402.

LeCheminant, A. N. & Heaman, L. M. (1989). Mackenzie igneous events, Canada: Middle Proterozoic hot spot magmatism associated with ocean opening. *Earth and Planetary Science Letters* **96**, 38–48.

Macgregor, I. H. (1974). The system $MgO–Al_2O_3–SiO_2$; solubility of Al_2O_3 in enstatite for spinel and garnet peridotite compositions. *American Mineralogist* **59**, 110–119.

Mahadevan, T. M. (1995). *Deep Continental Structure of India: a Review. Geological Society of India Memoir* **28**, 562 pp.

Mahotkin, I. L., Gibson, S. A., Thompson, R. N., Zhuravlev, D. Z. & Zherdev, P.U. (2000). Late Devonian diamondiferous kimberlite and alkaline picrite (proto-kimberlite?) magmatism in the Arkhangelsk region, NW Russia. *Journal of Petrology* **41**, 201–227.

Mallikharjuna Rao, J., Bhattacharjee, S., Rao, M. N. & Horne, O. (1995). $^{40}Ar/^{39}Ar$ ages and geochemistry of dyke swarms around the Cuddapah Basin. *Geological Society of India Memoir* **33**, 307–328.

Matson, D. W., Mucnow, D. W. & Garcia, M.O. (1986). Volatile contents of phlogopite micas from South African kimberlites. *Contributions to Mineralogy and Petrology* **93**, 399–408.

Maury, R., Defant, C. & Joron, M. J. (1992). Metasomatism of the sub-arc mantle inferred from trace elements in Philippines xenoliths. *Nature* **360**, 660–661.

McCulloch, M. T. & Bennett, V. C. (1994). Progressive growth of the Earth's continental crust and depleted mantle: geochemical constraints. *Geochimica et Cosmochimica Acta* **58**, 4717–4738.

McCulloch, M. T., Jaques, A. L., Nelson, D. R. & Lewis, J. D. (1983). Nd and Sr isotopes in kimberlites and lamproites from western Australia: an enriched mantle origin. *Nature* **302**, 400–403.

McDonald, I., De Wit, M. J., Smith, C. B., Bizzi, L. A. & Viljoen, K. S. (1995). The geochemistry of the Platinum Group of elements in Brazilian and southern African kimberlites. *Geochimica et Cosmochimica Acta* **59**, 2882–2903.

McKenzie, D. (1989). Some remarks on the movement of small melt fractions in the mantle. *Earth and Planetary Science Letters* **95**, 53–72.

McKenzie, D. P. & Bickle, M. J. (1988). The volume and composition of melt generated by extension of the lithosphere. *Journal of Petrology* **29**, 625–679.

McKenzie, D. & O'Nions, R. K. (1991). Partial melt distributions from the inversion of rare earth element concentrations. *Journal of Petrology* **32**, 1021–1091.

Menzies, M. A. & Wass, S.Y. (1983). CO_2 and LREE-rich mantle below eastern Australia: a REE and isotopic study of alkaline magmas and apatite-rich mantle xenoliths from the Southern Highlands Province, Australia. *Earth and Planetary Science Letters* **65**, 287–302.

Mitchell, R. H. (1985). A review of the mineralogy of lamproites. *Transactions of the Geological Society of South Africa* **88**, 411–437.

Mitchell, R. H. (1986). *Kimberlites: Mineralogy, Geochemistry and Petrology*. New York: Plenum, 442 pp.

Mitchell, R. H. (1995). *Kimberlites, Orangeites and Related Rocks*. New York: Plenum, 406 pp.

Mitchell, R. H. & Bergman, S. C. (1991). *Petrology of Lamproites*. New York: Plenum, 447 pp.

Mitchell, R. H. & Brunfelt, A.O. (1975). Rare earth geochemistry of kimberlite. *Physics and Chemistry of the Earth* **9**, 671–686.

Mitchell, R. H. & Reed, S. J. B. (1988). Ion microprobe determination of rare earth elements in perovskites from kimberlites and alnoites. *Mineralogical Magazine* **52**, 331–339.

Mitchell, R. H. & Steele, I. M. (1992). Potassium, zirconium and strontian cerian perovskite in lamproites from the Leucite Hills, Wyoming. *Canadian Mineralogist* **30**, 1153–1159.

Mitchell, R. H., Platt, R. G. & Downey, M. (1987). Petrology of lamproites from Smoky Butte, Montana. *Journal of Petrology* **28**, 645–677.

Moore, A. E. (1988). Olivine: a monitor of magma evolutionary paths in kimberlites and olivine melilitites. *Contributions to Mineralogy and Petrology* **99**, 238–248.

Moore, R.O., Gurney, J. J., Griffin, W. L. & Shimizu, N. (1991). Ultra-high pressure garnet inclusions in Monastery diamonds: trace element abundance patterns and conditions of origin. *European Journal of Mineralogy* **3**, 213–230.

Murphy, D. T., Collerson, K. D. & Kamber, B. S. (2002). Lamproites from Gaussberg, Antarctica: possible transition zone melts of Archaean subducted sediments. *Journal of Petrology* **43**, 981–1001.

Murthy, D. S. N., Dayal, A. M. & Natarajan, R. (1994). Mineralogy and geochemistry of Chigicherla kimberlite and its xenoliths, Anantapur district, South India. *Journal of the Geological Society of India* **43**, 329–341.

Murthy, D. S. N., Dayal, A. M., Natarajan, R., Balaram, V. & Govil, P. K. (1997). Petrology and geochemistry of Chigicherla (pipe-2) kimberlite, Anantapur district, A. P. *Journal of the Geological Society of India* **49**, 123–132.

Murthy, Y. G. K., Babu Rao, V., Guptasarma, D., Rao, J. M., Rao, M. N. & Bhattacharjee, S. (1987). Tectonic, petrochemical and geophysical studies of mafic dyke swarms around the Proterozoic Cuddapah Basin, South India. *Geological Association of Canada Special Paper* **34**, 303–316.

Nagaraja Rao, B. K., Rajurkar, S. T., Ramalingaswamy, G. & Ravindra Babu, B. (1987). Stratigraphy, structure and evolution of the Cuddapah Basin. *Geological Society of India Memoir* **6**, 33–86.

Naqvi, S. M. & Rogers, J. J. W. (1987). *Precambrian Geology of India. Oxford Monographs on Geology and Geophysics* **6**, 223 pp.

Naqvi, S. M., Divakara Rao, V. & Harinarain (1974). The Protocontinental growth of the Indian shield and the antiquity of its rift valleys. *Precambrian Research* **1**, 345–389.

Navon, O. & Stolper, E. (1987). Geochemical consequences of melt percolation: the upper mantle as a chromatographic column. *Journal of Geology* **95**, 435–453.

Nayak, S. S., Kasiviswanathan, C. V., Reddy, T. A. K. & Nagaraja Rao, B. K. (1988). New find of kimberlitic rocks in Andhra Pradesh near Maddur, Mahabubnagar district. *Journal of the Geological Society of India* **31**, 343–346.

Nayak, S. S., Rao, K. R. P., Kudari, S. A. K. & Ravi, S. (2001). Geology and tectonic setting of kimberlites and lamproites of southern India. *Geological Survey of India Special Publication* **58**, 603–613.

Nehru, C. E. & Reddy, T. A. K. (1989). Ultramafic xenoliths from Vajrakarur kimberlites, India. *Geological Society of Australia Special Publication* **14**, 745–758.

Nelson, D. R. (1989). Isotopic characteristics and petrogenesis of lamproites and kimberlites of central west Greenland. *Lithos* **22**, 265–275.

Nelson, D. R., Black, L. P. & McCulloch, M. T. (1989). Nd–Pb isotopic characteristics of the Mordor complex, Northern Territory: Mid-Proterozoic potassic magmatism from an enriched mantle. *Australian Journal of Earth Sciences* **36**, 541–551.

Nickel, K. G. & Green, D. H. (1985). Empirical geothermobarometry of garnet peridotites and implications for nature of the lithosphere, kimberlites and diamonds. *Earth and Planetary Science Letters* **73**, 157–170.

Nixon, P. H., Davies, G. R., Rex, D. C. & Gray, A. (1992). Venezuela kimberlites. *Journal of Volcanology and Geothermal Research* **50**, 101–115.

Norrish, M. & Hutton, J. T. (1969). An accurate X-ray spectrographic method for the analyses of a wide range of geological samples. *Geochimica et Cosmochimica Acta* **33**, 431–453.

Padmakumari, V. M. & Dayal, A. M. (1987). Geochronological studies of some mafic dykes around Cuddapah Basin, south India. *Geological Society of India Memoir* **6**, 369–379.

Paul, D. K. (1979). Isotopic composition of strontium in Indian kimberlites. *Geochimica et Cosmochimica Acta* **43**, 389–394.

Paul, D. K. & Ray Barman, T. (1988). Isotopic and geochemical evolution of granulites of the Eastern Ghats belt. *Workshop on 'Proterozoic Rocks of India' IGCP-217*. Calcutta: Geological Society of India (unpaginated).

Paul, D. K., Rex, D. C. & Harris, P. G. (1975). Chemical characteristics and K–Ar ages of Indian kimberlites. *Geological Society of America Bulletin* **86**, 364–366.

Peacock, S. M. (1990). Fluid processes in subduction zones. *Science* **248**, 329–337.

Pidgeon, R. T., Smith, C. B. & Fanning, C. M. (1989). Kimberlite and lamproite emplacement ages in Western Australia. *Geological Society of Australia Special Publication* **14**, 369–381.

Radhakrishna, T. & Piper, J. D. A. (eds) (1999). *The Indian Subcontinent and Gondwana: a Palaeomagnetic and Rock Magnetic Perspective. Geological Society of India Memoir* **44**, 270 pp.

Rajamani, V., Shiv Kumar, K., Hanson, G. N. & Shirey, S. B. (1985). Geochemistry and petrogenesis of amphibolites from Kolar schist belt, south India: evidence for komatiitic magma derived by low percentages of melting of the mantle. *Journal of Petrology* **96**, 92–123.

Rajamani, V., Shirey, S. B. & Hanson, G. N. (1989). Fe-rich Archaean tholeiites derived from melt-enriched mantle sources: evidence from Kolar schist belt, south India. *Journal of Geology* **32**, 487–501.

Rajaraman, S. & Deshpande, M. L. (1978). Banganapalle diamond-iferous conglomerate in Kurnool district, Andhra Pradesh. *Indian Minerals* **32**, 33–43.

Rao, K. R. P., Rao, K. S. B. & Satyanarayana, S. V. (1991). Assessment of diamond resources in kimberlites of Venkatampalle–Lattavaram areas, Anantapur district, Andhra Pradesh. *Records of the Geological Survey of India* **124**, 33–39.

Rao, P. V. & Puffer, J. H. (1996). Geochemistry, petrogenesis and tectonic setting of Proterozoic mafic dyke swarms, Eastern Dharwar Craton, India. *Journal of the Geological Society of India* **47**, 165–174.

Reddy, N. S. (1988). Pillowed spilitic lavas from the Tadpatri Formation of the Cuddapah Basin. *Journal of the Geological Society of India* **32**, 65–67.

Reddy, T. A. K. (1987). Kimberlite and lamproitic rocks of Wajrakarur area, Andhra Pradesh. *Journal of the Geological Society of India* **30**, 1–12.

Reddy, T. A. K., Ravi, S., Chakravarthi, V. & Neelakantam, S. (2000). Discovery of lamproite field in Krishna and Nalgonda districts in Andhra Pradesh, South India. Proceedings of a workshop on the status, complexities and challenges of diamond exploration in India held at Raipur, pp. 93–104.

Richter, F. M. (1988). A major change in the thermal state of the Earth at the Archean–Proterozoic boundary: consequences for the nature and preservation of continental lithosphere. *Journal of Petrology, Special Lithosphere Volume*, 39–52.

Ringwood, A. R., Kesson, S. E., Hibberson, W. & Ware, N. (1992). Origin of kimberlites and their related magmas. *Earth and Planetary Science Letters* **113**, 521–538.

Rogers, J. J. W., Unrug, R. & Sultan, M. (1995). Tectonic assembly of Gondwana. *Journal of Geodynamics* **19**, 1–34.

Rollinson, H. R., Windley, W. F. & Ramakrishnan, M. (1981). Contrasting high and intermediate pressures of metamorphism in

the Archaean Sargur belts of South India. *Contributions to Mineralogy and Petrology* **76**, 420–429.

Sato, K., Katsura, T. & Ito, E. (1997). Phase relations of natural phlogopite with and without enstatite up to 8 GPa; implication for mantle metasomatism. *Earth and Planetary Science Letters* **146**, 511–526.

Satyanarayana, S. V. (2002). Diamond Provinces of India: an overview. In: Proceedings of the International Conference on Diamond & Gemstones organized by South Asian Association of Economic Geologists (SAAEG) at Raipur, Chattisgarh, India, 9–15 February, Extended Abstracts, pp. 44–45.

Satyanarayana, S. V., Rao, K. R. P., Shivaji, K., Nayak, S. S., Rao, M. G. & Viswanathan, T. V. (1992). Geological setting of the diamondiferous primary and secondary rocks in Andhra Pradesh. Proceedings of the International Round Table Conference on Diamond Prospecting and Exploration (NMDC and UNESCO sponsored), New Delhi (unpaginated).

Scott, B. H. (1979). Petrogenesis of kimberlites and associated potassic lamprophyres from central west Greenland. In: Boyd, F. R. & Meyer, H. O. A. (eds) *Kimberlites, Diatremes and Diamonds: their Geology, Petrology and Geochemistry, Volume 1*. Washington, DC: American Geophysical Union, pp. 190–225.

Scott, B. H. (1981). Kimberlite and lamproite dykes from Holsteinsborg, West Greenland. *Meddelelser om Grønland, Geoscience* **3**, 13–24.

Scott-Smith, B. H. (1989). Lamproites and kimberlites in India. *Neues Jahrbuch für Mineralogie, Abhandlungen* **86**, 193–225.

Scott-Smith, B. H. & Skinner, E. M. W. (1984). A new look at the Prairie Creek, Arkansas. In: Kornprobst, J. (ed.) *Kimberlites I. Kimberlites and Related Rocks*. Amsterdam: Elsevier, pp. 255–284.

Scott-Smith, B. H., Danchin, R. V., Harris, J. W. & Stracke, K. J. (1984). Kimberlites near Orroroo, South Australia. In: Kornprobst, J. (ed.) *Kimberlites I. Kimberlites and Related Rocks*. Amsterdam: Elsevier, pp. 121–142.

Scott-Smith, B. H., Skinner, E. M. W. & Loney, P. E. (1989). The Kapamba lamproites of the Luangwa valley, eastern Zambia. *Geological Society of Australia Special Publication* **14**, 189–205.

Shee, S. R., Bristow, J. W., Bell, D. R., Smith, C. B., Allsopp, A. L. & Shee, P. B. (1989). The petrology of kimberlites, related rocks and associated mantle xenoliths from the Kuruman province, South Africa. *Geological Society of Australia Special Publication* **14**, 60–82.

Skinner, E. M. W., Smith, C. B., Bristow, J. W., Scott-Smith, B. H. & Dawson, J. B. (1985). Proterozoic kimberlites and lamproites and a preliminary age for the Argyle pipe, Western Australia. *Transactions of the Geological Society of South Africa* **88**, 335–340.

Smith, A. G. & Hallam, A. (1970). The fit of the southern continents. *Nature* **225**, 139–144.

Smith, C. B. (1983). Pb, Sr and Nd isotopic evidences for sources of southern African Cretaceous kimberlites. *Nature* **304**, 51–54.

Smith, C. B., Allsopp, H. L., Kramers, J. D., Hutchinson, G. & Roddick, J. C. (1985). Emplacement ages of Jurassic–Cretaceous South African kimberlites by the Rb–Sr method on phlogopite and whole-rock samples. *Transactions of the Geological Society of South Africa* **88**, 249–266.

Smith, J. V., Breunscholtz, R. & Dawson, J. B. (1978). Chemistry of micas from kimberlites and xenoliths—I micaceous kimberlites. *Geochimica et Cosmochimica Acta* **42**, 959–971.

Smith, J. V., Delaney, J. S., Hervig, R. L. & Dawson, J. B. (1981). Storage of F and Cl in the upper mantle: geochemical implications. *Lithos* **14**, 133–147.

Spriggs, A. J. (1988). An isotopic and geochemical study of kimberlites and associated alkaline rocks from Namibia. Ph.D. thesis, University of Leeds.

Sreeramachandra Rao, K. (1988). Geological setting of the kimberlite dykes in the Zangamarajupalle Lead Zinc prospect, Cuddapah district, Andhra Pradesh. *Records of the Geological Survey of India* **116**(3–8), 146–155.

Tainton, K. M. (1992). The petrogenesis of Group-2 kimberlites and lamproites from the Northern Cape Province, South Africa. Ph.D. thesis, University of Cambridge.

Tainton, K. M. & McKenzie, D. (1994). The generation of kimberlites, lamproites and their source rocks. *Journal of Petrology* **35**, 787–817.

Takahashi, M. (1988). On the Na_2O content of convergent zone high-alumina basalts. *Chemical Geology* **68**, 17–29.

Taylor, W. R., Tompkins, L. A. & Haggerty, S. E. (1994). Comparative geochemistry of West African kimberlites: evidence for a micaceous kimberlite end member of sub-lithospheric origin. *Geochimica et Cosmochimica Acta* **58**, 4017–4037.

Thompson, R. N. & Gibson, S. A. (2000). Transient high temperatures in mantle plume heads inferred from magnesian olivines in Phanerozoic picrites. *Nature* **407**, 502–505.

Thompson, R. N., Morrison, M. A., Hendry, G. L. & Parry, S. J. (1984). An assessment of the relative roles of crust and mantle in magma genesis: an elemental approach. *Philosophical Transactions of the Royal Society of London, Series A* **310**, 549–590.

Tomlinson, K. Y., Stevenson, R. K., Hughes, D. J., Hall, R. P., Thurston, P. C. & Hall, R. P. (1998). The Red Lake greenstone belt, Superior Province: evidence of plume-related magmatism at 3 Ga and evidence of an older enriched source. *Precambrian Research* **89**, 59–76.

Turcotte, D. L. & Schubert, G. (1982). *Geodynamics: Applications of Continuum Physics to Geological Problems*. New York: John Wiley, pp. 279–285.

Van der Laan, S. R. & Foley, S. F. (1994). MARIDs and mantle metasomatism. *Mineralogical Magazine* **58A**, 505–506.

Vollmer, R. & Norry, M. J. (1983). Possible origin of K-rich volcanic rocks from Virunga, East Africa, by metasomatism of continental crustal material: Pb, Nd and Sr isotope evidence. *Earth and Planetary Science Letters* **64**, 374–386.

Wagner, C., Deloule, E. & Mokhtari, A. (1996). Richterite-bearing peridotites and MARID-type inclusions in lavas from NE Morocco: mineralogy and O/H ratios. *Contributions to Mineralogy and Petrology* **124**, 406–421.

Wallace, M. E. & Green, D. H. (1988). Mantle metasomatism by ephemeral carbonate melts. *Nature* **336**, 459–462.

Wilson, M., Rosenbaum, J. M. & Dunworth, A. D. (1995). Melilitites: partial melts of the thermal boundary layer? *Contributions to Mineralogy and Petrology* **119**, 181–196.

Woolley, A. R., Bergman, S. C., Edgar, A. D., Le Bas, M. J., Mitchell, R. H., Rock, N. M. S. & Scott-Smith, B. H. (1996). Classification of lamprophyres, lamproites, kimberlites and the kalsilitic, melilitic and leucitic rocks. *Canadian Mineralogist* **34**, 175–186.

Wyllie, P. J. (1987). Discussion of recent papers on carbonated peridotites bearing on mantle metasomatism and magmatism. *Earth and Planetary Science Letters* **82**, 391–397.

Yoshida, M. (1995). Assembly of East Gondwanaland during the Mesoproterozoic and its rejuvenation during the Pan-African period. *Geological Society of India Memoir* **34**, 24–45.